Research in Optoelectronics (A)

2022 Reprints of

Professor Larry A. Coldren

and Collaborators

ECE Technical Report 23-01

Department of Electrical & Computer Engineering
University of California, Santa Barbara

A Review of Photonic Systems-on-Chip Enabled by Widely Tunable Lasers

Larry A. Coldren, *Life Fellow, IEEE*, Paul A. Verrinder, and Jonathan Klamkin, *Senior Member, IEEE*

***Abstract*— Photonic Integrated Circuits (PICs) on indium phosphide have matured significantly over the past couple of decades and have found use in many system applications. Some PIC efforts on other group III-V substrates have also been initiated. In numerous cases, the usefulness of these PICs is because of the reduction in size, weight, and power they provide, but in many cases also because of the higher performance made possible by the improved relative phase stability among optical paths as well as the reduction of inter-element coupling losses. In this paper, as part of this special issue in tribute to Prof. Daniel Dapkus, we focus on monolithic PICs that provide a system function, especially those that incorporate and build on widely-tunable laser technology as a key element. Some of the early widely-tunable laser work is reviewed, and a selection of past system-on-a-chip developments is presented as background. Then, more recent system-on-a-chip advances performed by the author's groups are reviewed in more detail. Key advances are highlighted.**

***Index Terms*— Optoelectronics, photonics, photonic-integrated-circuits, semiconductor lasers, tunable lasers.**

I. Introduction

THIS paper reviews recent research at the University of California Santa Barbara (UCSB) on relatively complex photonic integrated circuits (PICs) based on III-V materials that perform a useful optical system function. These PICs, denoted as System-on-Chip (SoC)-PICs [1], are generally closely packaged, or co-packaged, with control or complementary functional electronics. Similar work has also been carried out at other academic and industrial laboratories, and some of this work has been summarized in prior reviews [1]–[10].

The focus of this paper is on monolithic SoC-PICs on native III-V substrates, including both indium phosphide (InP) and gallium arsenide (GaAs), which incorporate tunable lasers as a key component. It is, however, worth noting that considerable work has also been carried out in recent years in the area of hybrid and heterogeneous integration of III-V materials on silicon. Approaches include, co-packaging, wafer bonding, micro-transfer printing, as well as direct growth of III-V materials on silicon [11]–[14]. These technologies were developed primarily for datacom applications [15], [16].

The UCSB work has especially highlighted the benefit of using widely-tunable lasers as an integral part of most of their SoC-PICs. As will be discussed in Section II below, past examples of these SoC-PICs have included: optical transmitters, receivers, all-optical switches, coherent receivers, vector transmitters, and LIDAR transceivers. Incorporation of widely-tunable lasers has provided full C-band operation, and in the case of LIDAR, wide beam sweep angles. The background in Section II will begin with some discussion of the origins of widely-tunable lasers.

In Section III, our recent work will show improved coherent receivers with lower power dissipation and noise, better SoC-PICs for RF-over-fiber transmission, very rapid switching and phase locking for agile frequency synthesis, high-power optical transmitters for free-space links, a SoC-PIC and electronics for gas absorption sensing using frequency-swept LIDAR, and the demonstration of a widely-tunable laser PIC on gallium arsenide for the 1 μm wavelength region.

II. Background

A. Early PICs on III-Vs

A history of III-V PICs has been recently reported by Kish, *et al.* in [1]. As outlined therein, the concept and promise of PICs was first suggested by Miller in 1969 [17]. Low-loss fiber in the 1300-1550 nm wavelength range soon followed in the early 1970s [18] leading to intensive research on quaternary indium gallium arsenide phosphide (InGaAsP) and related materials on InP that have bandgap wavelengths in this range. By the late-1970s many of the desired active and passive components—lasers, lasers with gratings, passive waveguide couplers, modulators, detectors, etc.—had been demonstrated [1].

Early in the 1980s, fiber optic links had been introduced at 1300 nm, but even at the modest data rates used then, links were limited in reach to 30-40 km by the available signal-to-noise ratio. Expensive electronic repeaters were required to regenerate the signals at that point. To avoid this optical-electrical-optical (OEO) conversion, research on coherent technologies was initiated to extend the reach to approximately 80 km by leveraging the increased sensitivity afforded by coherent detection. A relatively coarse wavelength division multiplexing (WDM) was also being employed, and coherent could assist with the demultiplexing. Coherent and WDM

Manuscript received 29 November 2021; revised 16 March 2022; accepted 4 April 2022. Date of publication 18 April 2022; date of current version 28 July 2022. This work was supported in part by the National Aeronautics and Space Administration (NASA) Research Opportunities in Space and Earth Sciences (ROSES) Advanced Component Technology Program and in part by the NASA Earth Science and Technology Office (ESTO) Advanced Component Technology Program. *(Corresponding author: Larry A. Coldren.)*

The authors are with the Department of Electrical and Computer Engineering, University of California at Santa Barbara, Santa Barbara, CA 93106 USA (e-mail: coldren@ucsb.edu; pverrinder@ucsb.edu; klamkin@ece.ucsb.edu).

Color versions of one or more figures in this article are available at https://doi.org/10.1109/JQE.2022.3168041.

Digital Object Identifier 10.1109/JQE.2022.3168041

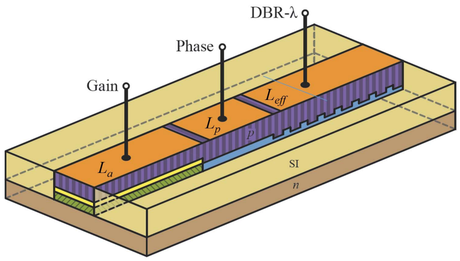

Fig. 1. Three-section tunable laser with one DBR and one cleaved facet mirror. Phase and DBR sections are passive (no gain), but tunable with current. The gain section provides gain with current injection, but little tuning. For more information see [21], [22].

stimulated some device researchers to begin work on tunable lasers, which could serve both as universal sources for WDM transmitters and tunable local oscillator (LO) sources that could be phase locked to the incoming signal in a coherent receiver [19], [20].

Researchers at the Tokyo Institute of Technology led by Prof. Suematsu were some of the first to focus on 1550 nm because optical fiber should ultimately have the lowest loss at this wavelength. They also realized that lasers should be tunable to operate as a WDM or coherent source, and they should have grating mirrors to be integrable with other passive waveguides and devices. They demonstrated such devices in the early 1980s [3].

By the late 1980s, relatively mature three-section DBR tunable lasers had been developed by several companies and universities [21], [22]. As shown in Fig. 1, these consisted of an active gain section, a passive phase tuner, and a passive Distributed-Bragg-Reflector (DBR) mirror, all connected to separate electrical sources. The active gain section contains gain material with a bandgap near the lasing wavelength in its *pn* junction, and the passive sections have higher bandgap material in their *pn* junctions, which change their index of refraction when current is injected. With current injected into the DBR, the narrow band over which it reflects is shifted in wavelength in proportion to the index shift. The optical cavity modes do not shift as much, so current must also be applied to the phase section to shift the cavity modes. In practice, approximately 6-7 nm of wavelength shift is possible at 1550 nm.

By the late 1980s coherent had still not been widely adopted. Higher data rates, denser WDM, as well as simply using more parallel fibers had been satisfying the increased demand, which was still due to a somewhat slowly increasing demand for voice, not data; the disruptive data crossover was not to occur until around 2000. By the late 1980s, research on the erbium-doped fiber amplifier (EDFA) was also beginning to show promise [23]. With the EDFA, OEO repeaters were no longer necessary and new links designed for the mid-1990s and beyond would no longer use OEO repeaters only for signal regeneration for modest distances. Work on coherent subsequently slowed.

B. Widely-Tunable Lasers

The EDFA enabled WDM over approximately 40 nm of bandwidth at 1550 nm in what was to be called the center

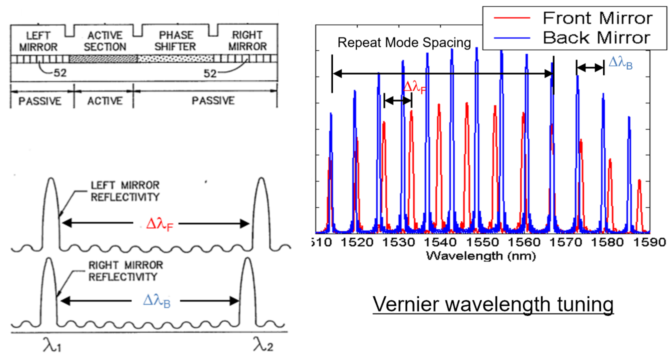

Fig. 2. Four-section widely-tunable laser. (Left) Excerpts from USP #4,896,325 illustrating basic structure and Vernier concept; (right) simulated mirror reflection spectra, expanding to many mirror reflection peaks, and showing eventual repeated overlaps.

or C-band. So, those researchers working on tunable lasers immediately began to search for concepts to make widely-tunable lasers, ones that could encompass the entire C-band.

There were a few ideas already being considered. For example, some of the early tunable laser work used coupled cavities, and these made use of Vernier tuning between the cavity modes of the two different length cavities to select a single mode [24]. However, these never led to a widely-tunable result, generally because the cavity modes were too close together. A relatively simple solution came in 1988 with the invention of the four-section tunable laser with two ‘differing multi-element mirrors’ [25], as described in Fig. 2.

By using periodically blanked, periodically modulated, or ‘sampled’ gratings, the reflection spectra of the gratings, instead of being a single sharp peak, are broken into a number of image peaks forming reflection combs. This is the so-called Sampled-Grating DBR, or SGDBR. If the two gratings are sampled with a different period, the period of the two reflection combs are different, but the separation of the reflection peaks can be large (~6-7 nm), and the separation difference can be tailorable (~1 nm). Thus, there is only one net reflection maximum for the laser (product of the two mirrors), and the repeat between these can be ~40 nm for single mode operation. By shifting both mirrors together, and then shifting one relative to the other slightly to select another pair of mirror maxima, and again repeating the shift together, it is possible to cover the full 40 nm with a single net maximum without missing any wavelengths [26].

Figure 3 shows the first results with the SGDBR laser in 1992 [27]. Although it did not include a phase tuner for fine tuning, it did illustrate the potential of the design with a total discontinuous tuning range of 57 nm and good single mode behavior over most of that range. Besides showing the fundamental attributes of the design, it should be noted that the material was grown by Prof. Dapkus’ group, illustrating one additional element of his influence on our field. Also, on this subject, we should mention that most of the early work at UCSB was supported by metalorganic chemical vapor deposition (MOCVD) growths performed by the group of Prof. DenBaars, an alumnus of Prof. Dapkus’ research group.

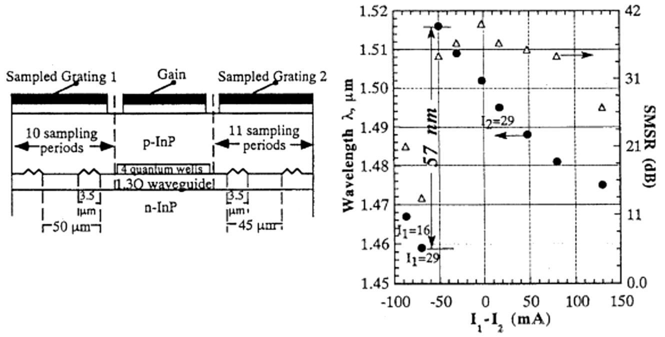

Fig. 3. First demonstration of wide range discontinuous tuning by a SGDBR laser. Adapted with permission from [27].

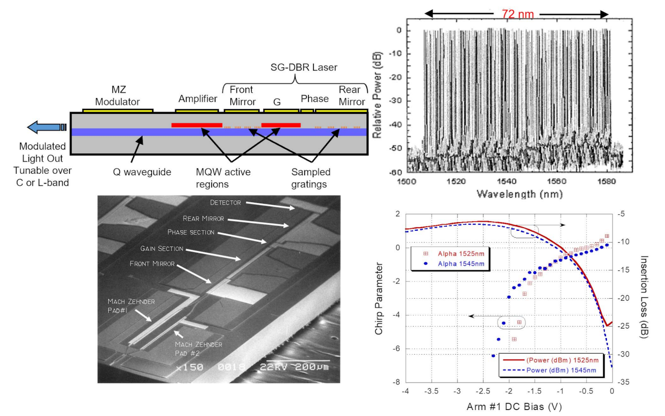

Fig. 4. SGDBR integrated with SOA and MZM schematic together with tuning results, a photograph, and modulator chirp vs. DC bias. For more information see [23] and [24].

The SGDBR design was to become one of the most successful of the options for widely-tunable lasers [28], perhaps the principal reason being that it was no more complex to manufacture than the three-section DBR illustrated in Fig. 1. The additional challenge was in the tuning control, and even that was only marginally more difficult. Following UCSB research, a company was formed, Agility Communications, to develop the concept into a product in 1998. This company also productized more complex PICs that incorporated SGDBRs with monitoring photodetectors, semiconductor optical amplifiers (SOAs), and modulators, either of the electroabsorption (EAM) [29] or Mach-Zehnder (MZM) [30] type.

Figure 4 shows the first UCSB prototype of the SGDBR-SOA-MZM along with chirp results reported in 2002 [23]. Also shown is a wavelength tuning spectrum of 72 nm from an earlier publication in 2000 [24], [25]. The output power at this tuning width was compromised to be $\sim$1 mW, so practical devices were later designed for $\sim$40 nm of tuning, which then allowed 40 mW in fiber reported by Agility in 2003 [31].

Agility was acquired by a more established optical components company in 2005, and many millions of these devices were sold into optical systems products that are still in use [32]. Analogous designs using ‘differing multi-element mirrors’ also appeared by other companies in the early 2000s,

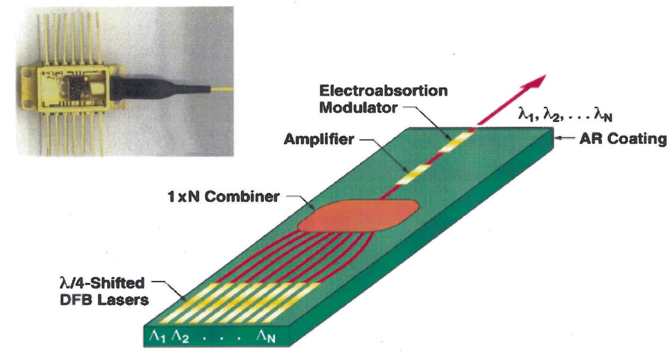

Fig. 5. DFB selectable-array PIC. Adapted with permission from [38].

and following some patent litigation, they were licensed to produce products [33].

Another early example stemmed from work on directional couplers between different waveguides. It was known that waveguides with slightly different effective indexes could be coupled if a coarse grating was added to one of them to provide the difference in propagation constants, or the phase matching. But, since this grating is fixed, and the waveguide propagation constants are proportional to frequency, phase matching is satisfied only over a limited bandwidth. However, this band can be tuned over a relatively large range by changing the index of one of the waveguides slightly; this is so because the difference between the waveguide indexes is small, and it is the *ratio* of the index change in one guide to this *difference* between the two waveguide indexes that counts. This concept was investigated by several research groups in the 1990s [34], [35], and eventually a company, Altitune, developed it into a product. However, following an acquisition, the acquiring company decided to abandon the concept.

There were a number of other examples of widely-tunable laser concepts developed in the late 1990s to early 2000s [36], mainly in response to the ‘telecom bubble’ that resulted from the realization that the rapidly increasing data bandwidth demand curve was overtaking the slowly increasing voice curve. But as dense WDM systems at higher data rates became available, this demand appeared to be satisfied, at least for a few years—perhaps just long enough to burst the bubble [37]. In any event, a couple of the widely-tunable solutions survived and that seemed to be sufficient.

Another concept not mentioned above, but very compelling to many at this time, was a DFB ‘selectable-array’ PIC, illustrated in Fig. 5. It typically consisted of 8-12 DFB lasers of slightly different wavelength that covered most of the C-band, and these could be tuned thermally by a few nanometers to fill in the gaps [38], [39]. These were all coupled by an MMI coupler into a single waveguide that incorporated an SOA, to compensate the 1/N coupling loss, as well as a possible integrated modulator.

This design was especially popular in Japan, because it seems many companies there were somewhat skeptical about the reliability and stability of the widely-tunable types discussed above [39]. Although the DFB selectable-array is not technically a widely-tunable laser, it does provide the same

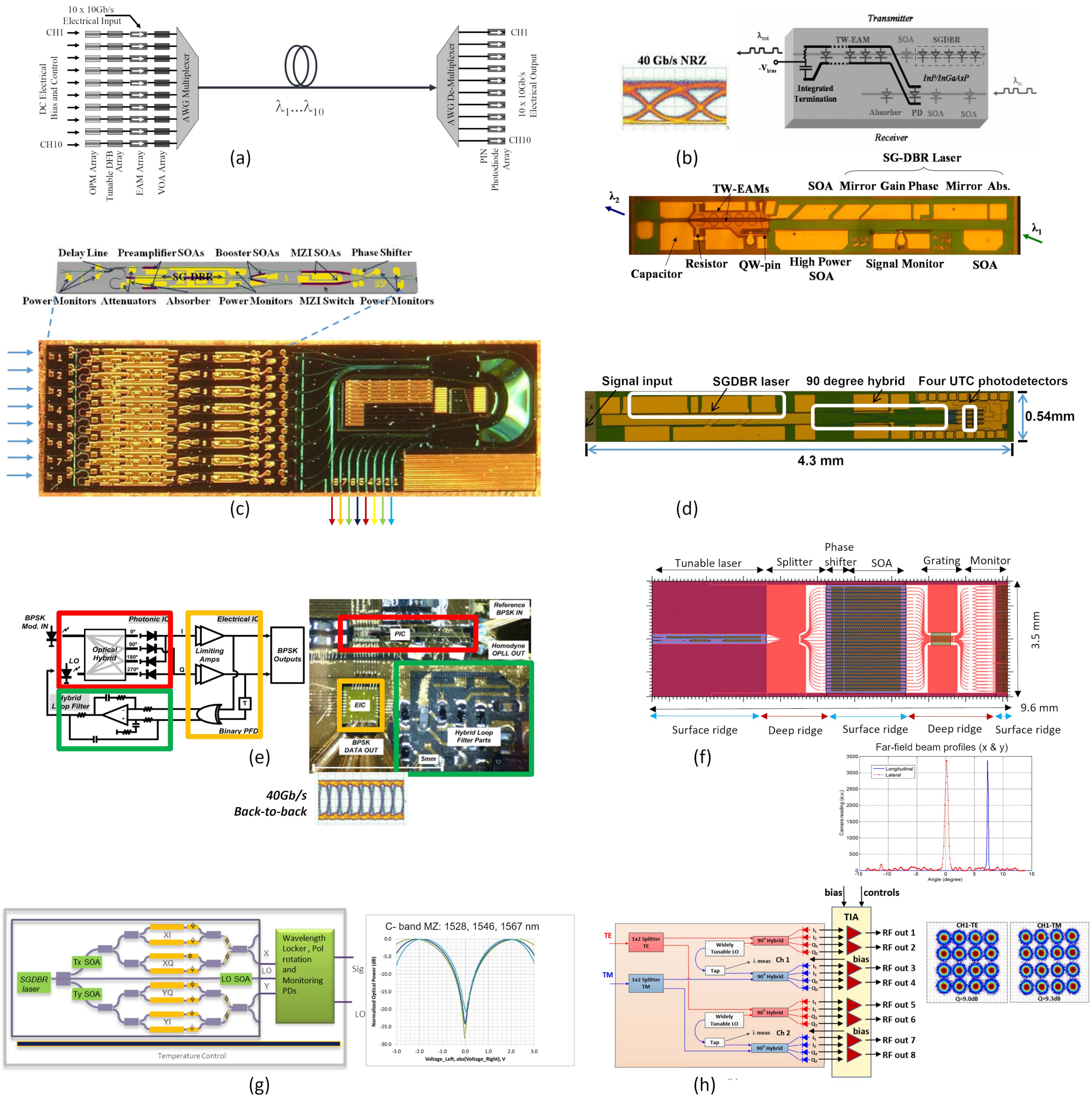

Fig. 6. Sampling of SoC-PIC results from 2004 to 2017. (a) Schematics of 10 × 10 Gb/s DFB/EAM integrated with AWG-MUX transmitter PIC and AWG-De-MUX integrated with 10 PIN PD array receiver PIC. Courtesy: Infinera; for more information see [43]; (b) full C-band wavelength-converter/transceiver PIC—SOA-PD input stage and SGDBR-Traveling-wave EAM output stage. Adapted with permission from [44]; (c) 8 × 8 all-optical packet switch PIC with 8 non-linear MZM wavelength converters integrated with an 8 × 8 AWGR. Adapted with permission from [45]; (d) coherent receiver PIC with high-power, widely-tunable SGDBR-LO, SOA, hybrid, and 4-high-bandwidth PDs. Adapted with permission from [46]; (e) Costa's loop phase-locked C-band coherent receiver. Adapted with permission from [47]; (f) 2-D LIDAR PIC with 32 × 120 resolution from 32 surface-emitting waveguides and tunable laser. Adapted with permission from [48]; (g) C-band vector transmitter PIC with supplemental LO output. Courtesy: Lumentum; for more information see [6]; (h) 2-Channel Rx PIC and TIA architecture and recovered constellations at 16 QAM for both polarizations @88 Gbaud. Courtesy: Infinera; for more information see [49].

functionality. Other 'selectable-array' types were also explored during the early 2000s [40]–[42].

III. System-on-Chip Demonstrations (2004-2017)

Figure 6 shows a sampling of SoC-PIC examples from the period 2004-2017.

The examples of Fig. 6 illustrate that SoC-PICs have provided many different functionalities and that significant savings in size, weight, and power have been demonstrated by integration. For example, as discussed in [1], the transmitter PIC in Fig. 6(a) comprises 10 transmitter channels that each include an optical power monitor, a DFB laser of a unique wavelength, an EAM, and a variable optical attenuator (VOA) (or SOA), all combined by an arrayed-waveguide grating (AWG) multiplexer. This is co-packaged with a 10-channel analog application specific integrated circuit (ASIC) modulator driver chip and a single thermoelectric cooler (TEC). The co-packaging with a single driver chip and a single TEC enables considerable power savings. A comparable description is provided for the receiver chip in [1], [43].

The discussion is somewhat similar for most of the SoC-PICs in Fig. 6. That is, many photonic elements are combined on a single PIC, the drive or control electronics are co-packaged, and a single TEC is used for the entire PIC. Figure 6(b) shows a data format and rate transparent wavelength converter/regenerator, which only requires DC bias connections, although data monitoring is available [39]. Operation from 5-40 Gb/s was demonstrated, and conversion from any input C-band wavelength to any output C-band wavelength was also confirmed. This SoC-PIC operates somewhat as a transceiver by using the input signal photocurrent from the receiving photodiode to dynamically change the bias on an EAM that follows an on-chip SGDBR laser. A regeneration function is possible by overdriving the EAM. Similar PICs have been constructed with MZMs [50].

Figure 6(c) shows the so-called MOTOR chip [45], which provides all-optical switching between its eight inputs and eight outputs. It operates in the return-to-zero (RZ) format at 40 Gb/s if nonlinear MZI-SOA wavelength converters are used [51]. This restriction is removed if the transceiver type of wavelength converter shown in Fig. 6(b) is employed. The outputs of the wavelength converters are coupled to an arrayed-waveguide-grating-router (AWGR), which sorts them according to their new wavelength to one of the outputs.

Figure 6(d) is a widely-tunable coherent receiver PIC. It includes SOA pre-amplifiers for the incoming signals, an integrated SGDBR-SOA as a high-power LO, a 90-degree hybrid and four uni-traveling-carrier (UTC)-photodiodes, which typically have bandwidths >30 GHz and good power handling capabilities, so that signal plus LO inputs well above the shot-noise level can be used. This receiver can be used with a number of different types of electronics, but it was used primarily in ‘analog’ coherent receivers in our work. For example, in Fig. 6(e), it is shown in the red box, and we have constructed a Costas phase/frequency locking circuit to phase-lock the LO to the carrier of the incoming signal with a wide frequency capture range [46], [47].

Figure 6(f) illustrates a 2-D optical beam-scanner chip that can be used in LIDAR or other direction-specific illumination or communication applications. The output of an SGDBR-SOA is split into 32 separate waveguides and coupled to an optical phased array via 32 phase shifters and SOAs. Light then emits from a weighted-grating surface-emitter region [48]. The angle of emission in the axial direction is varied by the wavelength. The angle in the lateral direction is varied by adjusting the individual phase shifters of the phased array using a particle-swarm optimization [52]. On-chip monitor photodiodes following the emitter array verify the calibration [52].

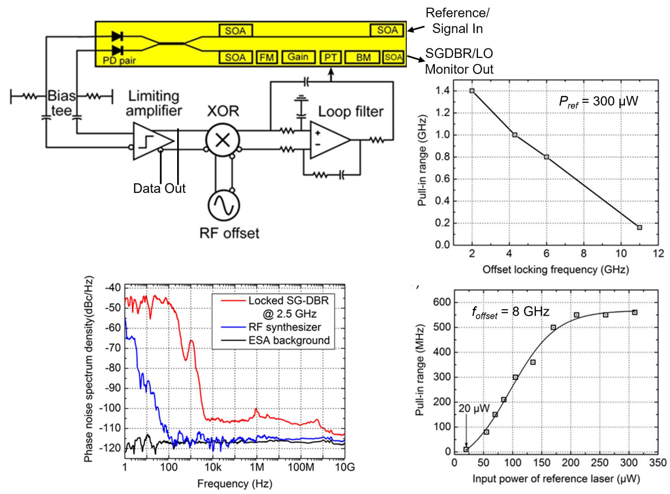

Fig. 7. Heterodyne optical phase locked loop with improved sensitivity and power consumption; schematic, locking frequency pull-in range vs. RF offset and input power of reference, and phase noise spectral density. Adapted with permission from [55].

Figure 6(g) is a schematic of a dual-polarization C-band vector transmitter PIC along with MZM characteristics from Lumentum [6]. This was co-packaged with modulator electronics and a TEC, and it was made available for system vendors. An LO output was also provided for use in a combined transmitter/receiver coherent module [6].

Figure 6(h) is a PIC receiver with transimpedance amplifier (TIA) architecture from Infinera, which uses a 1×2 splitter at the PIC input. This is capable of up to 720 Gb/s of input at 88 Gbaud over modest distances [49]. In [1], an analogous architecture is described in which the PIC employs a 1×6 splitter at its input to increase the practical data rate to 1.2 Tb/s at 33 Gbaud over considerably longer distances.

IV. Recent System-on-Chip Demonstrations

In the last five years there has been considerable activity at UCSB on SoC-PICs based on III-V materials grown at UCSB. The first section describes examples related to the use of optical phase lock loops (OPLLs) that are improvements on seminal work carried out a few years earlier [53], [54]. The following sections describe high power InP PICs for free space optical communications, InP PICs for remote sensing LIDAR, and tunable laser PICs for 1030 nm applications including topographical LIDAR.

A. Recent Optical Phase-Locked Loop Experiments

Figure 7 summarizes a more recent heterodyne OPLL effort with improved overall performance characteristics, and with significantly improved input optical sensitivity levels and power dissipation. The theoretical sensitivity was approximately 9 μW, and 20 μW was measured with a slight (2.5 GHz) offset [55].

The total dissipated power in the electronics was reduced dramatically to 1.12 W relative to circuits like those from Fig. 6(e), which consumed $\sim$3 W. The power consumption

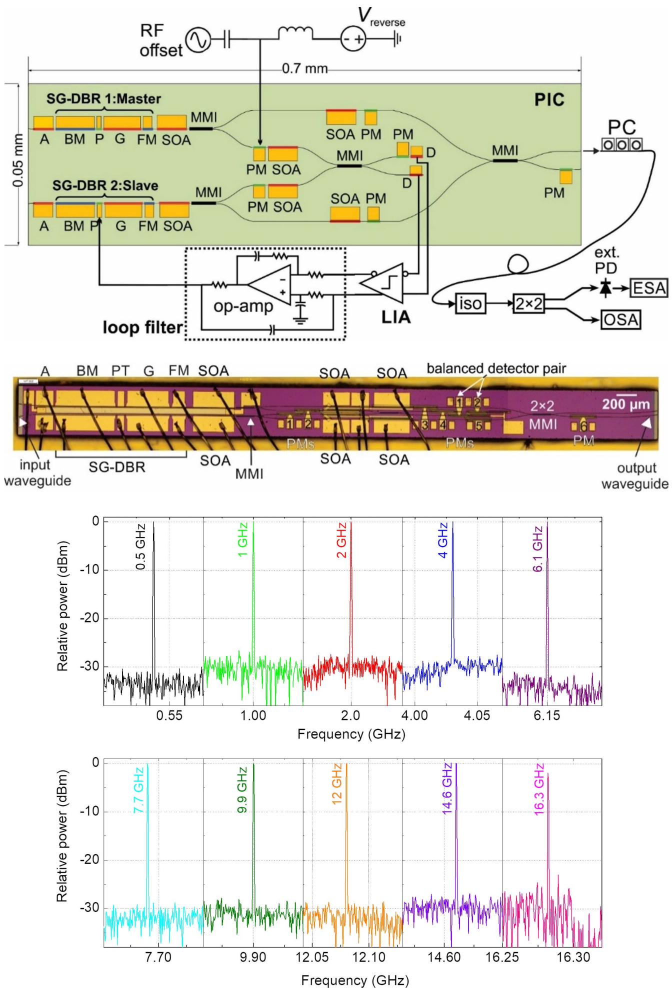

Fig. 8. RF-over-fiber SoC-PIC using an on-chip optical modulator for side-band generation. A schematic (top), PIC photo (center) and ESA spectra for various laser offsets due to RF applied to integrated phase modulator (PM) in center. Adapted with permission from [56].

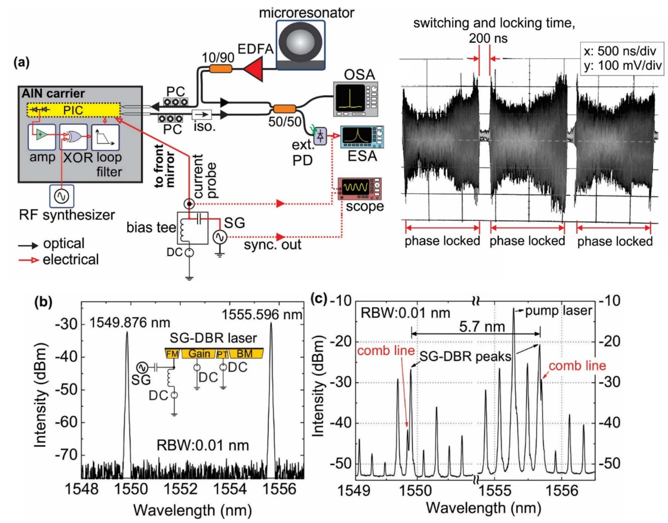

Fig. 9. Rapid locking of on-chip SGDBR laser to external microresonator for stable frequency synthesis. Schematic at top left. RF synthesizer set to 2.5 GHz; 800 kHz square wave applied to SGDBR front mirror to switch wavelength by 5.72 nm. ESA shows switching and locking time (top right); OSA shows spectra at bottom without and with microresonator reference. Adapted with permission from [57].

of the PIC with an SGDBR laser and SOA was 0.66 W with 10 mW output power. Experiments were also carried out with a Y-branch laser-PIC from Freedom Photonics; this PIC consumed only 0.18 W with 10 mW out, the difference being mostly that no SOA was employed [55].

As also illustrated in Fig. 7, the pull-in range of this simple OPLL is limited relative to the Costas-loop design of Fig. 6(e), which has a frequency locking and phase locking capability, because of the I and Q availability. In the case of Fig. 6(e) the pull-in range was ~20 GHz [46], but here it is limited to ~1 GHz, dependent in both cases on the signal strength and heterodyne offset.

Figure 8 shows results of an OPLL used to offset lock one SGDBR laser from another in an RF-over-fiber PIC [56]. This OPLL uses the sidebands from an on-chip optical modulator to lock the slave laser to the master rather than an electronic mixer, such as the XOR in Fig. 7. As illustrated by the electrical spectrum analyzer (ESA) spectra, master-slave offset locking up to 16.3 GHz was demonstrated.

In addition to the inner waveguide branches dedicated to the OPLL, this SoC-PIC also has outer waveguide branches that can be separately modulated to add signals to these two offset-locked laser carrier frequencies. They are combined near the output so that both carriers and possible modulation(s) are summed for transmission [56]. Thus, for example, if RF signal information, occupying e.g., the 4-6 GHz band, is modulated onto the outer branch of the slave laser path, one would be able to demodulate it with just a photodiode onto an IF equal to the chosen offset, e.g., at 12 GHz, some number of kilometers away from a coupled optical fiber.

Figure 9 shows a third example of the use of an OPLL for frequency synthesis [57]. Here, an external stable microresonator is used as the reference source, and an SGDBR-PIC and OPLL circuit similar to that in Fig. 7 is employed to select and lock to a microresonator line, providing a high-level stable output at the precise frequency of the reference resonator plus the tunable RF offset. What is particularly interesting is that the SGDBR can tune to a given line, lock to it, and provide a stable output within 200 ns, as shown by the repetitive switching back and forth between two SGDBR laser open loop frequencies some 5.72 nm or 720 GHz apart. The RF synthesizer is tuned to provide the difference necessary to get within locking range, here 2.5 GHz. The microresonator mode spacing in this wavelength range is ~25.7 GHz, suggesting that the SGDBR laser is jumping across 28 resonator modes to relock in this experiment. The mode spacing varies slightly due to dispersion.

B. High Power InP SoC-PICs for Free-Space Optical Links

The high data rates and low cost, size, weight and power (CSWaP) offered by SoC-PICs makes them desirable for free space laser communications to provide connectivity for intersatellite and deep-space links [58]. Figure 10(a) illustrates an InP-based PIC transmitter for free space optical communications [59]. The transmitter consists of a SGDBR

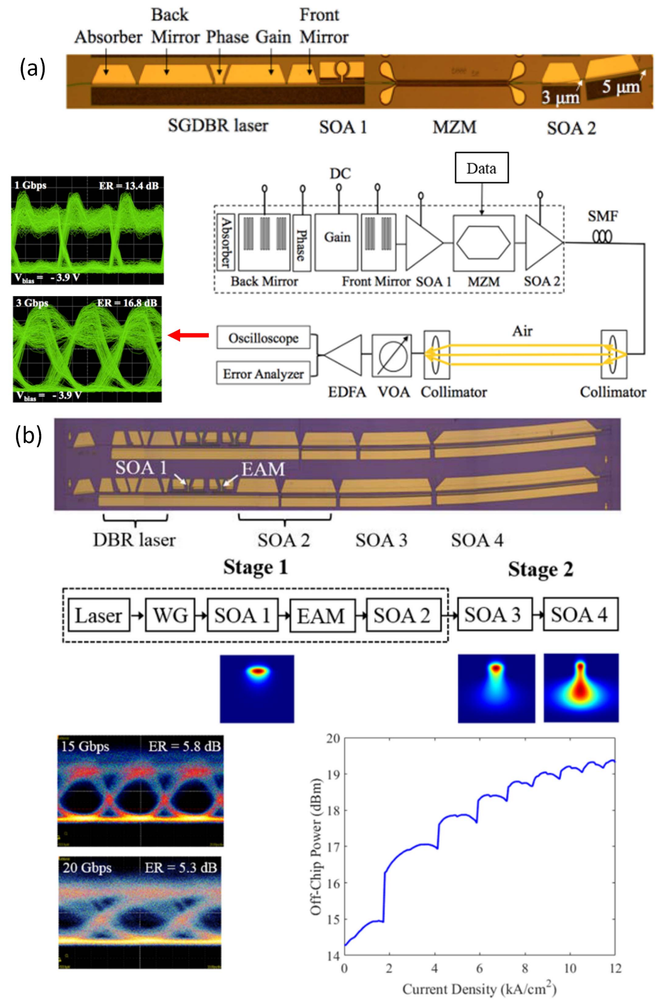

Fig. 10. Free-space link experiments. (a) SoC-PIC photo, schematic and data from free-space link experiment. Adapted with permission from [59]; (b) demonstration of high-power PIC with expanded mode SOA, and output power up to 19 dBm and 20 Gb/s data rate. Adapted with permission from [60].

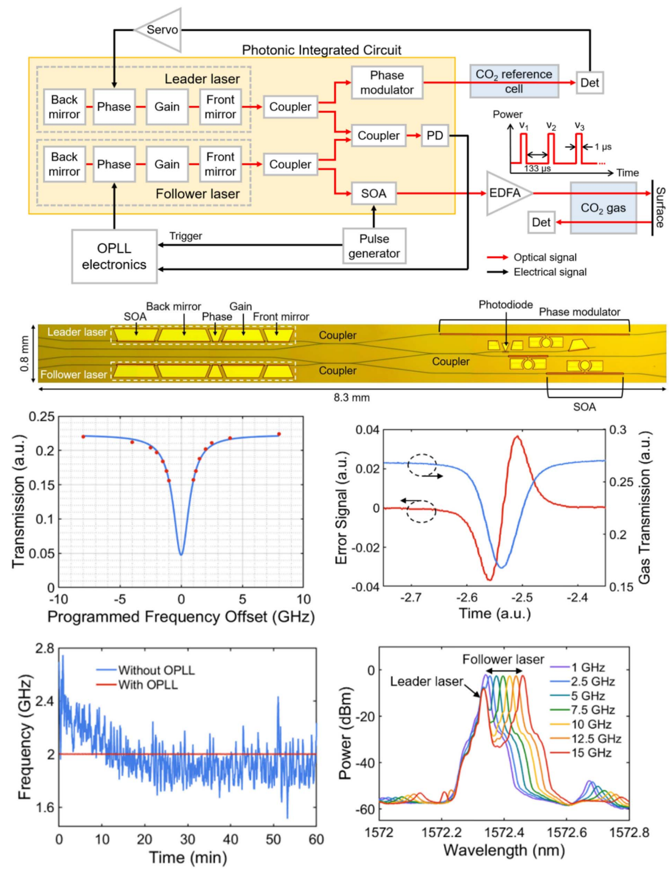

Fig. 11. CO_2 sensor SoC-PIC photo, schematic/electronics, and results. The first laser (leader) is frequency locked to a reference CO_2 cell, and a second laser (follower) is successively offset phase locked to the leader to trace out the CO_2 gas absorption in the atmosphere within a LIDAR path. Adapted with permission from [61].

laser, high-speed SOA, MZM, and a high-power output booster SOA. The SGDBR laser tunes from 1521 to 1565 nm with >45 dB side mode suppression ratio (SMSR). This InP PIC was incorporated into a free space optical link to demonstrate the potential for low size, weight and power demonstrating its suitability for deployment on small aircraft or satellites. Error-free operation was achieved at 3 Gbps for an equivalent link length of 180 m (up to 300 m with forward error correction) with a maximum output power of 14.5 dBm (28 mW).

A modified transmitter design for higher power operation is shown in Fig. 10(b) [60]. This PIC uses a quantum well intermixing (QWI) platform, rather than offset quantum well (OQW), for active-passive integration. The QWI transmitter consists of a DBR laser, high-speed SOA, an EAM, and an output SOA. The epitaxial structure and waveguide were modified in this design to achieve a lower confinement factor in the SOA for higher output saturation power. The measured off-chip power is 19.5 dBm (90 mW), and a data rate of 20 Gbps was demonstrated.

C. Remote Gas Sensing LIDAR

SoC-PICs for LIDAR have also been demonstrated recently at UCSB for gas sensing applications. The system shown in Figure 11 is for detection of atmospheric carbon dioxide (CO_2) using integrated path differential absorption LIDAR as described in [61]. Again, this system takes advantage of the low CSWaP offered by SoC-PICs to make it suitable for deployment on satellites. The InP PIC contains two SGDBR lasers, a leader and follower. The leader laser is locked to the center of the 1572.335 nm CO_2 absorption line, using the CO_2 reference cell as shown in the upper part of the system diagram. The frequency stability of the leader laser is improved 236-fold when locked to the gas cell, compared to free-running. The follower laser is tuned ±15 GHz around the 1572.335 nm absorption line and offset locked to the leader with an OPLL. The SOA is used to generate pulses at each frequency step to sample the CO_2 absorption line.

D. Widely Tunable 1030 nm SGDBR Laser PIC

The widely-tunable SoC-PICs discussed so far have all been demonstrated on InP and as such are restricted to wavelengths in the 1300-1600 nm range. Further development is being pursued, however, to develop widely-tunable PICs for

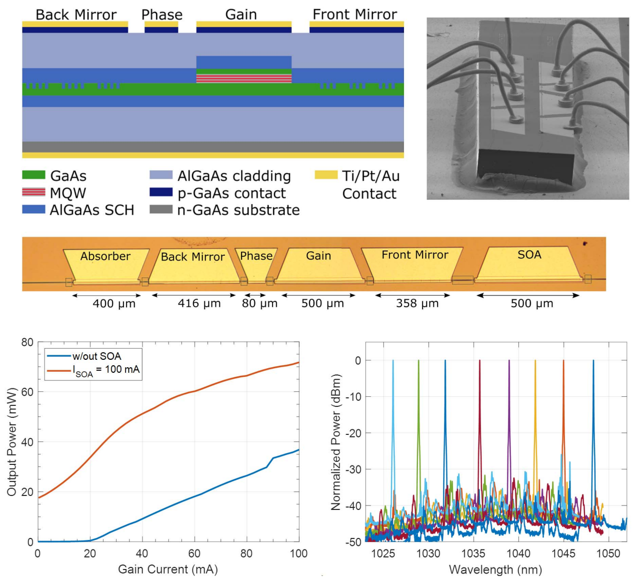

Fig. 12. Widely tunable SGDBR laser on GaAs, demonstrating 22 nm of continuous tuning around 1030 nm and up to 75 mW output power with amplification. For more information see [64] and [65].

applications in other spectral regions. Here, recent work on the development of widely-tunable SGDBR lasers on gallium arsenide (GaAs) for 1030 nm LIDAR is demonstrated. The spectral region near 1 μm is of particular interest for airborne terrain mapping LIDAR systems [62], owing to relatively low atmospheric absorption and the existence of high-quality detectors at this wavelength [63]. As with the remote gas sensing LIDAR system discussed above, the reduction of CSWaP offered by a SoC-PIC, compared to a system with commercial off-the-shelf (CoTS) components, is of critical importance for airborne topographical LIDAR.

A widely tunable SGDBR laser and integrated SOA on GaAs with a center wavelength near 1030 nm has been fabricated at UCSB and is shown in Fig. 12. This device was fabricated on an OQW PIC platform for active-passive integration, adapted for the GaAs material system [64]. The standalone SGDBR laser demonstrates 22.3 nm of continuous wavelength tuning with 30 dB SMSR (bottom right of Fig. 12) and 35 mW of output power [65]. With the addition of an integrated SOA, the output power can be increased to greater than 75 mW (bottom left of Fig. 12). The demonstration of a widely tunable laser and integrated SOA on GaAs lays a path for further development of more complex SoC-PICs in the 1 μm spectral range, analogous to those on InP for C-band applications.

V. Conclusion

Advanced materials growth and processing technologies together with highly-developed device designs have enabled complex PICs on III-Vs that can perform several photonic system functions. Many of these SoC-PICs can provide significant savings in cost, size, weight, and power compared to discrete implementations, even eliminating the need for some components, or required electronics, in many cases.

In this paper we have focused on the development, and benefits of widely-tunable lasers in such SoC-PICs. The use of such lasers can provide wavelength agility for broadband WDM communication systems, wavelength stability by phase locking to any of a number of references, and wavelength sweeping for a variety of sensing applications, such as in LIDAR or optical beam control.

Acknowledgment

A portion of this work was carried out at the University of California at Santa Barbara (UCSB) Nanofabrication Facility. For this special issue, the authors would like to acknowledge the many contributions of Prof. Daniel Dapkus to their field, especially his seminal MOCVD advances, which they depend upon for all of their PICs. Larry A. Coldren would like to specifically acknowledge him for growing their first SGDBR samples, which launched much of this work. The authors would also like to acknowledge contributions to the recent UCSB work reported by Shamsul Arafin, Hongwei Zhao, Sergio Pinna, Joseph Fridlander, Victoria Rosborough, Fengqiao Sang, and Bowen Song.

References

[1] F. Kish *et al.*, "System-on-chip photonic integrated circuits," *IEEE J. Sel. Topics Quantum Electron.*, vol. 24, no. 1, pp. 1–20, Feb. 2018.
[2] K. A. Williaams *et al.*, "InP photonic circuits using generic integration," *Photon. Res.*, vol. 3, no. 5, pp. 60–67, 2015.
[3] Y. Tohmori, Y. Suematsu, H. Tsushima, and S. Arai, "Wavelength tuning of GaInAsP/InP integrated laser with butt-jointed built-in distributed Bragg reflector," *Electron. Lett.*, vol. 19, no. 17, pp. 656–657, 1983.
[4] M. Zirngibl, C. H. Joyner, and L. W. Stulz, "WDM receiver by monolithic integration of an optical preamplifier, waveguide grating router and photodiode array," *Electron. Lett.*, vol. 31, no. 7, pp. 581–582, 1995.
[5] K. Kudo *et al.*, "1.55-μm wavelength-selectable microarray DFB-LD's with monolithically integrated MMI combiner, SOA, and EA-modulator," *IEEE Photon. Technol. Lett.*, vol. 12, no. 3, pp. 242–244, Mar. 2000.
[6] M. C. Larson *et al.*, "Narrow linewidth sampled-grating distributed Bragg reflector laser with enhanced side-mode suppression," in *Conf. Opt. Fiber Commun. Tech. Dig. Ser.*, Jun. 2015, pp. 2–4.
[7] G. Gilardi and M. K. Smit, "Generic InP-based integration technology: Present and prospects (invited review)," *Prog. Electromagn. Res.*, vol. 147, pp. 23–35, 2014.
[8] L. A. Coldren *et al.*, "High performance InP-based photonic ICs—A tutorial," *J. Lightw. Technol.*, vol. 29, no. 4, pp. 554–570, Feb. 15, 2011.
[9] M. Smit, K. Williams, and J. van der Tol, "Past, present, and future of InP-based photonic integration," *APL Photon.*, vol. 4, no. 5, May 2019, Art. no. 050901, doi: 10.1063/1.5087862.
[10] G. E. Hoefler *et al.*, "Foundry development of system-on-chip InP-based photonic integrated circuits," *IEEE J. Sel. Topics Quantum Electron.*, vol. 25, no. 5, pp. 1–17, Sep. 2019.
[11] M. Blaicher *et al.*, "Hybrid multi-chip assembly of optical communication engines by *in situ* 3D nano-lithography," *Light, Sci. Appl.*, vol. 9, no. 1, pp. 1–11, Dec. 2020, doi: 10.1038/s41377-020-0272-5.
[12] J. Zhang *et al.*, "III-V-on-Si photonic integrated circuits realized using micro-transfer-printing," *APL Photon.*, vol. 4, no. 11, Nov. 2019, Art. no. 110803, doi: 10.1063/1.5120004.
[13] B. Song, C. Stagarescu, S. Ristic, A. Behfar, and J. Klamkin, "3D integrated hybrid silicon laser," *Opt. Exp.*, vol. 24, no. 10, pp. 10435–10444, 2016.
[14] Y. Wan *et al.*, "Low threshold quantum dot lasers directly grown on unpatterned quasi-nominal (001) Si," *IEEE J. Sel. Topics Quantum Electron.*, vol. 26, no. 2, pp. 1–9, Mar. 2020.
[15] C. Xiang *et al.*, "High-performance silicon photonics using heterogeneous integration," *IEEE J. Sel. Topics Quantum Electron.*, vol. 28, no. 3, pp. 1–15, May 2022.

[16] N. Margalit, C. Xiang, S. M. Bowers, A. Bjorlin, R. Blum, and J. E. Bowers, "Perspective on the future of silicon photonics and electronics," *Appl. Phys. Lett.*, vol. 118, no. 22, May 2021, Art. no. 220501.

[17] S. E. Miller, "Integrated optics: An introduction," *Bell Syst. Tech. J.*, vol. 48, no. 7, pp. 2059–2069, Sep. 1969.

[18] D. B. Keck, R. D. Maurer, and P. C. Schultz, "On the ultimate lower limit of attenuation in glass optical waveguides," *Appl. Phys. Lett.*, vol. 22, no. 7, pp. 307–309, Apr. 1973.

[19] T. L. Koch *et al.*, "GaInAs/GaInAsP multiple-quantum-well integrated heterodyne receiver," *Electron. Lett.*, vol. 25, no. 24, pp. 1621–1623, 1989.

[20] R. C. Alferness and A. Glass, "Bell labs technology trends & developments," *Bell Labs Tech. J.*, vol. 2, no. 2, pp. 1–15, 1988.

[21] K. Murata, S. Mito, and I. Kobayashi, "Over 720 GHz (5.8 nm) frequency tuning by a 1.5 μm DBR laser with phase and Bragg wavelength control regions," *Electron. Lett.*, vol. 23, no. 8, pp. 403–405, 1987.

[22] T. L. Koch, U. Koren, and B. I. Miller, "High performance tunable 1.5 μm InGaAs/InGaAsP multiple quantum well distributed Bragg reflector lasers," *Appl. Phys. Lett.*, vol. 53, no. 12, pp. 1036–1038, 1988.

[23] R. J. Mears, L. Reekie, I. M. Jauncey, and D. N. Payne, "Low-noise erbium-doped fibre amplifier operating at 1.54 μm," *Electron. Lett.*, vol. 23, no. 19, pp. 1026–1028, 1987.

[24] L. A. Coldren, B. I. Miller, K. Iga, and J. A. Rentschler, "Monolithic two-section GaInAsP/InP active-optical-resonator devices formed by reactive ion etching," *Appl. Phys. Lett.*, vol. 38, no. 5, pp. 315–317, Mar. 1981.

[25] L. A. Coldren, "Multi-section tunable laser with differing multi-element mirrors," U.S. Patent 4 896 325, Jan. 23, 1990.

[26] V. Jayaraman, Z.-M. Chuang, and L. A. Coldren, "Theory, design, and performance of extended tuning range semiconductor lasers with sampled gratings," *IEEE J. Quantum Electron.*, vol. 29, no. 6, pp. 1824–1834, Jun. 1993.

[27] V. Jayaraman, A. Mathur, L. A. Coldren, and P. D. Dapkus, "Very wide tuning range in a sampled grating DBR laser," in *Proc. 13th IEEE Int. Semiconductor Laser Conf.* Takamatsu, Japan, 1992, Paper PD-11.

[28] T. L. Koch, "OFC tutorial: III–V and silicon photonic integrated circuit technologies," in *Proc. OFC/NFOEC*, 2012, pp. 1–45.

[29] Y. A. Akulova *et al.*, "Widely tunable electroabsorption-modulated sampled-grating DBR laser transmitter," *IEEE J. Sel. Top. Quantum Electron.*, vol. 8, no. 6, pp. 1349–1357, Nov./Dec. 2002.

[30] Y. A. Akulova *et al.*, "10 Gb/s Mach–Zehnder modulator integrated with widely-tunable sampled grating DBR laser," in *Proc. OSA Trends Opt. Photon. Ser.*, vol. 95, 2004, pp. 395–397.

[31] C. Coldren *et al.*, "Reliability of widely-tunable SGDBR lasers suitable for deployment in agile networks," in *OFC Tech. Dig.*, vol. 1, 2003, pp. 73–75.

[32] *Tunable Multiprotocal XFP Optical Transceiver—1550 nm for up to 80 km Reach JXP Series, P/N JXP01TMAC1CX5*, Lumentum, San Jose, CA, USA, 2015.

[33] Lumentum Operations LLC. (Mar. 2018).*Lumentum to acquire OCLARO for 1.8B in cash and stock*. San Jose, CA, Accessed: Apr. 26, 2022. [Online]. Available: https://www.lumentum.com/en/media-room/news-releases/lumentum-acquire-oclaro-18b-cash-and-stock

[34] R. C. Alferness *et al.*, "Broadly tunable InGaAsP/InP laser based on a vertical coupler filter with 57-nm tuning range," *Appl. Phys. Lett.*, vol. 60, no. 26, pp. 3209–3211, 1992.

[35] M. Öberg, S. Nilsson, K. Streubel, J. Wallin, L. Bäckbom, and T. Klinga, "74 nm wavelength tuning range of an InGaAsP/InP vertical grating assisted codirectional coupler laser with rear sampled grating reflector," *IEEE Photon. Technol. Lett.*, vol. 5, no. 7, pp. 735–738, Jul. 1993.

[36] L. A. Coldren, "Monolithic tunable diode lasers," *IEEE J. Sel. Topics Quantum Electron.*, vol. 6, no. 6, pp. 988–999, Nov./Dec. 2000.

[37] R.-J. Essiambre, G. Kramer, P. J. Winzer, G. J. Foschini, and B. Goebel, "Capacity limits of optical fiber networks," *J. Lightw. Technol.*, vol. 28, no. 4, pp. 662–701, Feb. 15, 2010.

[38] M. G. Young *et al.*, "Six wavelength laser array with integrated amplifier and modulator," *Electron. Lett.*, vol. 31, no. 21, pp. 1835–1836, Oct. 1995.

[39] H. M. Hatakeyama *et al.*, "Wavelength-selectable microarray light sources for S-, C-, and L-band WDM systems," *IEEE Photon. Technol. Lett.*, vol. 15, no. 7, pp. 903–905, Jul. 2003.

[40] N. Kikuchi *et al.*, "Monolithically integrated 64-channel WDM wavelength-selective receiver," *Electron. Lett.*, vol. 39, no. 3, pp. 312–314, 2003.

[41] J. Heanue, E. Vail, M. Sherback, and B. Pezeshki, "Widely tunable laser module using DFB array and MEMs selection with internal wavelength locker," in *Proc. OFC*, vol. 1, 2003, pp. 21–22.

[42] M. Smit *et al.*, "A generic foundry model for InP-based photonic ICs," in *Proc. Opt. InfoBase Conf. Paper*, 2012, pp. 2–4.

[43] R. Nagarajan *et al.*, "Large-scale photonic integrated circuits," *IEEE J. Sel. Top. Quantum Electron.*, vol. 11, no. 1, pp. 50–65, Jan./Feb. 2005.

[44] M. M. Dummer, J. Klamkin, A. Tauke-Pedretti, and L. A. Coldren, "A bit-rate-transparent monolithically integrated wavelength converter," in *Proc. Eur. Conf. Opt. Commun. (ECOC)*, vol. 4, Sep. 2008, pp. 77–80.

[45] S. C. Nicholes, M. L. Mašanović, B. Jevremović, E. Lively, L. A. Coldren, and D. J. Blumenthal, "An 8×8 InP monolithic tunable optical router (MOTOR) packet forwarding chip," *J. Lightw. Technol.*, vol. 28, no. 4, pp. 641–650, Feb. 15, 2010.

[46] M. Lu *et al.*, "An integrated 40 Gbit/s optical Costas receiver," *J. Lightw. Technol.*, vol. 31, no. 13, pp. 2244–2253, Jul. 1, 2013.

[47] H. C. Park *et al.*, "40 Gbit/s coherent optical receiver using a Costas loop," *Opt. Exp.*, vol. 20, no. 26, pp. 197–203, 2012.

[48] W. Guo, P. R. A. Binetti, M. L. Masanovic, L. A. Johansson, and L. A. Coldren, "Large-scale InP photonic integrated circuit packaged with ball grid array for 2D optical beam steering," in *Proc. IEEE Photon. Conf. (IPC)*, Sep. 2013, pp. 651–652.

[49] M. Lauermann *et al.*, "Multi-channel, widely-tunable coherent transmitter and receiver PICs operating at 88 Gbaud/16-QAM," in *Proc. Opt. Fiber Commun. Conf. Exhib. (OFC)*, vol. 1, 2017, pp. 8–10.

[50] A. Tauke-Pedretti *et al.*, "Separate absorption and modulation Mach–Zehnder wavelength converter," *J. Lightw. Technol.*, vol. 26, no. 1, pp. 91–98, Jan. 1, 2008.

[51] V. Lal, M. L. Mašanović, J. A. Summers, G. Fish, and D. J. Blumenthal, "Monolithic wavelength converters for high-speed packet-switched optical networks," *IEEE J. Sel. Top. Quantum Electron.*, vol. 13, no. 1, pp. 49–57, Jan./Feb. 2007.

[52] W. Guo *et al.*, "Two-dimensional optical beam steering with InP-based photonic integrated circuits," *IEEE J. Sel. Topics Quantum Electron.*, vol. 19, no. 4, Jul. 2013, Art. no. 6100212.

[53] M. Lu *et al.*, "A highly integrated optical phase-locked loop with singlesideband frequency sweeping," *CLEO Sci. Innov.*, vol. 20, no. 9, pp. 1090–1092, 2012.

[54] S. Ristic, A. Bhardwaj, M. J. Rodwell, L. A. Coldren, and L. A. Johansson, "An optical phase-locked loop photonic integrated circuit," *J. Lightw. Technol.*, vol. 28, no. 4, pp. 526–538, Feb. 15, 2010.

[55] A. Simsek *et al.*, "Evolution of chip-scale heterodyne optical phase-locked loops toward Watt level power consumption," *J. Lightw. Technol.*, vol. 36, no. 2, pp. 258–264, Jan. 15, 2018.

[56] S. Arafin, A. Simsek, M. Lu, M. J. Rodwell, and L. A. Coldren, "Heterodyne locking of a fully integrated optical phase-locked loop with on-chip modulators," *Opt. Lett.*, vol. 42, no. 19, pp. 3745–3748, 2017.

[57] S. Arafin *et al.*, "Towards chip-scale optical frequency synthesis based on optical heterodyne phase-locked loop," *Opt. Exp.*, vol. 25, no. 2, pp. 681–694, 2017.

[58] H. Hemmati, A. Biswas, and I. B. Djordjevic, "Deep-space optical communications: Future perspectives and applications," *Proc. IEEE*, vol. 99, no. 11, pp. 2020–2039, Nov. 2011.

[59] H. Zhao *et al.*, "Indium phosphide photonic integrated circuits for free space optical links," *IEEE J. Sel. Topics Quantum Electron.*, vol. 24, no. 6, pp. 1–6, Nov. 2018.

[60] H. Zhao *et al.*, "High-power indium phosphide photonic integrated circuits," *IEEE J. Sel. Topics Quantum Electron.*, vol. 25, no. 6, pp. 1–10, Nov. 2019.

[61] J. Fridlander *et al.*, "Dual laser indium phosphide photonic integrated circuit for integrated path differential absorption LiDAR," *IEEE J. Sel. Topics Quantum Electron.*, vol. 28, no. 1, pp. 1–8, Jan. 2022.

[62] A. W. Yu *et al.*, "A 16-beam non-scanning swath mapping laser altimeter instrument," *Proc. SPIE*, vol. 8599, Mar. 2013, Art. no. 85990P.

[63] M. A. Krainak, X. Sun, G. Yang, and W. Lu, "Comparison of linear-mode avalanche photodiode LiDAR receivers for use at one-micron wavelength," *Proc. SPIE*, vol. 7681, Apr. 2010, Art. no. 76810Y.

[64] P. Verrinder *et al.*, "Gallium arsenide photonic integrated circuit platform for tunable laser applications," *IEEE J. Sel. Topics Quantum Electron.*, vol. 28, no. 1, pp. 1–9, Jan. 2022.

[65] P. Verrinder, L. Wang, F. Sang, V. Rosborough, M. Nickerson, G. Yang, et al., "SGDBR tunable laser on gallium arsenide for 1030 nm lidar applications," in*Proc. 27th Int. Semiconductor Laser Conf.* Potsdam, Germany, Oct. 10/14, 2021, Paper no. WA2.2.

Larry A. Coldren (Life Fellow, IEEE) received the B.S. degree in electrical engineering and the B.A. degree in physics from Bucknell University and the M.S. and Ph.D. degrees in electrical engineering from Stanford University in 1969 and 1972, respectively, under the support of Bell Laboratories.

He joined Bell Laboratories in 1968. Following 13 years in the research area with Bell Laboratories, he joined the ECE Department of the University of California at Santa Barbara (UCSB) in 1984. In 1986, he was a Founding Member of the Materials Department. He became the Fred Kavli Professor of optoelectronics and sensors in 1999. From 2009 to 2011, he was the Acting Dean of the College of Engineering, and in 2017, he became a Emeritus Professor and a Distinguished Research Professor. In 1990, he co-founded Optical Concepts, later acquired as Gore Photonics, to develop novel VCSEL technology, and in 1998, he co-founded Agility Communications, later acquired by JDSU (now Lumentum), to develop widely-tunable integrated transmitters and transponders. At UCSB, he has worked on multiple-section widely-tunable lasers and efficient vertical-cavity surface-emitting lasers (VCSELs). He continues to research high-performance InP-based photonic integrated circuits, and high-speed and high-efficiency VCSELs for various applications. He has authored or coauthored over 1000 journals and conference papers, eight book chapters, a widely-used textbook, and 63 issued patents.

Prof. Coldren is a fellow of OSA, IEE, and the National Academy of Inventors as well as a member of the National Academy of Engineering. He was a recipient of the 2004 John Tyndall, the 2009 Aron Kressel, the 2014 David Sarnoff, the 2015 IPRM, and the 2017 Nick Holonyak, Jr., Awards.

Paul A. Verrinder received the B.S. degree in electrical engineering from California State University, Fresno, in 2015, and the M.S. degree in electrical and computer engineering from the University of California at Santa Barbara (UCSB), Santa Barbara, in 2020, where he is currently pursuing the Ph.D. degree with the Electrical and Computer Engineering Department. From 2015 to 2018, he was an Electrical Engineer with NAVAIR, China Lake. His research interests are in integrated photonics for optical communications and LIDAR.

Jonathan Klamkin (Senior Member, IEEE) received the B.S. degree from Cornell University, Ithaca, NY, USA, and the M.S. and Ph.D. degrees from the University of California at Santa Barbara (UCSB), Santa Barbara, CA, USA. From 2008 to 2011, he was a member of the Technical Staff with the Electro-Optical Materials and Devices Group, MIT Lincoln Laboratory, Lexington, MA, USA. From 2011 to 2013, he was an Assistant Professor with the Institute of Communication, Information and Perception Technologies, Scuola Superiore Sant'Anna, Pisa, Italy. From 2013 to 2015, he was an Assistant Professor of electrical and computer engineering (ECE) and materials with Boston University, Boston, MA. In 2015, he joined the ECE Department, University of California at Santa Barbara, where he is currently a Professor and the Director of the UCSB Nanotech. He has authored or coauthored 200 journals and conference papers. He or his group members were the recipient of Best Paper Awards at the 2006 Conference on Optoelectronic and Microelectronic Materials and Devices, the 2007 Microwave Photonics Conference, and the 2017 and 2019 Asia Communications and Photonics Conference. He was the recipient of the NASA Early Career Faculty Award, the DARPA Young Faculty Award, and the DARPA Director's Fellowship.

A Review of Photonic Systems-on-Chip Enabled by Widely Tunable Lasers

Larry A. Coldren, *Life Fellow, IEEE*, Paul A. Verrinder, and Jonathan Klamkin, *Senior Member, IEEE*

***Abstract*— Photonic Integrated Circuits (PICs) on indium phosphide have matured significantly over the past couple of decades and have found use in many system applications. Some PIC efforts on other group III-V substrates have also been initiated. In numerous cases, the usefulness of these PICs is because of the reduction in size, weight, and power they provide, but in many cases also because of the higher performance made possible by the improved relative phase stability among optical paths as well as the reduction of inter-element coupling losses. In this paper, as part of this special issue in tribute to Prof. Daniel Dapkus, we focus on monolithic PICs that provide a system function, especially those that incorporate and build on widely-tunable laser technology as a key element. Some of the early widely-tunable laser work is reviewed, and a selection of past system-on-a-chip developments is presented as background. Then, more recent system-on-a-chip advances performed by the author's groups are reviewed in more detail. Key advances are highlighted.**

***Index Terms*— Optoelectronics, photonics, photonic-integrated-circuits, semiconductor lasers, tunable lasers.**

I. Introduction

THIS paper reviews recent research at the University of California Santa Barbara (UCSB) on relatively complex photonic integrated circuits (PICs) based on III-V materials that perform a useful optical system function. These PICs, denoted as System-on-Chip (SoC)-PICs [1], are generally closely packaged, or co-packaged, with control or complementary functional electronics. Similar work has also been carried out at other academic and industrial laboratories, and some of this work has been summarized in prior reviews [1]–[10].

The focus of this paper is on monolithic SoC-PICs on native III-V substrates, including both indium phosphide (InP) and gallium arsenide (GaAs), which incorporate tunable lasers as a key component. It is, however, worth noting that considerable work has also been carried out in recent years in the area of hybrid and heterogeneous integration of III-V materials on silicon. Approaches include, co-packaging, wafer bonding, micro-transfer printing, as well as direct growth of III-V materials on silicon [11]–[14]. These technologies were developed primarily for datacom applications [15], [16].

The UCSB work has especially highlighted the benefit of using widely-tunable lasers as an integral part of most of their SoC-PICs. As will be discussed in Section II below, past examples of these SoC-PICs have included: optical transmitters, receivers, all-optical switches, coherent receivers, vector transmitters, and LIDAR transceivers. Incorporation of widely-tunable lasers has provided full C-band operation, and in the case of LIDAR, wide beam sweep angles. The background in Section II will begin with some discussion of the origins of widely-tunable lasers.

In Section III, our recent work will show improved coherent receivers with lower power dissipation and noise, better SoC-PICs for RF-over-fiber transmission, very rapid switching and phase locking for agile frequency synthesis, high-power optical transmitters for free-space links, a SoC-PIC and electronics for gas absorption sensing using frequency-swept LIDAR, and the demonstration of a widely-tunable laser PIC on gallium arsenide for the 1 μm wavelength region.

II. Background

A. Early PICs on III-Vs

A history of III-V PICs has been recently reported by Kish, *et al.* in [1]. As outlined therein, the concept and promise of PICs was first suggested by Miller in 1969 [17]. Low-loss fiber in the 1300-1550 nm wavelength range soon followed in the early 1970s [18] leading to intensive research on quaternary indium gallium arsenide phosphide (InGaAsP) and related materials on InP that have bandgap wavelengths in this range. By the late-1970s many of the desired active and passive components—lasers, lasers with gratings, passive waveguide couplers, modulators, detectors, etc.—had been demonstrated [1].

Early in the 1980s, fiber optic links had been introduced at 1300 nm, but even at the modest data rates used then, links were limited in reach to 30-40 km by the available signal-to-noise ratio. Expensive electronic repeaters were required to regenerate the signals at that point. To avoid this optical-electrical-optical (OEO) conversion, research on coherent technologies was initiated to extend the reach to approximately 80 km by leveraging the increased sensitivity afforded by coherent detection. A relatively coarse wavelength division multiplexing (WDM) was also being employed, and coherent could assist with the demultiplexing. Coherent and WDM

Manuscript received 29 November 2021; revised 16 March 2022; accepted 4 April 2022. Date of publication 18 April 2022; date of current version 28 July 2022. This work was supported in part by the National Aeronautics and Space Administration (NASA) Research Opportunities in Space and Earth Sciences (ROSES) Advanced Component Technology Program and in part by the NASA Earth Science and Technology Office (ESTO) Advanced Component Technology Program. *(Corresponding author: Larry A. Coldren.)*

The authors are with the Department of Electrical and Computer Engineering, University of California at Santa Barbara, Santa Barbara, CA 93106 USA (e-mail: coldren@ucsb.edu; pverrinder@ucsb.edu; klamkin@ece.ucsb.edu).

Color versions of one or more figures in this article are available at https://doi.org/10.1109/JQE.2022.3168041.

Digital Object Identifier 10.1109/JQE.2022.3168041

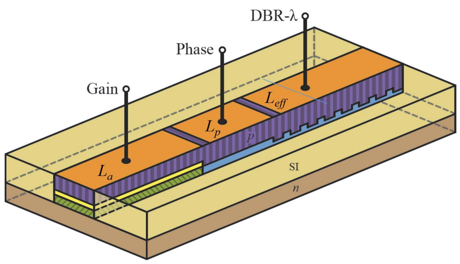

Fig. 1. Three-section tunable laser with one DBR and one cleaved facet mirror. Phase and DBR sections are passive (no gain), but tunable with current. The gain section provides gain with current injection, but little tuning. For more information see [21], [22].

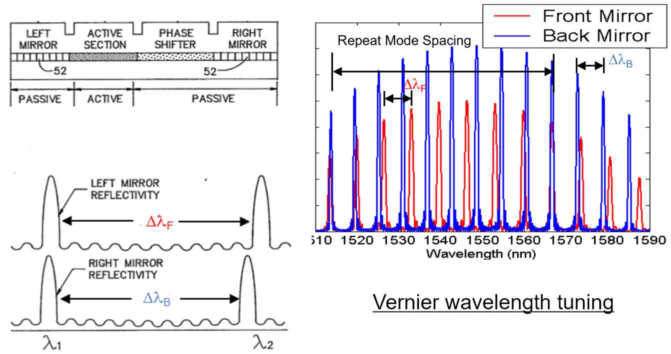

Fig. 2. Four-section widely-tunable laser. (Left) Excerpts from USP #4,896,325 illustrating basic structure and Vernier concept; (right) simulated mirror reflection spectra, expanding to many mirror reflection peaks, and showing eventual repeated overlaps.

stimulated some device researchers to begin work on tunable lasers, which could serve both as universal sources for WDM transmitters and tunable local oscillator (LO) sources that could be phase locked to the incoming signal in a coherent receiver [19], [20].

Researchers at the Tokyo Institute of Technology led by Prof. Suematsu were some of the first to focus on 1550 nm because optical fiber should ultimately have the lowest loss at this wavelength. They also realized that lasers should be tunable to operate as a WDM or coherent source, and they should have grating mirrors to be integrable with other passive waveguides and devices. They demonstrated such devices in the early 1980s [3].

By the late 1980s, relatively mature three-section DBR tunable lasers had been developed by several companies and universities [21], [22]. As shown in Fig. 1, these consisted of an active gain section, a passive phase tuner, and a passive Distributed-Bragg-Reflector (DBR) mirror, all connected to separate electrical sources. The active gain section contains gain material with a bandgap near the lasing wavelength in its *pn* junction, and the passive sections have higher bandgap material in their *pn* junctions, which change their index of refraction when current is injected. With current injected into the DBR, the narrow band over which it reflects is shifted in wavelength in proportion to the index shift. The optical cavity modes do not shift as much, so current must also be applied to the phase section to shift the cavity modes. In practice, approximately 6-7 nm of wavelength shift is possible at 1550 nm.

By the late 1980s coherent had still not been widely adopted. Higher data rates, denser WDM, as well as simply using more parallel fibers had been satisfying the increased demand, which was still due to a somewhat slowly increasing demand for voice, not data; the disruptive data crossover was not to occur until around 2000. By the late 1980s, research on the erbium-doped fiber amplifier (EDFA) was also beginning to show promise [23]. With the EDFA, OEO repeaters were no longer necessary and new links designed for the mid-1990s and beyond would no longer use OEO repeaters only for signal regeneration for modest distances. Work on coherent subsequently slowed.

B. Widely-Tunable Lasers

The EDFA enabled WDM over approximately 40 nm of bandwidth at 1550 nm in what was to be called the center or C-band. So, those researchers working on tunable lasers immediately began to search for concepts to make widely-tunable lasers, ones that could encompass the entire C-band.

There were a few ideas already being considered. For example, some of the early tunable laser work used coupled cavities, and these made use of Vernier tuning between the cavity modes of the two different length cavities to select a single mode [24]. However, these never led to a widely-tunable result, generally because the cavity modes were too close together. A relatively simple solution came in 1988 with the invention of the four-section tunable laser with two ‘differing multi-element mirrors’ [25], as described in Fig. 2.

By using periodically blanked, periodically modulated, or ‘sampled’ gratings, the reflection spectra of the gratings, instead of being a single sharp peak, are broken into a number of image peaks forming reflection combs. This is the so-called Sampled-Grating DBR, or SGDBR. If the two gratings are sampled with a different period, the period of the two reflection combs are different, but the separation of the reflection peaks can be large (∼6-7 nm), and the separation difference can be tailorable (∼1 nm). Thus, there is only one net reflection maximum for the laser (product of the two mirrors), and the repeat between these can be ∼40 nm for single mode operation. By shifting both mirrors together, and then shifting one relative to the other slightly to select another pair of mirror maxima, and again repeating the shift together, it is possible to cover the full 40 nm with a single net maximum without missing any wavelengths [26].

Figure 3 shows the first results with the SGDBR laser in 1992 [27]. Although it did not include a phase tuner for fine tuning, it did illustrate the potential of the design with a total discontinuous tuning range of 57 nm and good single mode behavior over most of that range. Besides showing the fundamental attributes of the design, it should be noted that the material was grown by Prof. Dapkus’ group, illustrating one additional element of his influence on our field. Also, on this subject, we should mention that most of the early work at UCSB was supported by metalorganic chemical vapor deposition (MOCVD) growths performed by the group of Prof. DenBaars, an alumnus of Prof. Dapkus’ research group.

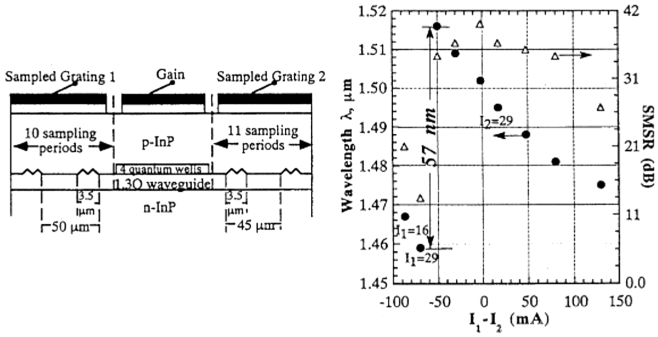

Fig. 3. First demonstration of wide range discontinuous tuning by a SGDBR laser. Adapted with permission from [27].

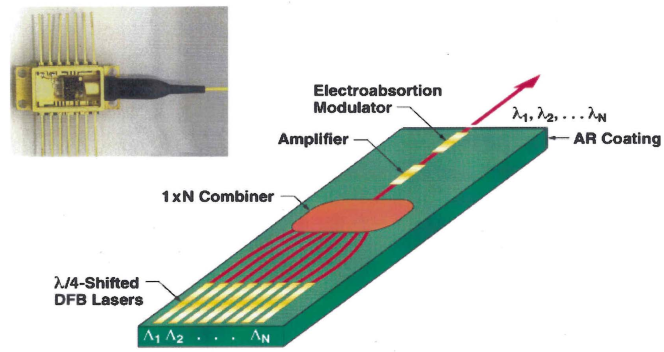

Fig. 5. DFB selectable-array PIC. Adapted with permission from [38].

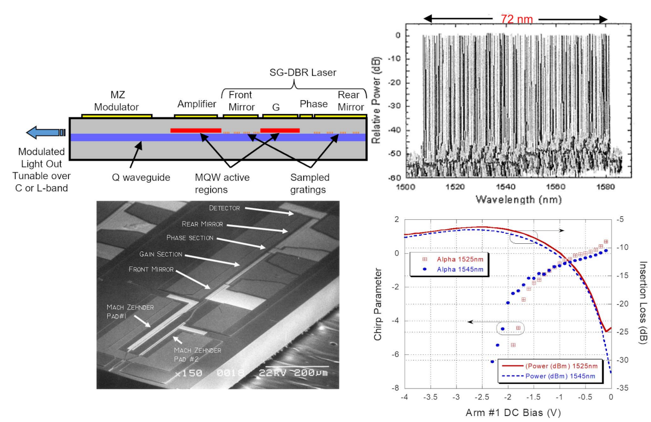

Fig. 4. SGDBR integrated with SOA and MZM schematic together with tuning results, a photograph, and modulator chirp vs. DC bias. For more information see [23] and [24].

The SGDBR design was to become one of the most successful of the options for widely-tunable lasers [28], perhaps the principal reason being that it was no more complex to manufacture than the three-section DBR illustrated in Fig. 1. The additional challenge was in the tuning control, and even that was only marginally more difficult. Following UCSB research, a company was formed, Agility Communications, to develop the concept into a product in 1998. This company also productized more complex PICs that incorporated SGDBRs with monitoring photodetectors, semiconductor optical amplifiers (SOAs), and modulators, either of the electroabsorption (EAM) [29] or Mach-Zehnder (MZM) [30] type.

Figure 4 shows the first UCSB prototype of the SGDBR-SOA-MZM along with chirp results reported in 2002 [23]. Also shown is a wavelength tuning spectrum of 72 nm from an earlier publication in 2000 [24], [25]. The output power at this tuning width was compromised to be ~1 mW, so practical devices were later designed for ~40 nm of tuning, which then allowed 40 mW in fiber reported by Agility in 2003 [31].

Agility was acquired by a more established optical components company in 2005, and many millions of these devices were sold into optical systems products that are still in use [32]. Analogous designs using ‘differing multi-element mirrors’ also appeared by other companies in the early 2000s, and following some patent litigation, they were licensed to produce products [33].

Another early example stemmed from work on directional couplers between different waveguides. It was known that waveguides with slightly different effective indexes could be coupled if a coarse grating was added to one of them to provide the difference in propagation constants, or the phase matching. But, since this grating is fixed, and the waveguide propagation constants are proportional to frequency, phase matching is satisfied only over a limited bandwidth. However, this band can be tuned over a relatively large range by changing the index of one of the waveguides slightly; this is so because the difference between the waveguide indexes is small, and it is the *ratio* of the index change in one guide to this *difference* between the two waveguide indexes that counts. This concept was investigated by several research groups in the 1990s [34], [35], and eventually a company, Altitune, developed it into a product. However, following an acquisition, the acquiring company decided to abandon the concept.

There were a number of other examples of widely-tunable laser concepts developed in the late 1990s to early 2000s [36], mainly in response to the ‘telecom bubble’ that resulted from the realization that the rapidly increasing data bandwidth demand curve was overtaking the slowly increasing voice curve. But as dense WDM systems at higher data rates became available, this demand appeared to be satisfied, at least for a few years—perhaps just long enough to burst the bubble [37]. In any event, a couple of the widely-tunable solutions survived and that seemed to be sufficient.

Another concept not mentioned above, but very compelling to many at this time, was a DFB ‘selectable-array’ PIC, illustrated in Fig. 5. It typically consisted of 8-12 DFB lasers of slightly different wavelength that covered most of the C-band, and these could be tuned thermally by a few nanometers to fill in the gaps [38], [39]. These were all coupled by an MMI coupler into a single waveguide that incorporated an SOA, to compensate the 1/N coupling loss, as well as a possible integrated modulator.

This design was especially popular in Japan, because it seems many companies there were somewhat skeptical about the reliability and stability of the widely-tunable types discussed above [39]. Although the DFB selectable-array is not technically a widely-tunable laser, it does provide the same

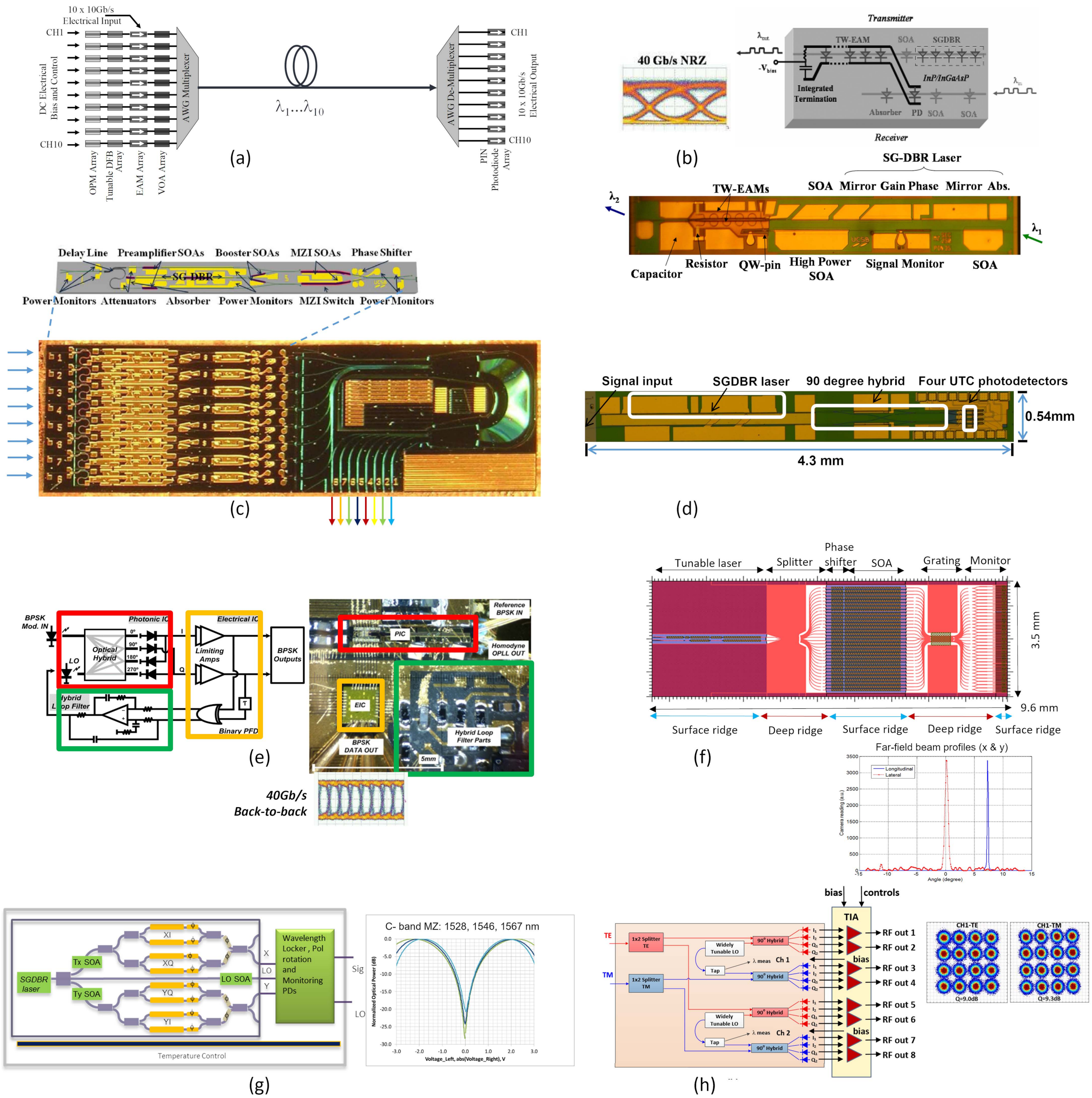

Fig. 6. Sampling of SoC-PIC results from 2004 to 2017. (a) Schematics of 10 × 10 Gb/s DFB/EAM integrated with AWG-MUX transmitter PIC and AWG-De-MUX integrated with 10 PIN PD array receiver PIC. Courtesy: Infinera; for more information see [43]; (b) full C-band wavelength-converter/transceiver PIC—SOA-PD input stage and SGDBR-Traveling-wave EAM output stage. Adapted with permission from [44]; (c) 8 × 8 all-optical packet switch PIC with 8 non-linear MZM wavelength converters integrated with an 8 × 8 AWGR. Adapted with permission from [45]; (d) coherent receiver PIC with high-power, widely-tunable SGDBR-LO, SOA, hybrid, and 4-high-bandwidth PDs. Adapted with permission from [46]; (e) Costa's loop phase-locked C-band coherent receiver. Adapted with permission from [47]; (f) 2-D LIDAR PIC with 32 × 120 resolution from 32 surface-emitting waveguides and tunable laser. Adapted with permission from [48]; (g) C-band vector transmitter PIC with supplemental LO output. Courtesy: Lumentum; for more information see [6]; (h) 2-Channel Rx PIC and TIA architecture and recovered constellations at 16 QAM for both polarizations @88 Gbaud. Courtesy: Infinera; for more information see [49].

functionality. Other 'selectable-array' types were also explored during the early 2000s [40]–[42].

III. System-on-Chip Demonstrations (2004-2017)

Figure 6 shows a sampling of SoC-PIC examples from the period 2004-2017.

The examples of Fig. 6 illustrate that SoC-PICs have provided many different functionalities and that significant savings in size, weight, and power have been demonstrated by integration. For example, as discussed in [1], the transmitter PIC in Fig. 6(a) comprises 10 transmitter channels that each include an optical power monitor, a DFB laser of a unique wavelength, an EAM, and a variable optical attenuator (VOA) (or SOA), all combined by an arrayed-waveguide grating (AWG) multiplexer. This is co-packaged with a 10-channel analog application specific integrated circuit (ASIC) modulator driver chip and a single thermoelectric cooler (TEC). The co-packaging with a single driver chip and a single TEC enables considerable power savings. A comparable description is provided for the receiver chip in [1], [43].

The discussion is somewhat similar for most of the SoC-PICs in Fig. 6. That is, many photonic elements are combined on a single PIC, the drive or control electronics are co-packaged, and a single TEC is used for the entire PIC. Figure 6(b) shows a data format and rate transparent wavelength converter/regenerator, which only requires DC bias connections, although data monitoring is available [39]. Operation from 5-40 Gb/s was demonstrated, and conversion from any input C-band wavelength to any output C-band wavelength was also confirmed. This SoC-PIC operates somewhat as a transceiver by using the input signal photocurrent from the receiving photodiode to dynamically change the bias on an EAM that follows an on-chip SGDBR laser. A regeneration function is possible by overdriving the EAM. Similar PICs have been constructed with MZMs [50].

Figure 6(c) shows the so-called MOTOR chip [45], which provides all-optical switching between its eight inputs and eight outputs. It operates in the return-to-zero (RZ) format at 40 Gb/s if nonlinear MZI-SOA wavelength converters are used [51]. This restriction is removed if the transceiver type of wavelength converter shown in Fig. 6(b) is employed. The outputs of the wavelength converters are coupled to an arrayed-waveguide-grating-router (AWGR), which sorts them according to their new wavelength to one of the outputs.

Figure 6(d) is a widely-tunable coherent receiver PIC. It includes SOA pre-amplifiers for the incoming signals, an integrated SGDBR-SOA as a high-power LO, a 90-degree hybrid and four uni-traveling-carrier (UTC)-photodiodes, which typically have bandwidths >30 GHz and good power handling capabilities, so that signal plus LO inputs well above the shot-noise level can be used. This receiver can be used with a number of different types of electronics, but it was used primarily in ‘analog’ coherent receivers in our work. For example, in Fig. 6(e), it is shown in the red box, and we have constructed a Costas phase/frequency locking circuit to phase-lock the LO to the carrier of the incoming signal with a wide frequency capture range [46], [47].

Figure 6(f) illustrates a 2-D optical beam-scanner chip that can be used in LIDAR or other direction-specific illumination or communication applications. The output of an SGDBR-SOA is split into 32 separate waveguides and coupled to an optical phased array via 32 phase shifters and SOAs. Light then emits from a weighted-grating surface-emitter region [48]. The angle of emission in the axial direction is varied by the wavelength. The angle in the lateral direction is varied by adjusting the individual phase shifters of the phased array using a particle-swarm optimization [52]. On-chip monitor photodiodes following the emitter array verify the calibration [52].

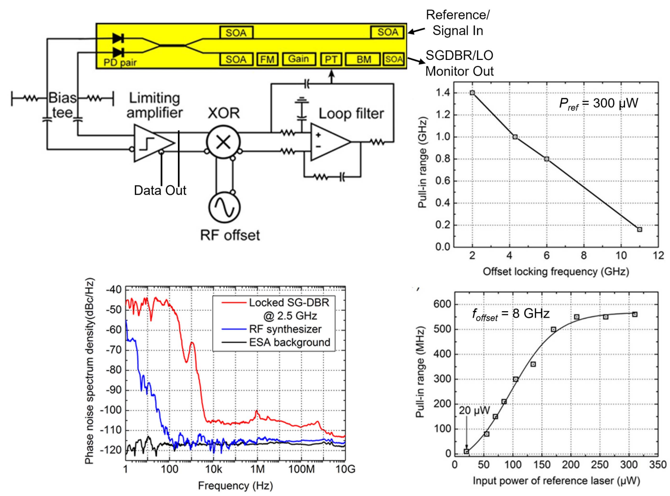

Fig. 7. Heterodyne optical phase locked loop with improved sensitivity and power consumption; schematic, locking frequency pull-in range vs. RF offset and input power of reference, and phase noise spectral density. Adapted with permission from [55].

Figure 6(g) is a schematic of a dual-polarization C-band vector transmitter PIC along with MZM characteristics from Lumentum [6]. This was co-packaged with modulator electronics and a TEC, and it was made available for system vendors. An LO output was also provided for use in a combined transmitter/receiver coherent module [6].

Figure 6(h) is a PIC receiver with transimpedance amplifier (TIA) architecture from Infinera, which uses a 1 × 2 splitter at the PIC input. This is capable of up to 720 Gb/s of input at 88 Gbaud over modest distances [49]. In [1], an analogous architecture is described in which the PIC employs a 1 × 6 splitter at its input to increase the practical data rate to 1.2 Tb/s at 33 Gbaud over considerably longer distances.

IV. Recent System-on-Chip Demonstrations

In the last five years there has been considerable activity at UCSB on SoC-PICs based on III-V materials grown at UCSB. The first section describes examples related to the use of optical phase lock loops (OPLLs) that are improvements on seminal work carried out a few years earlier [53], [54]. The following sections describe high power InP PICs for free space optical communications, InP PICs for remote sensing LIDAR, and tunable laser PICs for 1030 nm applications including topographical LIDAR.

A. Recent Optical Phase-Locked Loop Experiments

Figure 7 summarizes a more recent heterodyne OPLL effort with improved overall performance characteristics, and with significantly improved input optical sensitivity levels and power dissipation. The theoretical sensitivity was approximately 9 μW, and 20 μW was measured with a slight (2.5 GHz) offset [55].

The total dissipated power in the electronics was reduced dramatically to 1.12 W relative to circuits like those from Fig. 6(e), which consumed ∼3 W. The power consumption

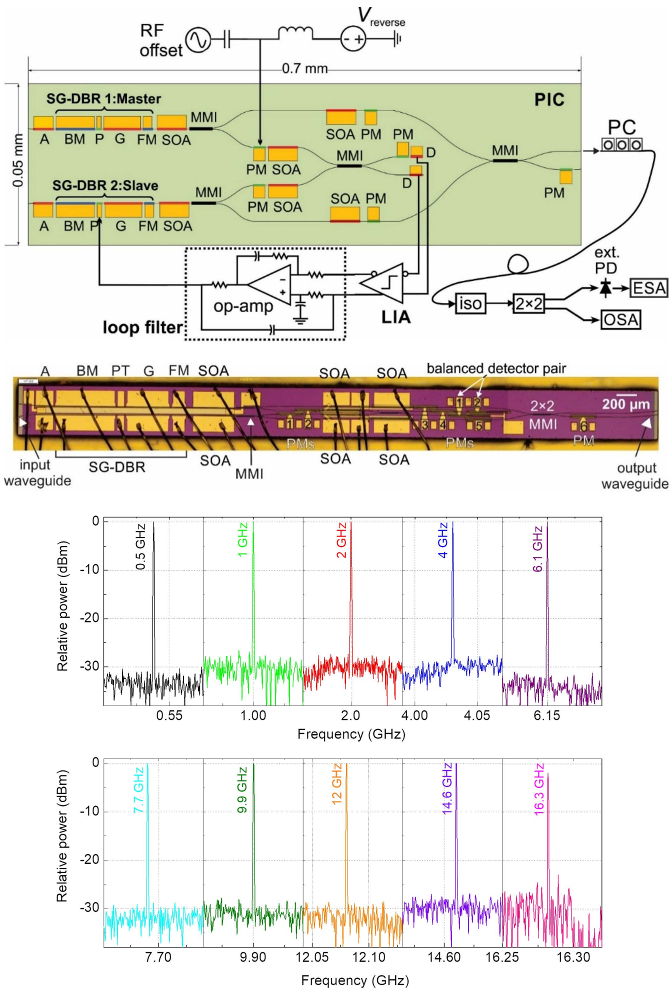

Fig. 8. RF-over-fiber SoC-PIC using an on-chip optical modulator for side-band generation. A schematic (top), PIC photo (center) and ESA spectra for various laser offsets due to RF applied to integrated phase modulator (PM) in center. Adapted with permission from [56].

of the PIC with an SGDBR laser and SOA was 0.66 W with 10 mW output power. Experiments were also carried out with a Y-branch laser-PIC from Freedom Photonics; this PIC consumed only 0.18 W with 10 mW out, the difference being mostly that no SOA was employed [55].

As also illustrated in Fig. 7, the pull-in range of this simple OPLL is limited relative to the Costas-loop design of Fig. 6(e), which has a frequency locking and phase locking capability, because of the I and Q availability. In the case of Fig. 6(e) the pull-in range was ~20 GHz [46], but here it is limited to ~1 GHz, dependent in both cases on the signal strength and heterodyne offset.

Figure 8 shows results of an OPLL used to offset lock one SGDBR laser from another in an RF-over-fiber PIC [56]. This OPLL uses the sidebands from an on-chip optical modulator to lock the slave laser to the master rather than an electronic mixer, such as the XOR in Fig. 7. As illustrated by the electrical spectrum analyzer (ESA) spectra, master-slave offset locking up to 16.3 GHz was demonstrated.

In addition to the inner waveguide branches dedicated to the OPLL, this SoC-PIC also has outer waveguide branches

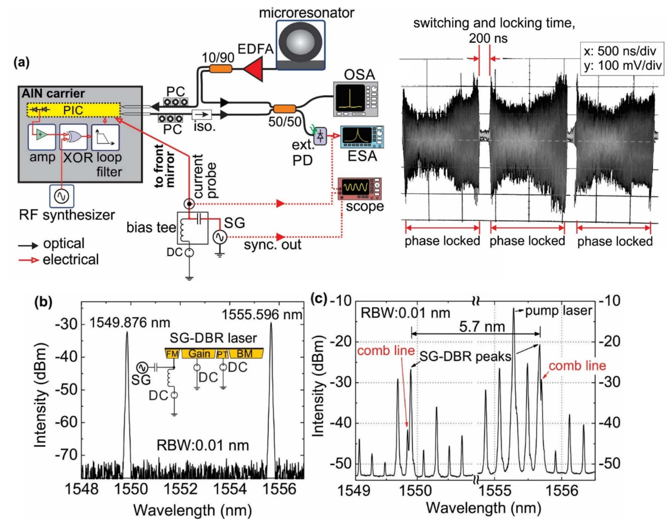

Fig. 9. Rapid locking of on-chip SGDBR laser to external microresonator for stable frequency synthesis. Schematic at top left. RF synthesizer set to 2.5 GHz; 800 kHz square wave applied to SGDBR front mirror to switch wavelength by 5.72 nm. ESA shows switching and locking time (top right); OSA shows spectra at bottom without and with microresonator reference. Adapted with permission from [57].

that can be separately modulated to add signals to these two offset-locked laser carrier frequencies. They are combined near the output so that both carriers and possible modulation(s) are summed for transmission [56]. Thus, for example, if RF signal information, occupying e.g., the 4-6 GHz band, is modulated onto the outer branch of the slave laser path, one would be able to demodulate it with just a photodiode onto an IF equal to the chosen offset, e.g., at 12 GHz, some number of kilometers away from a coupled optical fiber.

Figure 9 shows a third example of the use of an OPLL for frequency synthesis [57]. Here, an external stable microresonator is used as the reference source, and an SGDBR-PIC and OPLL circuit similar to that in Fig. 7 is employed to select and lock to a microresonator line, providing a high-level stable output at the precise frequency of the reference resonator plus the tunable RF offset. What is particularly interesting is that the SGDBR can tune to a given line, lock to it, and provide a stable output within 200 ns, as shown by the repetitive switching back and forth between two SGDBR laser open loop frequencies some 5.72 nm or 720 GHz apart. The RF synthesizer is tuned to provide the difference necessary to get within locking range, here 2.5 GHz. The microresonator mode spacing in this wavelength range is ~25.7 GHz, suggesting that the SGDBR laser is jumping across 28 resonator modes to relock in this experiment. The mode spacing varies slightly due to dispersion.

B. High Power InP SoC-PICs for Free-Space Optical Links

The high data rates and low cost, size, weight and power (CSWaP) offered by SoC-PICs makes them desirable for free space laser communications to provide connectivity for intersatellite and deep-space links [58]. Figure 10(a) illustrates an InP-based PIC transmitter for free space optical communications [59]. The transmitter consists of a SGDBR

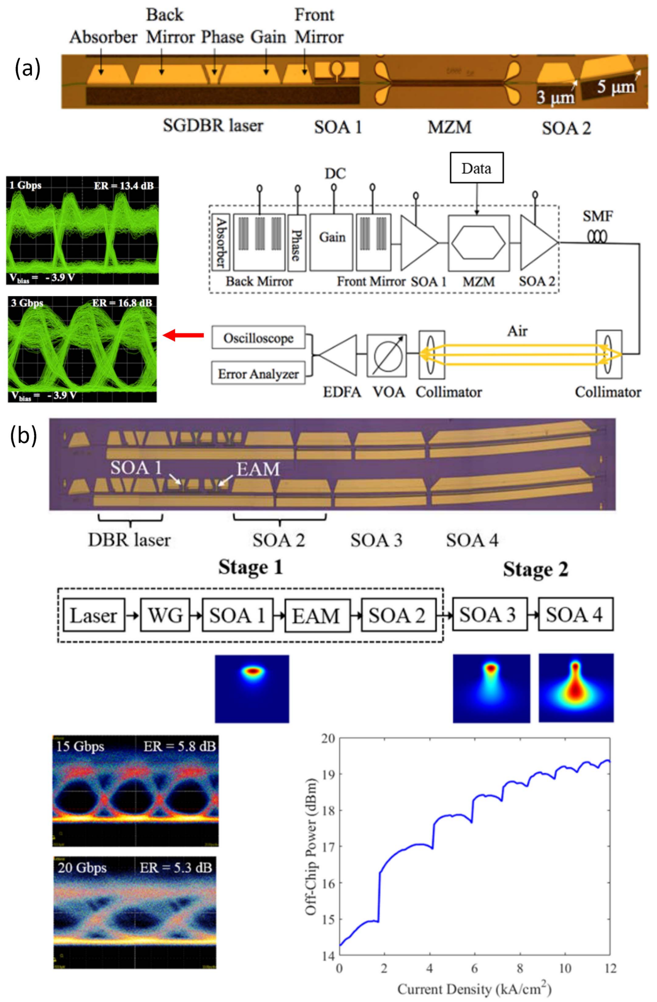

Fig. 10. Free-space link experiments. (a) SoC-PIC photo, schematic and data from free-space link experiment. Adapted with permission from [59]; (b) demonstration of high-power PIC with expanded mode SOA, and output power up to 19 dBm and 20 Gb/s data rate. Adapted with permission from [60].

laser, high-speed SOA, MZM, and a high-power output booster SOA. The SGDBR laser tunes from 1521 to 1565 nm with >45 dB side mode suppression ratio (SMSR). This InP PIC was incorporated into a free space optical link to demonstrate the potential for low size, weight and power demonstrating its suitability for deployment on small aircraft or satellites. Error-free operation was achieved at 3 Gbps for an equivalent link length of 180 m (up to 300 m with forward error correction) with a maximum output power of 14.5 dBm (28 mW).

A modified transmitter design for higher power operation is shown in Fig. 10(b) [60]. This PIC uses a quantum well intermixing (QWI) platform, rather than offset quantum well (OQW), for active-passive integration. The QWI transmitter consists of a DBR laser, high-speed SOA, an EAM, and an output SOA. The epitaxial structure and waveguide were modified in this design to achieve a lower confinement factor in the SOA for higher output saturation power. The measured off-chip power is 19.5 dBm (90 mW), and a data rate of 20 Gbps was demonstrated.

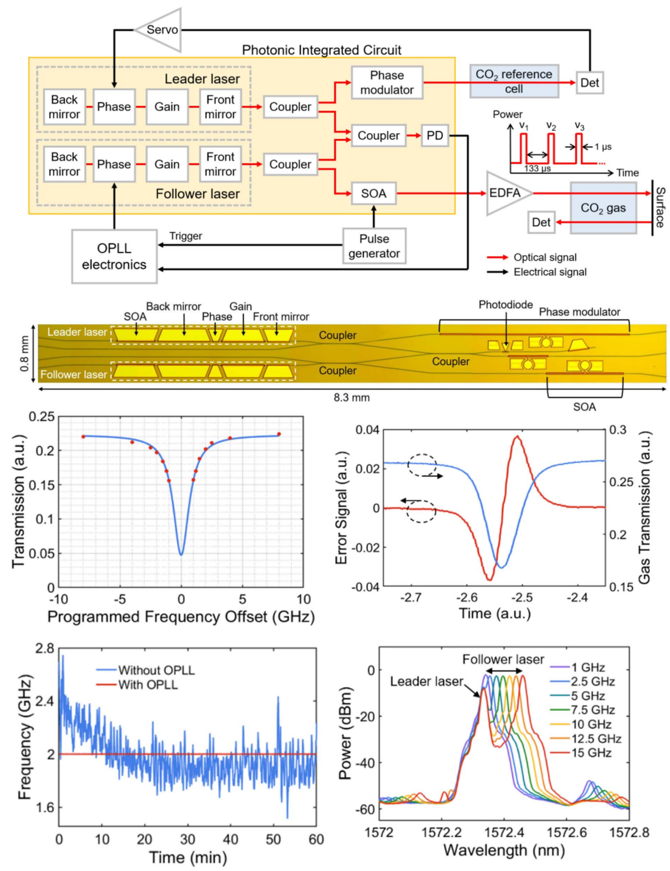

Fig. 11. CO_2 sensor SoC-PIC photo, schematic/electronics, and results. The first laser (leader) is frequency locked to a reference CO_2 cell, and a second laser (follower) is successively offset phase locked to the leader to trace out the CO_2 gas absorption in the atmosphere within a LIDAR path. Adapted with permission from [61].

C. Remote Gas Sensing LIDAR

SoC-PICs for LIDAR have also been demonstrated recently at UCSB for gas sensing applications. The system shown in Figure 11 is for detection of atmospheric carbon dioxide (CO_2) using integrated path differential absorption LIDAR as described in [61]. Again, this system takes advantage of the low CSWaP offered by SoC-PICs to make it suitable for deployment on satellites. The InP PIC contains two SGDBR lasers, a leader and follower. The leader laser is locked to the center of the 1572.335 nm CO_2 absorption line, using the CO_2 reference cell as shown in the upper part of the system diagram. The frequency stability of the leader laser is improved 236-fold when locked to the gas cell, compared to free-running. The follower laser is tuned ±15 GHz around the 1572.335 nm absorption line and offset locked to the leader with an OPLL. The SOA is used to generate pulses at each frequency step to sample the CO_2 absorption line.

D. Widely Tunable 1030 nm SGDBR Laser PIC

The widely-tunable SoC-PICs discussed so far have all been demonstrated on InP and as such are restricted to wavelengths in the 1300-1600 nm range. Further development is being pursued, however, to develop widely-tunable PICs for

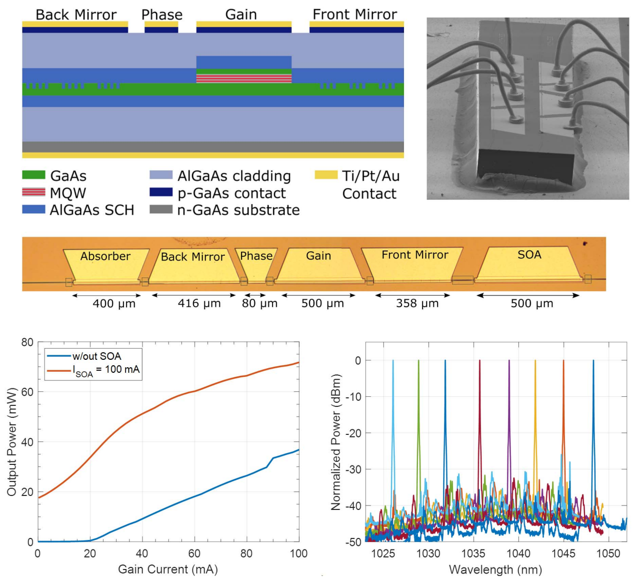

Fig. 12. Widely tunable SGDBR laser on GaAs, demonstrating 22 nm of continuous tuning around 1030 nm and up to 75 mW output power with amplification. For more information see [64] and [65].

applications in other spectral regions. Here, recent work on the development of widely-tunable SGDBR lasers on gallium arsenide (GaAs) for 1030 nm LIDAR is demonstrated. The spectral region near 1 μm is of particular interest for airborne terrain mapping LIDAR systems [62], owing to relatively low atmospheric absorption and the existence of high-quality detectors at this wavelength [63]. As with the remote gas sensing LIDAR system discussed above, the reduction of CSWaP offered by a SoC-PIC, compared to a system with commercial off-the-shelf (CoTS) components, is of critical importance for airborne topographical LIDAR.

A widely tunable SGDBR laser and integrated SOA on GaAs with a center wavelength near 1030 nm has been fabricated at UCSB and is shown in Fig. 12. This device was fabricated on an OQW PIC platform for active-passive integration, adapted for the GaAs material system [64]. The standalone SGDBR laser demonstrates 22.3 nm of continuous wavelength tuning with 30 dB SMSR (bottom right of Fig. 12) and 35 mW of output power [65]. With the addition of an integrated SOA, the output power can be increased to greater than 75 mW (bottom left of Fig. 12). The demonstration of a widely tunable laser and integrated SOA on GaAs lays a path for further development of more complex SoC-PICs in the 1 μm spectral range, analogous to those on InP for C-band applications.

V. Conclusion

Advanced materials growth and processing technologies together with highly-developed device designs have enabled complex PICs on III-Vs that can perform several photonic system functions. Many of these SoC-PICs can provide significant savings in cost, size, weight, and power compared to discrete implementations, even eliminating the need for some components, or required electronics, in many cases.

In this paper we have focused on the development, and benefits of widely-tunable lasers in such SoC-PICs. The use of such lasers can provide wavelength agility for broadband WDM communication systems, wavelength stability by phase locking to any of a number of references, and wavelength sweeping for a variety of sensing applications, such as in LIDAR or optical beam control.

Acknowledgment

A portion of this work was carried out at the University of California at Santa Barbara (UCSB) Nanofabrication Facility. For this special issue, the authors would like to acknowledge the many contributions of Prof. Daniel Dapkus to their field, especially his seminal MOCVD advances, which they depend upon for all of their PICs. Larry A. Coldren would like to specifically acknowledge him for growing their first SGDBR samples, which launched much of this work. The authors would also like to acknowledge contributions to the recent UCSB work reported by Shamsul Arafin, Hongwei Zhao, Sergio Pinna, Joseph Fridlander, Victoria Rosborough, Fengqiao Sang, and Bowen Song.

References

[1] F. Kish *et al.*, "System-on-chip photonic integrated circuits," *IEEE J. Sel. Topics Quantum Electron.*, vol. 24, no. 1, pp. 1–20, Feb. 2018.
[2] K. A. Williaams *et al.*, "InP photonic circuits using generic integration," *Photon. Res.*, vol. 3, no. 5, pp. 60–67, 2015.
[3] Y. Tohmori, Y. Suematsu, H. Tsushima, and S. Arai, "Wavelength tuning of GaInAsP/InP integrated laser with butt-jointed built-in distributed Bragg reflector," *Electron. Lett.*, vol. 19, no. 17, pp. 656–657, 1983.
[4] M. Zirngibl, C. H. Joyner, and L. W. Stulz, "WDM receiver by monolithic integration of an optical preamplifier, waveguide grating router and photodiode array," *Electron. Lett.*, vol. 31, no. 7, pp. 581–582, 1995.
[5] K. Kudo *et al.*, "1.55-μm wavelength-selectable microarray DFB-LD's with monolithically integrated MMI combiner, SOA, and EA-modulator," *IEEE Photon. Technol. Lett.*, vol. 12, no. 3, pp. 242–244, Mar. 2000.
[6] M. C. Larson *et al.*, "Narrow linewidth sampled-grating distributed Bragg reflector laser with enhanced side-mode suppression," in *Conf. Opt. Fiber Commun. Tech. Dig. Ser.*, Jun. 2015, pp. 2–4.
[7] G. Gilardi and M. K. Smit, "Generic InP-based integration technology: Present and prospects (invited review)," *Prog. Electromagn. Res.*, vol. 147, pp. 23–35, 2014.
[8] L. A. Coldren *et al.*, "High performance InP-based photonic ICs—A tutorial," *J. Lightw. Technol.*, vol. 29, no. 4, pp. 554–570, Feb. 15, 2011.
[9] M. Smit, K. Williams, and J. van der Tol, "Past, present, and future of InP-based photonic integration," *APL Photon.*, vol. 4, no. 5, May 2019, Art. no. 050901, doi: 10.1063/1.5087862.
[10] G. E. Hoefler *et al.*, "Foundry development of system-on-chip InP-based photonic integrated circuits," *IEEE J. Sel. Topics Quantum Electron.*, vol. 25, no. 5, pp. 1–17, Sep. 2019.
[11] M. Blaicher *et al.*, "Hybrid multi-chip assembly of optical communication engines by *in situ* 3D nano-lithography," *Light, Sci. Appl.*, vol. 9, no. 1, pp. 1–11, Dec. 2020, doi: 10.1038/s41377-020-0272-5.
[12] J. Zhang *et al.*, "III-V-on-Si photonic integrated circuits realized using micro-transfer-printing," *APL Photon.*, vol. 4, no. 11, Nov. 2019, Art. no. 110803, doi: 10.1063/1.5120004.
[13] B. Song, C. Stagarescu, S. Ristic, A. Behfar, and J. Klamkin, "3D integrated hybrid silicon laser," *Opt. Exp.*, vol. 24, no. 10, pp. 10435–10444, 2016.
[14] Y. Wan *et al.*, "Low threshold quantum dot lasers directly grown on unpatterned quasi-nominal (001) Si," *IEEE J. Sel. Topics Quantum Electron.*, vol. 26, no. 2, pp. 1–9, Mar. 2020.
[15] C. Xiang *et al.*, "High-performance silicon photonics using heterogeneous integration," *IEEE J. Sel. Topics Quantum Electron.*, vol. 28, no. 3, pp. 1–15, May 2022.

[16] N. Margalit, C. Xiang, S. M. Bowers, A. Bjorlin, R. Blum, and J. E. Bowers, "Perspective on the future of silicon photonics and electronics," *Appl. Phys. Lett.*, vol. 118, no. 22, May 2021, Art. no. 220501.

[17] S. E. Miller, "Integrated optics: An introduction," *Bell Syst. Tech. J.*, vol. 48, no. 7, pp. 2059–2069, Sep. 1969.

[18] D. B. Keck, R. D. Maurer, and P. C. Schultz, "On the ultimate lower limit of attenuation in glass optical waveguides," *Appl. Phys. Lett.*, vol. 22, no. 7, pp. 307–309, Apr. 1973.

[19] T. L. Koch *et al.*, "GaInAs/GaInAsP multiple-quantum-well integrated heterodyne receiver," *Electron. Lett.*, vol. 25, no. 24, pp. 1621–1623, 1989.

[20] R. C. Alferness and A. Glass, "Bell labs technology trends & developments," *Bell Labs Tech. J.*, vol. 2, no. 2, pp. 1–15, 1988.

[21] K. Murata, S. Mito, and I. Kobayashi, "Over 720 GHz (5.8 nm) frequency tuning by a 1.5 μm DBR laser with phase and Bragg wavelength control regions," *Electron. Lett.*, vol. 23, no. 8, pp. 403–405, 1987.

[22] T. L. Koch, U. Koren, and B. I. Miller, "High performance tunable 1.5 μm InGaAs/InGaAsP multiple quantum well distributed Bragg reflector lasers," *Appl. Phys. Lett.*, vol. 53, no. 12, pp. 1036–1038, 1988.

[23] R. J. Mears, L. Reekie, I. M. Jauncey, and D. N. Payne, "Low-noise erbium-doped fibre amplifier operating at 1.54 μm," *Electron. Lett.*, vol. 23, no. 19, pp. 1026–1028, 1987.

[24] L. A. Coldren, B. I. Miller, K. Iga, and J. A. Rentschler, "Monolithic two-section GaInAsP/InP active-optical-resonator devices formed by reactive ion etching," *Appl. Phys. Lett.*, vol. 38, no. 5, pp. 315–317, Mar. 1981.

[25] L. A. Coldren, "Multi-section tunable laser with differing multi-element mirrors," U.S. Patent 4 896 325, Jan. 23, 1990.

[26] V. Jayaraman, Z.-M. Chuang, and L. A. Coldren, "Theory, design, and performance of extended tuning range semiconductor lasers with sampled gratings," *IEEE J. Quantum Electron.*, vol. 29, no. 6, pp. 1824–1834, Jun. 1993.

[27] V. Jayaraman, A. Mathur, L. A. Coldren, and P. D. Dapkus, "Very wide tuning range in a sampled grating DBR laser," in *Proc. 13th IEEE Int. Semiconductor Laser Conf.* Takamatsu, Japan, 1992, Paper PD-11.

[28] T. L. Koch, "OFC tutorial: III–V and silicon photonic integrated circuit technologies," in *Proc. OFC/NFOEC*, 2012, pp. 1–45.

[29] Y. A. Akulova *et al.*, "Widely tunable electroabsorption-modulated sampled-grating DBR laser transmitter," *IEEE J. Sel. Top. Quantum Electron.*, vol. 8, no. 6, pp. 1349–1357, Nov./Dec. 2002.

[30] Y. A. Akulova *et al.*, "10 Gb/s Mach–Zehnder modulator integrated with widely-tunable sampled grating DBR laser," in *Proc. OSA Trends Opt. Photon. Ser.*, vol. 95, 2004, pp. 395–397.

[31] C. Coldren *et al.*, "Reliability of widely-tunable SGDBR lasers suitable for deployment in agile networks," in *OFC Tech. Dig.*, vol. 1, 2003, pp. 73–75.

[32] *Tunable Multiprotocal XFP Optical Transceiver—1550 nm for up to 80 km Reach JXP Series, P/N JXP01TMAC1CX5*, Lumentum, San Jose, CA, USA, 2015.

[33] Lumentum Operations LLC. (Mar. 2018).*Lumentum to acquire OCLARO for 1.8B in cash and stock.* San Jose, CA, Accessed: Apr. 26, 2022. [Online]. Available: https://www.lumentum.com/en/media-room/news-releases/lumentum-acquire-oclaro-18b-cash-and-stock

[34] R. C. Alferness *et al.*, "Broadly tunable InGaAsP/InP laser based on a vertical coupler filter with 57-nm tuning range," *Appl. Phys. Lett.*, vol. 60, no. 26, pp. 3209–3211, 1992.

[35] M. Öberg, S. Nilsson, K. Streubel, J. Wallin, L. Bäckbom, and T. Klinga, "74 nm wavelength tuning range of an InGaAsP/InP vertical grating assisted codirectional coupler laser with rear sampled grating reflector," *IEEE Photon. Technol. Lett.*, vol. 5, no. 7, pp. 735–738, Jul. 1993.

[36] L. A. Coldren, "Monolithic tunable diode lasers," *IEEE J. Sel. Topics Quantum Electron.*, vol. 6, no. 6, pp. 988–999, Nov./Dec. 2000.

[37] R.-J. Essiambre, G. Kramer, P. J. Winzer, G. J. Foschini, and B. Goebel, "Capacity limits of optical fiber networks," *J. Lightw. Technol.*, vol. 28, no. 4, pp. 662–701, Feb. 15, 2010.

[38] M. G. Young *et al.*, "Six wavelength laser array with integrated amplifier and modulator," *Electron. Lett.*, vol. 31, no. 21, pp. 1835–1836, Oct. 1995.

[39] H. M. Hatakeyama *et al.*, "Wavelength-selectable microarray light sources for S-, C-, and L-band WDM systems," *IEEE Photon. Technol. Lett.*, vol. 15, no. 7, pp. 903–905, Jul. 2003.

[40] N. Kikuchi *et al.*, "Monolithically integrated 64-channel WDM wavelength-selective receiver," *Electron. Lett.*, vol. 39, no. 3, pp. 312–314, 2003.

[41] J. Heanue, E. Vail, M. Sherback, and B. Pezeshki, "Widely tunable laser module using DFB array and MEMs selection with internal wavelength locker," in *Proc. OFC*, vol. 1, 2003, pp. 21–22.

[42] M. Smit *et al.*, "A generic foundry model for InP-based photonic ICs," in *Proc. Opt. InfoBase Conf. Paper*, 2012, pp. 2–4.

[43] R. Nagarajan *et al.*, "Large-scale photonic integrated circuits," *IEEE J. Sel. Top. Quantum Electron.*, vol. 11, no. 1, pp. 50–65, Jan./Feb. 2005.

[44] M. M. Dummer, J. Klamkin, A. Tauke-Pedretti, and L. A. Coldren, "A bit-rate-transparent monolithically integrated wavelength converter," in *Proc. Eur. Conf. Opt. Commun. (ECOC)*, vol. 4, Sep. 2008, pp. 77–80.

[45] S. C. Nicholes, M. L. Mašanović, B. Jevremović, E. Lively, L. A. Coldren, and D. J. Blumenthal, "An 8×8 InP monolithic tunable optical router (MOTOR) packet forwarding chip," *J. Lightw. Technol.*, vol. 28, no. 4, pp. 641–650, Feb. 15, 2010.

[46] M. Lu *et al.*, "An integrated 40 Gbit/s optical Costas receiver," *J. Lightw. Technol.*, vol. 31, no. 13, pp. 2244–2253, Jul. 1, 2013.

[47] H. C. Park *et al.*, "40 Gbit/s coherent optical receiver using a Costas loop," *Opt. Exp.*, vol. 20, no. 26, pp. 197–203, 2012.

[48] W. Guo, P. R. A. Binetti, M. L. Masanovic, L. A. Johansson, and L. A. Coldren, "Large-scale InP photonic integrated circuit packaged with ball grid array for 2D optical beam steering," in *Proc. IEEE Photon. Conf. (IPC)*, Sep. 2013, pp. 651–652.

[49] M. Lauermann *et al.*, "Multi-channel, widely-tunable coherent transmitter and receiver PICs operating at 88 Gbaud/16-QAM," in *Proc. Opt. Fiber Commun. Conf. Exhib. (OFC)*, vol. 1, 2017, pp. 8–10.

[50] A. Tauke-Pedretti *et al.*, "Separate absorption and modulation Mach–Zehnder wavelength converter," *J. Lightw. Technol.*, vol. 26, no. 1, pp. 91–98, Jan. 1, 2008.

[51] V. Lal, M. L. Mašanović, J. A. Summers, G. Fish, and D. J. Blumenthal, "Monolithic wavelength converters for high-speed packet-switched optical networks," *IEEE J. Sel. Top. Quantum Electron.*, vol. 13, no. 1, pp. 49–57, Jan./Feb. 2007.

[52] W. Guo *et al.*, "Two-dimensional optical beam steering with InP-based photonic integrated circuits," *IEEE J. Sel. Topics Quantum Electron.*, vol. 19, no. 4, Jul. 2013, Art. no. 6100212.

[53] M. Lu *et al.*, "A highly integrated optical phase-locked loop with singlesideband frequency sweeping," *CLEO Sci. Innov.*, vol. 20, no. 9, pp. 1090–1092, 2012.

[54] S. Ristic, A. Bhardwaj, M. J. Rodwell, L. A. Coldren, and L. A. Johansson, "An optical phase-locked loop photonic integrated circuit," *J. Lightw. Technol.*, vol. 28, no. 4, pp. 526–538, Feb. 15, 2010.

[55] A. Simsek *et al.*, "Evolution of chip-scale heterodyne optical phase-locked loops toward Watt level power consumption," *J. Lightw. Technol.*, vol. 36, no. 2, pp. 258–264, Jan. 15, 2018.

[56] S. Arafin, A. Simsek, M. Lu, M. J. Rodwell, and L. A. Coldren, "Heterodyne locking of a fully integrated optical phase-locked loop with on-chip modulators," *Opt. Lett.*, vol. 42, no. 19, pp. 3745–3748, 2017.

[57] S. Arafin *et al.*, "Towards chip-scale optical frequency synthesis based on optical heterodyne phase-locked loop," *Opt. Exp.*, vol. 25, no. 2, pp. 681–694, 2017.

[58] H. Hemmati, A. Biswas, and I. B. Djordjevic, "Deep-space optical communications: Future perspectives and applications," *Proc. IEEE*, vol. 99, no. 11, pp. 2020–2039, Nov. 2011.

[59] H. Zhao *et al.*, "Indium phosphide photonic integrated circuits for free space optical links," *IEEE J. Sel. Topics Quantum Electron.*, vol. 24, no. 6, pp. 1–6, Nov. 2018.

[60] H. Zhao *et al.*, "High-power indium phosphide photonic integrated circuits," *IEEE J. Sel. Topics Quantum Electron.*, vol. 25, no. 6, pp. 1–10, Nov. 2019.

[61] J. Fridlander *et al.*, "Dual laser indium phosphide photonic integrated circuit for integrated path differential absorption LiDAR," *IEEE J. Sel. Topics Quantum Electron.*, vol. 28, no. 1, pp. 1–8, Jan. 2022.

[62] A. W. Yu *et al.*, "A 16-beam non-scanning swath mapping laser altimeter instrument," *Proc. SPIE*, vol. 8599, Mar. 2013, Art. no. 85990P.

[63] M. A. Krainak, X. Sun, G. Yang, and W. Lu, "Comparison of linear-mode avalanche photodiode LiDAR receivers for use at one-micron wavelength," *Proc. SPIE*, vol. 7681, Apr. 2010, Art. no. 76810Y.

[64] P. Verrinder *et al.*, "Gallium arsenide photonic integrated circuit platform for tunable laser applications," *IEEE J. Sel. Topics Quantum Electron.*, vol. 28, no. 1, pp. 1–9, Jan. 2022.

[65] P. Verrinder, L. Wang, F. Sang, V. Rosborough, M. Nickerson, G. Yang, et al., "SGDBR tunable laser on gallium arsenide for 1030 nm lidar applications," in*Proc. 27th Int. Semiconductor Laser Conf.* Potsdam, Germany, Oct. 10/14, 2021, Paper no. WA2.2.

Larry A. Coldren (Life Fellow, IEEE) received the B.S. degree in electrical engineering and the B.A. degree in physics from Bucknell University and the M.S. and Ph.D. degrees in electrical engineering from Stanford University in 1969 and 1972, respectively, under the support of Bell Laboratories.

He joined Bell Laboratories in 1968. Following 13 years in the research area with Bell Laboratories, he joined the ECE Department of the University of California at Santa Barbara (UCSB) in 1984. In 1986, he was a Founding Member of the Materials Department. He became the Fred Kavli Professor of optoelectronics and sensors in 1999. From 2009 to 2011, he was the Acting Dean of the College of Engineering, and in 2017, he became a Emeritus Professor and a Distinguished Research Professor. In 1990, he co-founded Optical Concepts, later acquired as Gore Photonics, to develop novel VCSEL technology, and in 1998, he co-founded Agility Communications, later acquired by JDSU (now Lumentum), to develop widely-tunable integrated transmitters and transponders. At UCSB, he has worked on multiple-section widely-tunable lasers and efficient vertical-cavity surface-emitting lasers (VCSELs). He continues to research high-performance InP-based photonic integrated circuits, and high-speed and high-efficiency VCSELs for various applications. He has authored or coauthored over 1000 journals and conference papers, eight book chapters, a widely-used textbook, and 63 issued patents.

Prof. Coldren is a fellow of OSA, IEE, and the National Academy of Inventors as well as a member of the National Academy of Engineering. He was a recipient of the 2004 John Tyndall, the 2009 Aron Kressel, the 2014 David Sarnoff, the 2015 IPRM, and the 2017 Nick Holonyak, Jr., Awards.

Paul A. Verrinder received the B.S. degree in electrical engineering from California State University, Fresno, in 2015, and the M.S. degree in electrical and computer engineering from the University of California at Santa Barbara (UCSB), Santa Barbara, in 2020, where he is currently pursuing the Ph.D. degree with the Electrical and Computer Engineering Department. From 2015 to 2018, he was an Electrical Engineer with NAVAIR, China Lake. His research interests are in integrated photonics for optical communications and LIDAR.

Jonathan Klamkin (Senior Member, IEEE) received the B.S. degree from Cornell University, Ithaca, NY, USA, and the M.S. and Ph.D. degrees from the University of California at Santa Barbara (UCSB), Santa Barbara, CA, USA. From 2008 to 2011, he was a member of the Technical Staff with the Electro-Optical Materials and Devices Group, MIT Lincoln Laboratory, Lexington, MA, USA. From 2011 to 2013, he was an Assistant Professor with the Institute of Communication, Information and Perception Technologies, Scuola Superiore Sant'Anna, Pisa, Italy. From 2013 to 2015, he was an Assistant Professor of electrical and computer engineering (ECE) and materials with Boston University, Boston, MA. In 2015, he joined the ECE Department, University of California at Santa Barbara, where he is currently a Professor and the Director of the UCSB Nanotech. He has authored or coauthored 200 journals and conference papers. He or his group members were the recipient of Best Paper Awards at the 2006 Conference on Optoelectronic and Microelectronic Materials and Devices, the 2007 Microwave Photonics Conference, and the 2017 and 2019 Asia Communications and Photonics Conference. He was the recipient of the NASA Early Career Faculty Award, the DARPA Young Faculty Award, and the DARPA Director's Fellowship.

Dual Laser Indium Phosphide Photonic Integrated Circuits for Remote Active Carbon Dioxide Sensing

Fengqiao Sang[1*], Victoria Rosborough[1], Joseph Fridlander[1], Fabrizio Gambini[2,3], Simone Šuran Brunelli[1], Jeffrey R. Chen[2], Stephan R. Kawa[2], Kenji Numata[2], Mark Stephen[2], Larry Coldren[1], Jonathan Klamkin[1]

[1]*Electrical and Computer Engineering Department, University of California, Santa Barbara, Santa Barbara, CA 93106 USA*
[2]*NASA Goddard Space Flight Center, Greenbelt, MD 20771 USA*
[3]*University of Maryland Baltimore County, Baltimore, MD 21250 USA*
[*]*fsang@ece.ucsb.edu*

Abstract: Two generations of indium phosphide photonic integrated circuits were fabricated, characterized, and their performance compared. Successful sampling of carbon dioxide was performed in a laboratory setting under continuous wave sampling.

1. Introduction

In recent years, there has been increasing interest in photonic integrated circuits (PICs) for remote sensing and free space communication applications because of their low size, weight, and power (SWaP) [1-5]. Remote carbon dioxide (CO_2) sensing is one such application. Currently, remote spectrometers rely on reflected sunlight to passively measure CO_2 concentrations in the atmosphere. Engineers at NASA Goddard Space Flight Center (GSFC) have developed an active CO_2 sensor with an on-board infrared laser source to realize approximately 1 ppm precision [6,7]. The integrated path differential absorption lidar system includes a leader laser locked to the center of the CO_2 absorption line at 1572.335 nm and a follower laser offset locked to the leader laser. The follower laser is scanned ±15 GHz around 1572.335 nm to measure the CO_2 concentration from the shape of the absorption line. In this work, we present progress toward a low SWaP PIC-based module leveraging the architecture of the NASA GSFC system, which was built from discrete commercial off the shelf components.

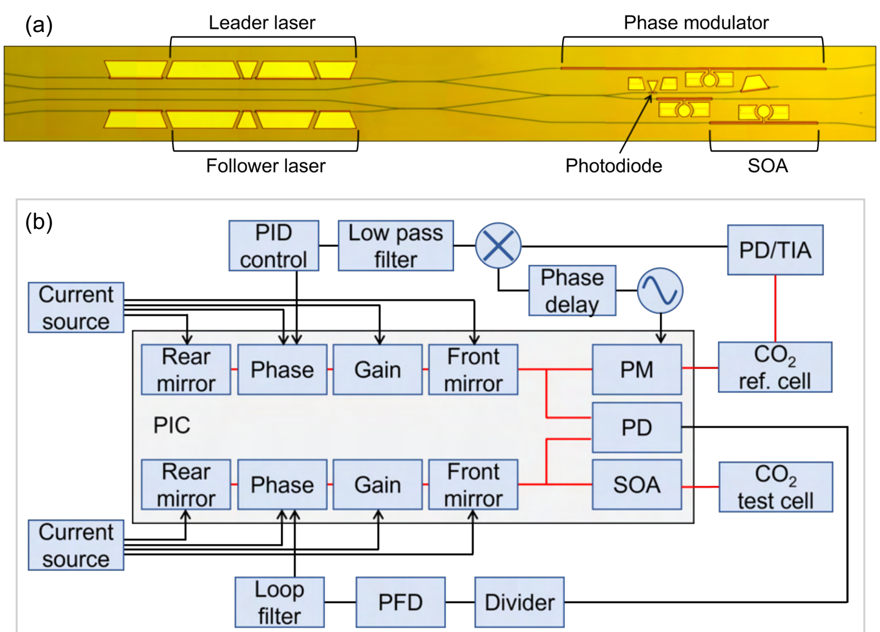

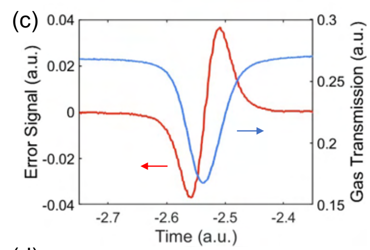

(d)

	Generation 1	Generation 2
Couplers	Directional couplers only	Directional and MMI couplers
Phase modulator length (mm)	2.5	1.2
SOA length (mm)	1	1
PIC dimensions (mm)	8.2 x 0.8	9.5 x 0.8
On-chip photodiode	Insufficient performance	Suitable performance
Locked leader laser SMSR (dB)	54	47
Leader laser frequency std. dev. (MHz) (30 mins)	0.332	0.466
Follower laser frequency std. dev. (kHz) (30 mins)	33.126	3.614
Maximum follower laser power (mW)	12	16.5

Fig. 1. (a) Microscope image of fabricated first generation PIC. (b) Test setup used to characterize PIC. PID = proportional-integral-derivative. PD/TIA = photodiode/transimpedance amplifier. PM = phase modulator. PFD = phase frequency detector. (c) Absorption and error signal at the reference gas cell detector. (d) Table comparing the layout and performance of first and second generations.

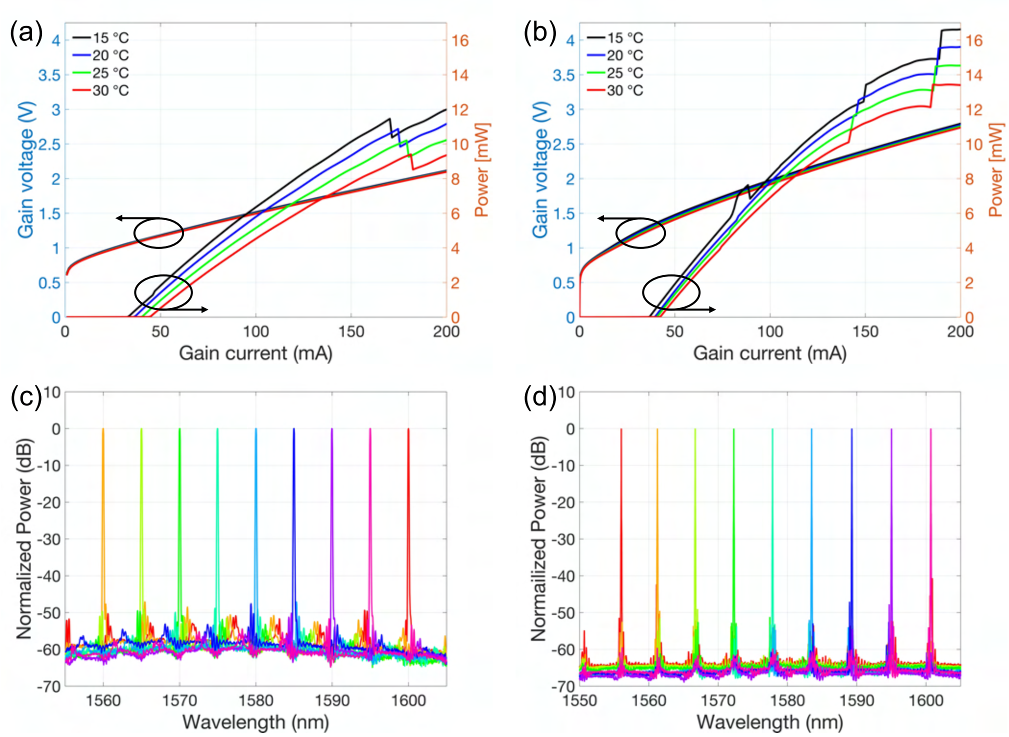

Fig. 2. (a) First generation light-current-voltage curve measured at the SOA. (b) Second generation light-current-voltage curve measured at the SOA. (c) First generation laser tuning. (d) Second generation laser tuning.

2. PIC Layout and Characterization

Two generations of InP PICs are designed and fabricated. One of the fabricated PICs is shown in Fig. 1(a), and the testing system is shown in Fig. 1(b). The overall system mainly consists of two parts, leader laser stabilization and follower laser offset locking. The overall gas sensing is achieved by performing both systems together.

The leader laser stabilization is achieved using a frequency modulation technique [6-8], where the leader laser is locked to a CO_2 reference cell by modulating the phase of the laser output signal at 125 MHz. The CO_2 reference cell works as a frequency discriminator; it generates a phase dependent error signal as shown in Fig. 1(c). The signal is extracted using a mixer, further filtered with a low pass filter, and processed using PID controls. The processed error signal is sent back into the phase section of the leader laser to achieve locking and stabilization.

The follower laser offset locking is accomplished using the optical phase lock loop technique [6,7]. An integrated photodiode detects the beat note signal from the leader and follower laser. The beat note signal is sent into PLL electronics, and is divided into a lower frequency signal through a multi-stage divider. Then, a phase frequency detector is used to detect the frequency difference between the divided signal and target frequency to generate a feedback signal. A loop filter was designed carefully to provide the best in-band phase noise and bandwidth for the feedback signal. The filtered feedback signal is sent back into the phase section of the follower laser to accomplish offset locking.

The two generations are compared here, where the first generation was reported to have accomplished gas sensing with continuous wave (CW) sampling using an external photodiode due to insufficient performance of the integrated photodiode [3-5,9]. Fig. 1(d) lists the major differences between the first and second generation PICs and corresponding performance, where the key difference is that the second generation used an integrated photodiode instead of an external photodiode. Fig. 2 shows a comparison of the device level characterization between the two generations. The second generation achieved a 45 nm tuning range and 12.7 mW output power with 150 mA current injection at 20 degrees Celsius, whereas the first generation has a 40 nm tuning range and 9.36 mW output power for the same conditions. However, the side mode suppression ratio (SMSR) of the second generation laser is slightly worse at some frequencies compared to the first generation laser. Since the two generations used the same laser design, this difference is mainly caused by fabrication variations, especially the depth of the etched grating.

Finally, system level characterization is compared in Fig. 3. Both generations successfully performed the gas sensing measurement using CW sampling, yielding an absorption spectrum with a fitted full-width half maximum of 1600 MHz. The leader laser stabilization performance is comparable between the two generations because a similar

PIC design and measurement setup were used for both generations. Leader laser stabilization over 30 minutes gave a standard deviation of 0.33 MHz and 0.46 MHz for the first and second generations, respectively. But, since the second generation used an integrated photodiode for the follower laser locking, the follower laser stabilization performance for the second generation achieved an order of magnitude improvement compared with the first generation. Over 30 minutes, the standard deviation of the follower laser frequency stability was 33.12 kHz for the first generation and 3.61 kHz for the second generation.

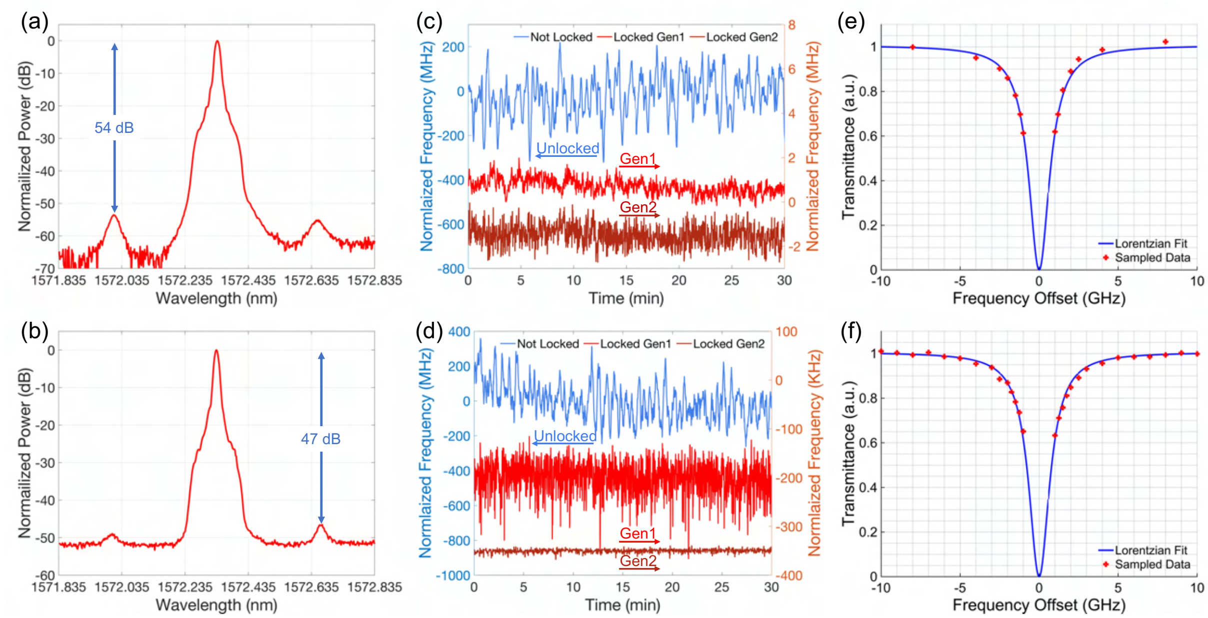

Fig. 3. (a) First generation locked leader laser spectrum. (b) Second generation locked leader laser spectrum. (c) Comparison of leader laser stabilization. (d) Comparison of follower laser stabilization. (e) First generation CW sampling of CO_2 with Lorentzian fit. (f) Second generation CW sampling of CO_2 with Lorentzian fit.

3. Conclusion

Successful laboratory CO_2 sensing was performed with compact PIC technology. The performance between the first and second generation PICs was compared for CW gas sampling. Improved stabilization was achieved for the second generation because an integrated photodiode was used instead of an external photodiode. Future work will focus on pulsed gas sampling and further SWaP reduction using close integration with control electronics in a compact package.

4. Acknowledgements

The authors acknowledge funding from NASA's Earth Science Technology Office (ESTO) Advanced Component Technology (ACT) program. A portion of this work was performed in the UCSB Nanofabrication Facility.

5. References

[1] Zhao, Hongwei, et al. "High-power indium phosphide photonic integrated circuits." IEEE Journal of Selected Topics in Quantum Electronics 25.6 (2019): 1-10.
[2] Isaac, Brandon J., et al. "Indium phosphide photonic integrated circuit transceiver for FMCW LiDAR." IEEE Journal of Selected Topics in Quantum Electronics 25.6 (2019): 1-7.
[3] Fridlander, Joseph, et al. "Dual Laser Indium Phosphide Photonic Integrated Circuit for Integrated Path Differential Absorption Lidar." IEEE Journal of Selected Topics in Quantum Electronics (2021).
[4] Fridlander, Joseph, et al. "Monolithic Indium Phosphide Dual Laser Photonic Integrated Circuit for Remote Sensing Lidar." CLEO: Science and Innovations. Optical Society of America, 2021.
[5] Fridlander, Joseph, et al. "Photonic integrated circuits for precision spectroscopy." CLEO: Science and Innovations. Optical Society of America, 2020.
[6] Numata, Kenji, et al. "Frequency stabilization of distributed-feedback laser diodes at 1572 nm for lidar measurements of atmospheric carbon dioxide." Applied optics 50.7 (2011):1047-1056.
[7] Numata, Kenji, Jeffrey R. Chen, and Stewart T. Wu. "Precision and fast wavelength tuning of a dynamically phase-locked widely-tunable laser." Optics express 20.13 (2012): 14234-14243.
[8] Bjorklund, Gary C. "Frequency-modulation spectroscopy: a new method for measuring weak absorptions and dispersions." Optics letters 5.1 (1980): 15-17.
[9] Rosborough, Victoria, et al. "Residual Amplitude Modulation Reduction in Integrated Indium Phosphide Phase Modulators." CLEO: Science and Innovations. Optical Society of America, 2021.

High Speed Etched Facet Traveling Wave Modulators for Micro Transfer Print Integration

Thomas Meissner[1*], Si Zhu[1], Simone Šuran Brunelli[1], Andrew Carter[2], Adam Young[2], Chongxin Zhang[1], Lei Wang[1], Gopikrishnan G. Meena[3], Renan Moreira[3], Larry Coldren[1] and Jonathan Klamkin[1]
[1]*Electrical and Computer Engineering Department, University of California Santa Barbara, Santa Barbara, CA 93106 USA*
[2]*Teledyne Scientific & Imaging, Thousand Oaks, CA 91360 USA*
[3]*Ultra Low Loss Technologies, Goleta, CA 93117 USA*
[*]*thomas_meissner@ucsb.edu*

Abstract: Traveling wave etched facet waveguide modulators are designed and fabricated. Measurements demonstrate a 56 GHz bandwidth at 1275 nm with power handling greater than 20 dBm. Micro transfer printing onto silicon has also been demonstrated.

OCIS codes: (250.5300) Photonic Integrated Circuits; (250.7360) Waveguide Modulators; (230.4110) Modulators

1. Introduction

Traveling wave (TW) modulators are often leveraged in applications requiring both high bandwidth and high efficiency such as short reach optical links in data centers [1], beam steering [2], and optical isolators [3]. To utilize the high efficiency of indium phosphide (InP) for modulators and the low loss of other platforms such as silicon nitride (SiN), etched facets can be utilized to enable heterogeneous integration [4]. In this paper, we report on high speed InP TW electro-absorption modulators (EAMs) fabricated with epitaxy that includes an indium aluminum arsenide (InAlAs) release layer for micro transfer printing (MTP). Modulators characterized in discrete form demonstrated 56 GHz 3-dB bandwidth and preliminary MTP onto bare silicon (Si) was performed.

2. Device Design, Fabrication and Results

A cross section and CAD layout of the TW modulator is shown in Fig. 1(a). A periodically loaded Au-based microstrip feed using BCB dielectric is used as the RF feed. Series resistance, line inductance, parallel conductance, and capacitance of the unloaded line was simulated using Ansys HFSS. Diode series resistance and junction capacitance was added analytically using measured values from devices with similar epitaxy. The equivalent circuit model is shown in Fig. 1(b).

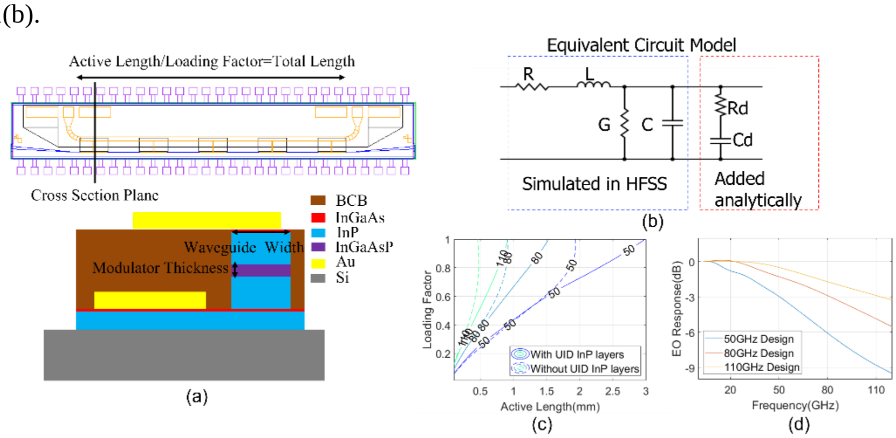

Fig. 1. (a) Cross section of designed microstrip modulator transferred to silicon; (b) Distributed circuit model for loaded microstrip transmission line; (c) Design space for modified and conventional epitaxy for several bandwidth targets; (d) Simulated response for 2.6 mm,1.2 mm and 0.6 mm traveling wave modulators with a 20 Ω load impedance and 100% loading.

Diode junction capacitance is the primary limiter of InP TW modulator bandwidth. To combat this effect, this work includes 75 nm thick unintentionally doped (UID) layers of InP above and below the indium gallium arsenide phosphide (InGaAsP) waveguide core. This increases the thickness of the depletion region, significantly reducing capacitance. For this modified epitaxy design, the UID layer significantly increases the maximum modulator length for a specific bandwidth requirement as illustrated in Fig. 1(c). The lower capacitance also allows for a higher impedance transmission line feed, reducing mismatch to standard 50 Ω sources and therefore lowering drive requirements. The simulated EO responses for several designs meeting common bandwidth targets are shown in Fig. 1(d). For direct comparison of MTP and discrete devices, both were fabricated on the same substrate. Fabricated devices on the native InP substrate are shown in Fig. 2(a). The development of a high-quality etched facet is necessary for MTP integration (shown in Fig. 2(b)). For MTP, two-port devices with input and output on opposite sides of the chip present integration challenges, so it is desirable to have turns to enable single-sided device geometries. This was realized with a convex turning mirror bend demonstrating a measured loss of 1.27 dB per 180˚ bend. This loss was measured via test structures with multiple 180˚ bends as shown in Fig. 2(c). A CAD layout of a single-sided TW EAM with a compact 180˚ turning mirror is shown in Fig. 2(d).

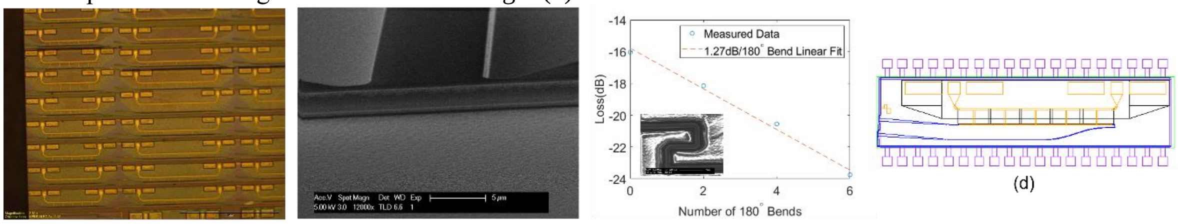

(a) (b) (c)

Fig. 2. (a) Microscope image of fabricated TW modulators; (b) High quality vertical etched facet for MTP devices; (c) Loss measurements for 180˚ bends with inset test structure; (d) CAD layout for single-sided MTP device with 180° turning mirror.

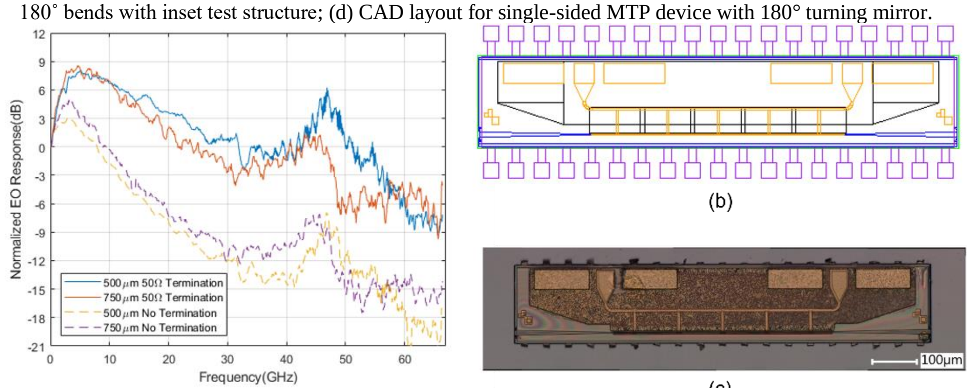

(a)

Fig. 3. (a) Bandwidth measurements of discrete TW modulators; (b) CAD layout of MTP TW EAM (c) TW modulator printed onto bare Si.

Preliminary measurements demonstrate bandwidth up to 56 GHz for a 500 µm long modulator and 30 GHz bandwidth for a 750 µm long modulator, both of which are terminated with a 50 Ω probe impedance. Comparison of resistive and open terminated devices clearly illustrate traveling wave effects (Fig. 3(a)). The peaking near 45 GHz matches closely with the free spectral range of the of the optical waveguides. Simulations show that a lower and on-chip termination of 15 Ω, along with a 25 pF capacitor, would enable a bandwidth in excess of 100 GHz for both 500 µm and 750 µm long devices. Implementation of lower termination impedance is ongoing. Finally, Fig. 3(b) and Fig. 3(c) show the CAD layout and a microscope image of a TW modulator that was released from the InP and successfully transfer printed to a bare Si wafer respectively. Future work will characterize printed devices and demonstrate alignment and coupling to SiN waveguides on Si.

3. Conclusions

TW modulators with etched facets for MTP were designed and fabricated. Some devices included 180° bends to enable simplified MTP; these bends demonstrated a measured loss of 1.27 dB per 180˚ bend. A 56 GHz bandwidth was measured for a discrete 500 µm TW modulator at wavelength of 1275 nm and using a 50 Ω probe termination. Preliminary MTP on bare Si was also demonstrated.

4. Acknowledgement

The authors acknowledge funding support from DARPA through the LUMOS program. A portion of this work was performed in the UCSB Nanofabrication Facility.

5. References

[1] T. Hirokawa, et al., “Analog Coherent Detection for Energy Efficient Intra-Data Center Links at 200 Gbps Per Wavelength,” J. Lightwave Technol. 39, 520-531 (2021)
[2] M. Jarrahi, et al., “Optical switching based on high-speed phased array optical beam steering,” Appl. Phys. Lett. 92, 014106 (2008)
[3] P. Dong, “Travelling-wave Mach-Zehnder modulators functioning as optical isolators,” Opt. Express 23, 10498-10505 (2015)
[4] R. Loi, *et al*., “Micro-transfer-printing of InP Photonic Devices to Silicon Photonics,” *2019 Photonics & Electromagnetics Research Symposium - Spring (PIERS-Spring)*, 2019, pp. 242-248, doi: 10.1109/PIERS-Spring46901.2019.9017709.

High-Speed SiGe EAMs at Cryogenic Temperatures

Evan Chansky[1], Thomas Dorch[2], Aaron Maharry[1], Roshanak Shafiiha[3], Guomin Yu[3], Aaron Zilkie[3], Steven Estrella[1,2], Larry Coldren[1], Clint Schow[1]

[1] Department of Electrical & Computer Engineering, University of California Santa Barbara, Santa Barbara, CA, USA

[2] Freedom Photonics LLC., Goleta CA, USA

[3] Rockley Photonics Inc., Pasadena, CA, USA

***Abstract*—Electro-optic modulators capable of operating at cryogenic temperatures are of interest to a host of sensing, quantum, and supercomputing applications. Silicon photonics is compelling for its low cost and CMOS compatibility, but conventional tuning mechanisms are impacted at low temperatures. Bulk electro-absorption modulators are appealing since only the wavelength of the absorption band edge varies with temperature. Cryogenic effects on a fabricated high-speed modulator are shown, with consistent extinction ratio from 5-300K. (*Abstract*)**

Keywords—Silicon Photonics, cryogenic optical links, Electro-absorption Modulator, EAM, Franz-Keldysh Effect

I. Introduction

High-bandwidth readout from cryogenic environments is desired for a wide range of applications including both classical and quantum supercomputing, infrared focal-plane arrays, and high energy physics experiments. Optical fiber preferrable to electrical cables given their superior loss, bandwidth, and low thermal conductivity. However, development of energy efficient and easily manufacturable electro-optic modulators capable of operating at cryogenics is still required. Silicon photonics are appealing for their low-cost and CMOS compatibility, but most conventional electro-optic mechanisms in Si break down at low temperatures. Even ignoring the large heat dissipation, the thermo-optic coefficient of Silicon decreases by multiple orders of magnitude at 5K from 300K rendering thermal tuning inadvisable. Junction-based devices in Si are impacted by carrier freeze-out below 40K but spoked micro rings have shown promising results so far [1].

Electro-absorption modulators (EAMs) offer a compromise between mm-scale Mach-Zehnder modulators (MZMs) and compact (~10 um) but sensitive ring resonator modulators (RRMs). Including control electronics for resonance stabilization puts RRMs on the same size scale as EAMs but it should be noted that novel link architectures could remove stabilization from the cold environment [2].

To date, there has only been one investigation of the behavior of EAMs at cryogenic temperatures [3] which showed that bulk EAMs making use of the Franz-Keldysh Effect (FKE) fared better than the more sensitive quantum well QCSE devices. However, this investigation was limited to 77K, had a low bandwidth, and required impressive but still experimental fabrication techniques. In this work a SiGe bulk EAM initially intended for datacenter operation at 1550 nm at 60°C (343K) and has demonstrated 50 Gbps modulation at room temperature [4].

II. Experimental Setup

Devices were fabricated in a Rockley Photonics multi-micron process [5] and epoxied to a printed circuit board (PCB), fiber attached with a pigtail fiber array unit (FAU), and wirebonded. Due to inaccessible bondpads, a second PCB with a cutout was brought over the PIC to shorten the wirebonds. Additional height clearance was given to the signal bond to avoid a short from thermal expansion, but the length can be reduced in future builds. The completed assembly was secured in a cryostat with coaxial cable and fiber vacuum feedthroughs to be cooled with liquid He. Insertion loss sweeps were obtained from 1240-1640nm using three EXFO T100S-HP tunable lasers (O+, ES, and CL band varieties) which were controlled by an EXFO CTP10 passive optical component tester as shown in Fig. 1(a-b). DC biases and IV sweeps were controlled by a Keithley 2401. At intervals of 5K, from 300K to 5K, a current voltage (IV) sweep was taken first, followed by insertion loss sweeps biased at 0V, -1V, -3V, and -5V. At 300K and 5K, electro-optic bandwidth measurements were acquired with an Agilent HP 8073A lightwave component analyzer.

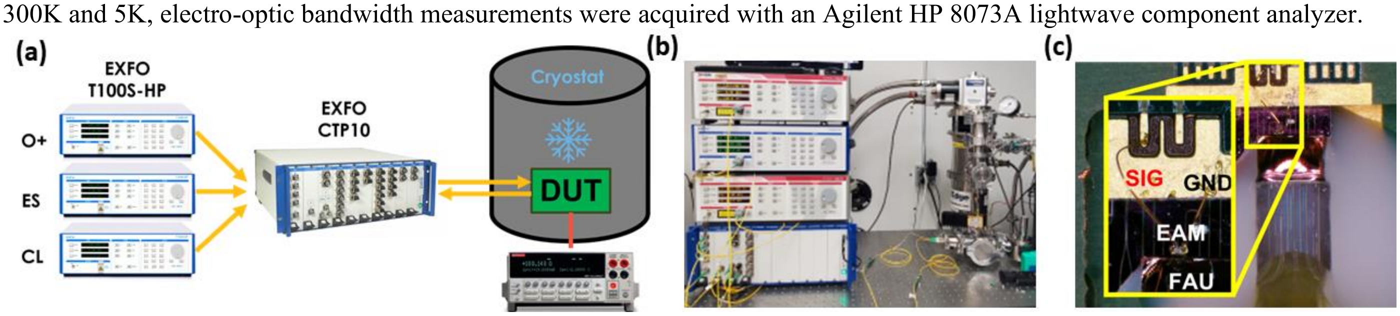

Fig. 1. Experimental setup for insertion loss sweeps from 1260-1640 nm using an EXFO CTP10 and TS-100HP lasers (a) system diagram (b) picture of setup (c) Microscope image of device assembly with fiber attach and wire bonds to PCB

2022 IEEE Photonics Conference (IPC) | 978-1-6654-3487-4/22/$31.00 ©2022 IEEE | DOI: 10.1109/IPC53466.2022.9975738

III. RESULTS AND DISCUSSION

From 300K to 5K, the absorption band edge shifted by around 120 nm, resulting in an operation point around 1400 nm as opposed to 1520 nm at room temperature. Most notably, the strength of the FKE-induced extinction was not impacted at all, just the wavelength at which it peaks. The extinction ratio shown in Fig. 2(a) is defined between 0 V and -5 V bias. The I-V curves in Fig. 2(d) denote a reduction in leakage current at low reverse biases, but DC power consumption is only one component of total power. Capacitance would also need to be measured as a function of temperature to indicate the effects on RF power consumption, which would be largely determined by the required driving electronics.

Due to damage to the fiber attach during assembly, the total coupling loss is 15 dB, although 5 dB was achieved on other assemblies. Insertion loss of the EAM itself was measured to be 7 dB by calibrating to a waveguide loopback test structure on chip. Fig. 2(e) shows the electro-optic bandwidth at -2 V bias to be about 18 GHz and unaffected by temperature. The 5K measurement was done with a wavelength of 1390 nm resulting in an 18.3 GHz bandwidth, whereas the 300K curve was at a wavelength of 1530 nm and produced an 18.7 GHz bandwidth. Test equipment, including cabling and bias tees were calibrated out, but device packaging parasitics remain. The long wire bonds for the complex assembly shown in Fig. 1(c) are limiting the speed of the device which has previously been open eye diagrams at 50 Gbps with high-speed probes [4]. Despite packaging limitations, this device has a high bandwidth compared to existing cryogenic modulators require more complex fabrication.

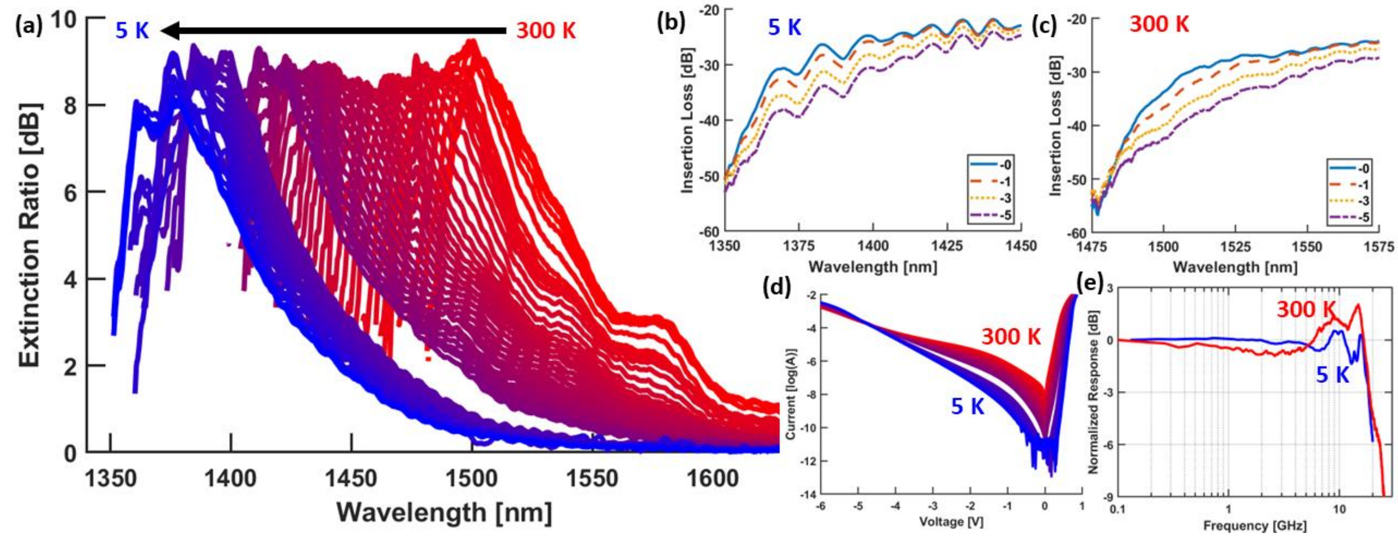

Fig. 2. Temperature dependent data (a) Extinction ratio between at 0 and -5 V bias (b) Insertion loss at cryogenic temperature (c) Insertion loss at room temperature (d) I-V characteristics from 300K-5K (e) Electro-optic bandwidth at 300K and 5K

IV. CONCLUSION

Bulk EAMs provide a promising mechanism for electro-optic modulation at cryogenic temperatures and shows little degradation in the extinction ratio or 18 GHz bandwidth from 300K to 5K. However, a shift in wavelength by about 120 nm is observed due to the temperature dependence of the absorption edge. More high-speed characterization is required to investigate the expected power consumption and heat dissipation and a new assembly can improve the packaged device's performance.

ACKNOWLEDGMENTS

The authors would like to thank Andre Dubois at Tritek Solutions and Lawrence Van der Vegt of EXFO for technical support, Junqian Liu for wire bonding assistance, and Paolo Pintus, Yujie Xia, and Xinhong Du for their insight.

REFERENCES

[1] H. Gevorgyan, et al., "Cryo-Compatible, Silicon Spoked-Ring Modulator in a 45nm CMOS Platform for 4K-to-Room-Temperature Optical Links," in *Optical Fiber Communication Conference (OFC)*, 2021.

[2] S. B. Estrella et al., "Novel Link Architecture Minimizing Thermal Energy Dissipation for Cryogenic Optical Interconnects," in *Optical Fiber Communications Conference and Exhibition (OFC)*, 2021.

[3] P. Pintus, et al., "Characterization of heterogeneous InP-on-Si optical modulators operating between 77 K and room temperature.," *APL Photon.,* vol. 4, p. 100805, 2019.

[4] A. H. Talkhooncheh, A. Zilkie, G. Yu, R. Shafiiha and A. Emami, , "A 100 Gb/s PAM-4 Silicon Photonic Transmitter with Two Binary-Driven EAMs in MZI Structure," in *2021 IEEE Photonics Conference (IPC)*, 2021.

[5] A. Zilkie, et al., "Multi-micron silicon photonics platform for highly manufacturable and versatile photonic integrated circuits,”," *IEEE Journal of Selected Topics in Quantum Electronics,* vol. 25, no. 5, pp. 1-13, 2019.

Monolithic Indium Phosphide Photonic Integrated Circuit for Remote Lidar Active Carbon Dioxide Sensing

Fengqiao Sang[1*], Victoria Rosborough[1], Joseph Fridlander[1], Fabrizio Gambini[2], Simone Šuran Brunelli[1], Jeffrey R. Chen[2], Stephan R. Kawa[2], Kenji Numata[2], Mark Stephen[2], Larry Coldren[1], Jonathan Klamkin[1]
[1]*Electrical and Computer Engineering Department, University of California, Santa Barbara, Santa Barbara, CA 93106 USA*
[2]*NASA Goddard Space Flight Center, Greenbelt, MD 20771 USA*
[*]*fsang@ece.ucsb.edu*

Abstract: A monolithic indium phosphide photonic integrated circuit was designed and fabricated for remote active carbon dioxide sensing. Successful measurement of carbon dioxide in a laboratory setting under pulsed sampling was demonstrated.

1. Introduction

Several investigations and demonstrations have been carried out for passive carbon dioxide (CO_2) sensing and monitoring including the OCO-3 from NASA and GOSAT-2 from JAXA [1,2]. Different from passive sensing, which utilizes reflection of solar light, active sensing uses a laser light source for sensing. Laser remote-sensing techniques allow accurate measurements to be taken day and night, over ocean and land surfaces, in the presence of thin and/or scattered clouds, at all times of year, and with less susceptibility to bias errors [3], however space-based laser instruments can be large and power hungry. To reduce the size, weight, and power (SWaP) of such systems, one based on photonic integrated circuit (PIC) technology was designed and demonstrated for active CO_2 sensing. The indium phosphide (InP) PIC platform can integrate both active and passive components making it ideal for this application [4,5]. In this work, we have designed and fabricated InP PICs for active CO_2 sensing and successfully demonstrated sampling of the 1572.335 nm CO_2 absorption line under pulsed sampling.

2. Lidar Photonic Integrated Circuit Demonstration

The InP PIC leverages a dual-laser architecture that integrates a leader laser and a follower laser, splitters, a phase modulator, a photodiode, and a pulse carver based on a semiconductor optical amplifier (SOA). The PIC system is shown in Fig. 1. The system can be divided into two main parts, that for the leader laser stabilization and that for the follower laser offset locking. The leader and follower lasers are both sampled grating distributed Bragg reflector (SGDBR) lasers. The leader laser functions as an absolute optical reference for the follower laser; the leader is locked to the center of the CO_2 absorption line with a CO_2 reference cell using the frequency modulation technique [6-8]. While locked, it achieves a 44.5 dB side mode suppression ratio as shown in Fig. 2(a). The corresponding error signal

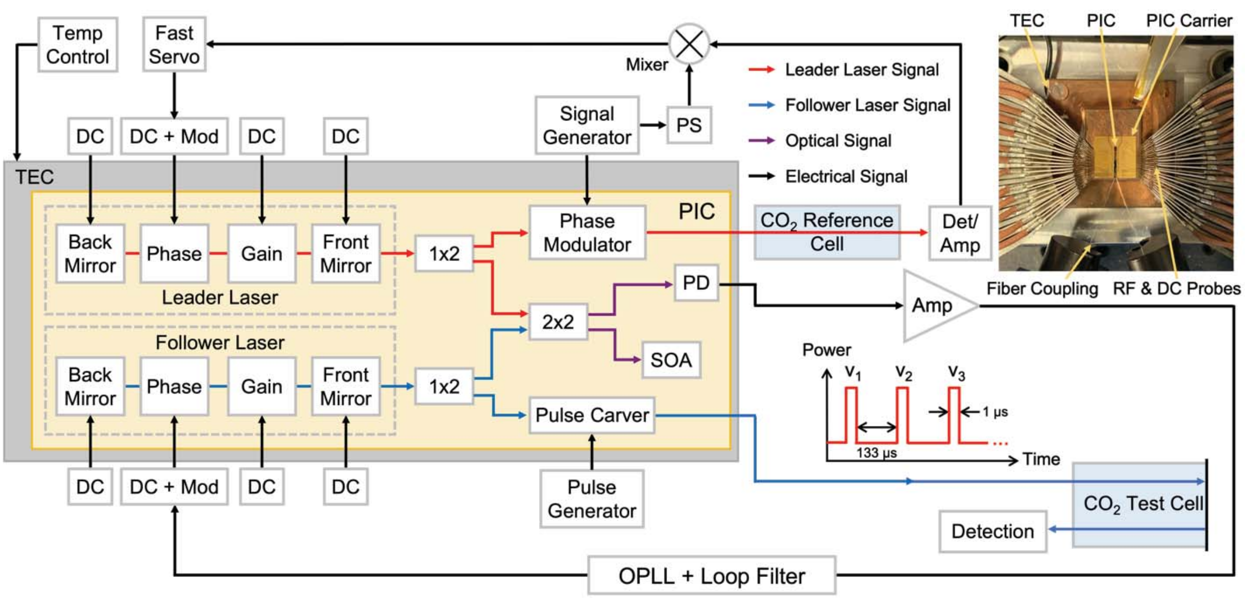

Figure 1: PIC details and system architecture for CO_2 sensing along with photograph of PIC on carrier under test.

used for the locking is shown in Fig. 2(c). The follower laser is offset locked to the leader laser by way of the integrated beat note photodiode and an optical phase lock loop (OPLL) [7-9]. From the OPLL electronics, the leader laser can be controlled to sweep over a 30 GHz range centered at 1572.335 nm to enable sensing measurement [9-11]. The SOA pulse carver converts the continuous wave (CW) output into a frequency-stepped pulse train with 1 μs pulse width and 133 μs period to prevent crosstalk between wavelengths due to cloud scattering [7,9]. The pulsed output achieved an extinction ratio of 45 dB as shown in Fig. 2(b).

The leader laser stabilization performance was also characterized, and results are shown in Fig. 2(d). Over a period of 30 minutes, the peak-to-peak frequency drift without feedback was around 675 MHz. With feedback, the drift was 2.7 MHz, demonstrating an improvement of 24 dB. The follower laser stabilization is shown in Fig. 2(e). The peak-to-peak frequency drift compared to leader laser without the OPLL engaged was around 1 GHz, and with the OPLL it was 29 kHz thereby demonstrating an improvement of more than 45 dB. Finally, a sensing experiment was successfully performed under pulsed sampling and the results are shown in Fig. 2(f). A Lorentzian fitted full-width half maximum of 1600 MHz was demonstrated.

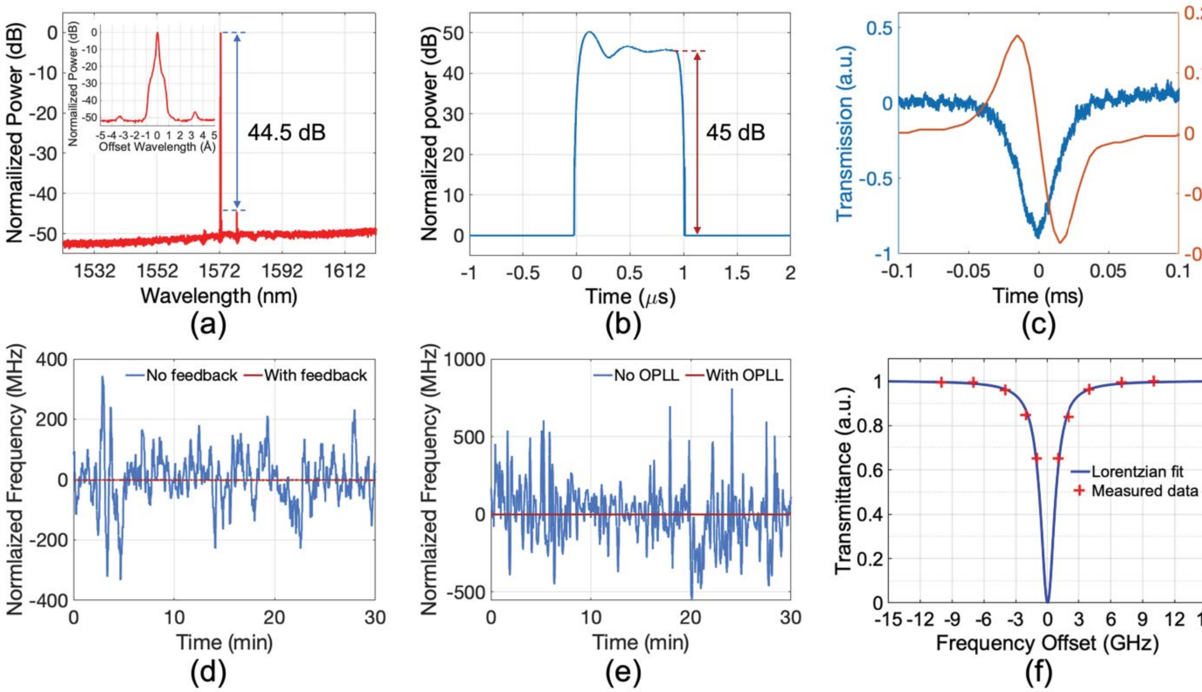

Figure 2: (a) Optical spectrum of leader laser when locked to 1572.335 nm with zoomed in spectrum inset. (b) Pulsed output optical signal after pulse carver. (c) CO_2 reference cell absorption and the frequency-discriminating error signal. (d) Beat note between the leader laser and an external cavity laser with and without feedback to the leader laser phase section. (e) Beat note between the leader and follower laser with and without the OPLL engaged. (f) Measured absorption of a CO_2 test cell at several wavelengths overlaid with a Lorentzian fit.

3. Conclusions

We designed and fabricated InP PICs for CO_2 active remote Lidar sensing. The PIC-based Lidar system successfully demonstrated CO_2 active sensing in a laboratory environment under pulsed sampling. Future work will focus on packaging and photonic-electronic integration to further reduce SWaP of the overall system.

4. References

[1] Srivastava, Priyanka, et al. IGARSS 2020-2020 IEEE International Geoscience and Remote Sensing Symposium. IEEE, 2020.
[2] Glumb, Ronald, et al. 2014 IEEE Geoscience and Remote Sensing Symposium. IEEE, 2014.
[3] Abshire, James B., et al. Lidar Technologies, Techniques, and Measurements for Atmospheric Remote Sensing VI. Vol. 7832. International Society for Optics and Photonics, 2010.
[4] Zhao, Hongwei, et al. IEEE Journal of Selected Topics in Quantum Electronics 25.6 (2019): 1-10.
[5] Isaac, Brandon J., et al. IEEE Journal of Selected Topics in Quantum Electronics 25.6 (2019): 1-7.
[6] Bjorklund, Gary C. Optics letters 5.1 (1980): 15-17.
[7] Numata, Kenji, et al. Applied optics 50.7 (2011): 1047-1056.
[8] Numata, Kenji, et al. Optics express 20.13 (2012): 14234-14243.
[9] Fridlander, Joseph, et al. IEEE Journal of Selected Topics in Quantum Electronics (2021).
[10] Fridlander, Joseph, et al. 2021 Conference on Lasers and Electro-Optics (CLEO). IEEE, 2021.
[11] Sang, Fengqiao, et al. 2021 IEEE International Geoscience and Remote Sensing Symposium IGARSS. IEEE, 2021.

From coupled cavities to photonic ICs—
It didn't begin with lasers

(1968-1978) Surface Acoustic Waves (SAW)

Stanford — Bell Labs

- $v_a \sim 10^{-5}\, v_l$ → ~3 µs/cm vs ~3 µs/km for fiber
- SAW wavelength @ UHF ~ near IR photonic wavelengths
- Large time-bandwidths possible on small crystals → [0.5GHz x 3 µs = 1500]

- Typical SAW filter:

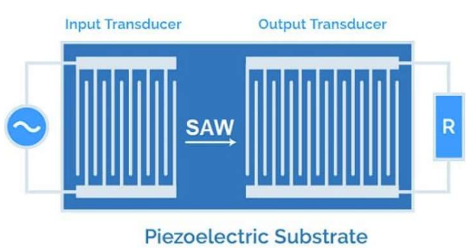

- In this time period, SAW most useful in defense applications—radar, electronic warfare

Monolithic Acoustic Surface Wave Amplifier

(PhD work: 1969-72)

- Traveling-wave amplifier—interaction of carriers and the acousto-electric field due to the piezoelectric effect
- Drift carriers faster than the velocity of acoustic waves for gain
- Vacuum deposition of InSb on $LiNbO_3$ (*Heterogeneous integration*)

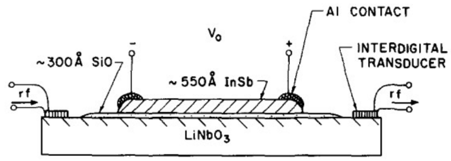

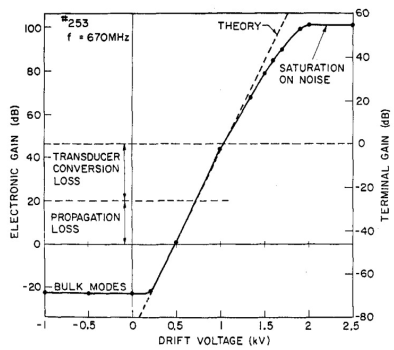

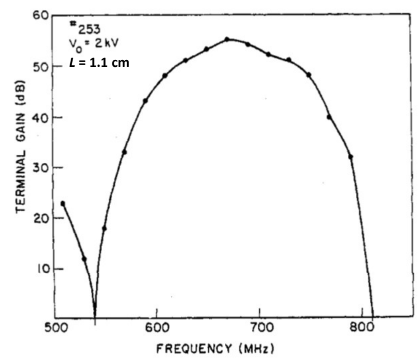

L. A. Coldren, *PhD Thesis Stanford*—same title (1972); also L. A. Coldren and G. S. Kino, " The InSb on piezoelectric Rayleigh wave amplifier, " *IEEE Trans. Electron Devices*, **ED-21** (7), July, 1974.

Wrap-around Long-delay Lines

- ~3 µs/cm
- Bell Labs interested in Frame store for Picture Phone
- Digital storage limited to 1 kb/DIP package in 1972 → entire 6 ft cabinet for frame

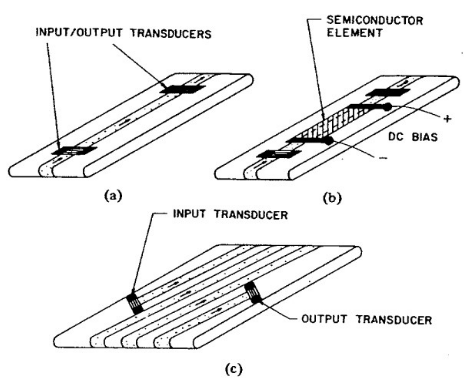

$Bi_{12}GeO_{20}$ delay lines

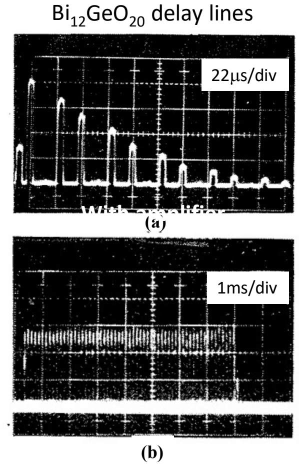

L. A. Coldren and H. J. Shaw, *Proc. of the IEEE*, **64** (5) 1976

ZnO/Si Signal/Image Storage Read by Two Interfering SAWs

Bell Labs

Nonlinear SAW correlators weighted by stored charge at ZnO/SiO2 interface (charge could be modulated by light)

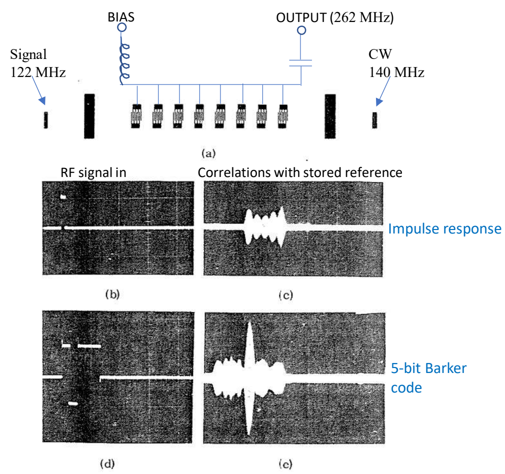

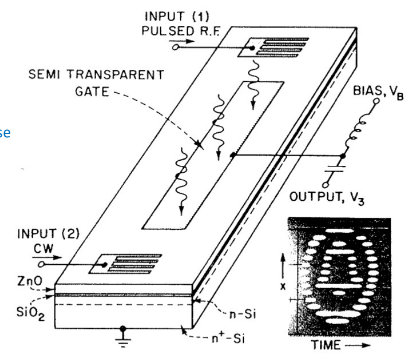

L. A. Coldren, *Appl. Phys. Letts*, **26** (4) (1975)

L. A. Coldren, *Appl. Phys. Letts*, **27** (1) (1975)

See also, L. A. Coldren, *Proc. of the IEEE*, **64** (5) (1976)

SAW Resonator Filters (1974-1979)

L. A. Coldren and R. L. Rosenberg, *Proc. of the IEEE*, **67** (1) 1979

Bell Labs

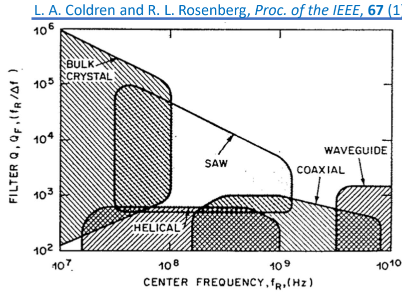

Two-port single-section

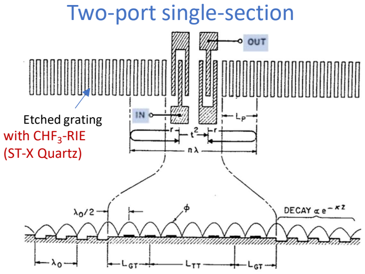

Transfer function from Scattering Theory (C_0 resonated out):

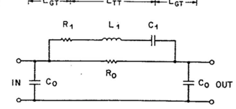

$$T \approx \frac{t^2(1+r)^2}{1 - r^2 t^4\left[1 - S_{13}^2(2 + 1/r + 1/rt^4)\right]}\, S_{13}^2, \qquad |S_{13}|^2 << 1.$$

Example:

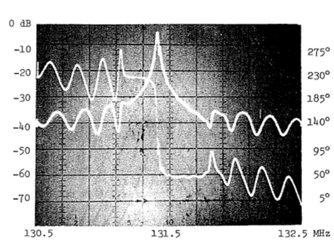

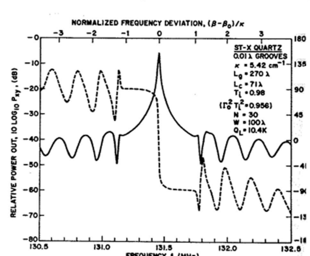

Two-section SAW Resonator Filters (and higher-order)

Bell Labs

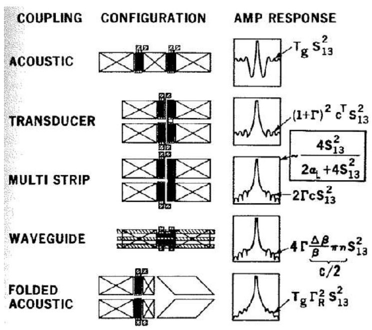

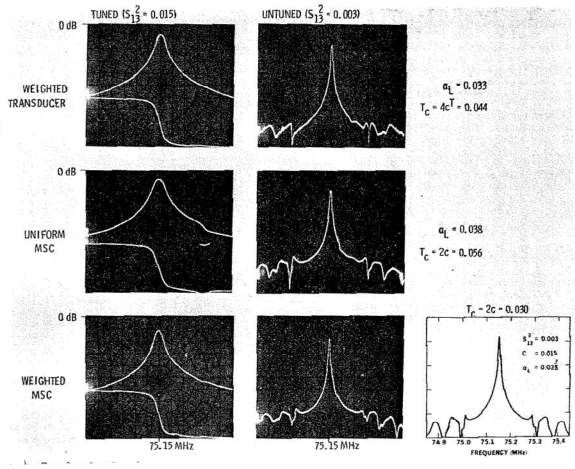

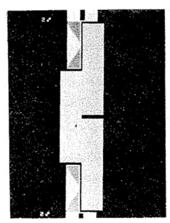

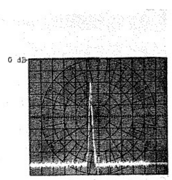

4-section MSC result

- Scattering theory worked well

L. A. Coldren and R. L. Rosenberg, *Proc. of the IEEE*, **67** (1) 1979

7

SAW Filters (Today) > $5B market

Applications:

Smart phones and tables	Radar
GPS	Aerospace
WiFi	RFID sensors
Wireless Sensing	Digital TV
Base Stations	

The global surface acoustic wave (SAW) filters market size was valued at $4.56 billion in 2020, and is projected to reach $9.94 billion by 2030, registering a CAGR of 8.5% from 2021 to 2030.

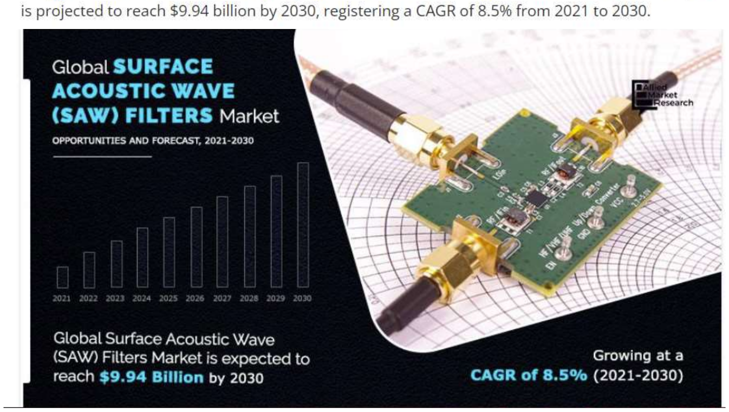

Allied Market Research®

Author(s) : N N Kundan, Asavari Patil , Vineet Kumar

8

Energy to transport a bit across the ocean—TAT-8 first optical system (used SAW—TR filters)

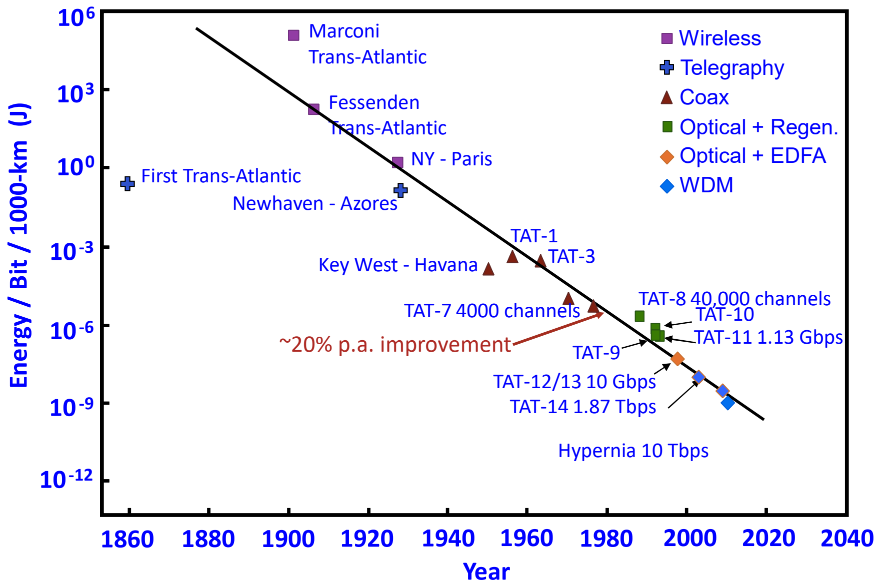

IEEE Fellow

- 1982
- No mention of photonics

Early Tunable, Single-Frequency Diode Lasers

Bell Labs

- Coupling mirrors between integrated active and passive sections

First integrated InP (laser – X) devices

→ Etched grooves/RIE: Cl-Ar-O_2

- Tunable single frequency @ 1.3 µm
- Laser-modulator
- Laser-detector

L.A. Coldren, B.I. Miller, K. Iga, and J.A. Rentschler, "Monolithic two-section GaInAsP/InP active-optical-resonator devices formed by RIE," *Appl. Phys. Letts.*, 38 (5) 315-7 (March, 1981).

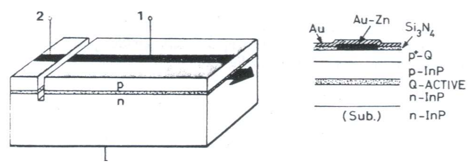

→ DBR gratings

- Tunable single frequency @ 1.55 µm
- Combined integration technologies

Y. Tohmori, Y. Suematsu, Y. Tushima, and S. Arai, "Wavelength tuning of GaInAsP/InP integrated laser with butt-jointed built-in DBR," *Electron. Lett.*, 19 (17) 656-7 (1983).

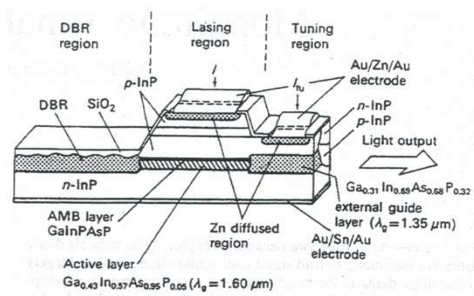

Vernier Tuning Between Modes of Two Cavities

Bell Labs

- **Long-short configuration more stable**

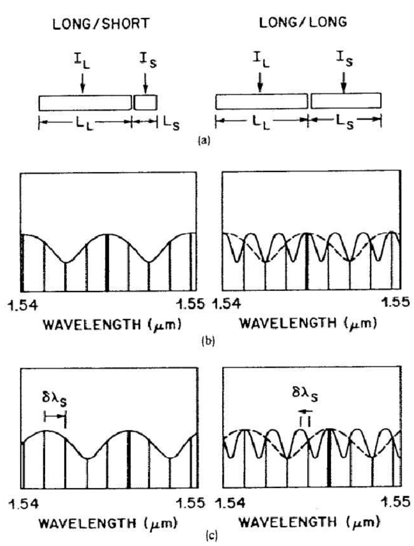

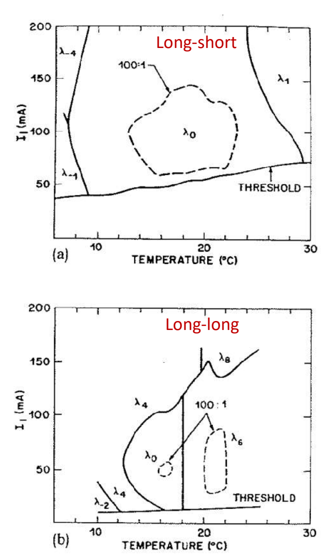

Early Tuning Result with Etched Coupling Grooves

Bell Labs

Monolithic two-section tunable laser

-- Broad-area lasers

-- No regrowth required

-- Single longitudinal mode (> 20:1) with short pulses

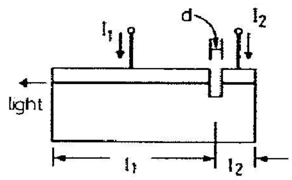

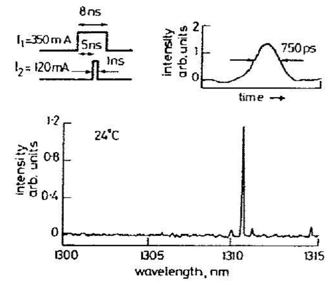

Tuning between two modes of short cavity ~7 nm)

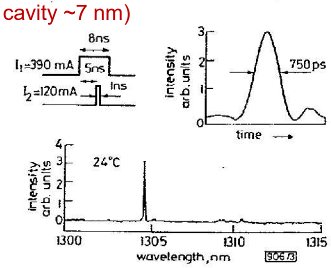

K. J. Ebeling, L. A. Coldren, B. I. Miller, J. A. Rentschler, "Generation of single-longitutional mode subnanosecond light pulses by high-speed current modulation of monolithic two-section semiconductor lasers," *Electronic Letts*., **18** (21) 901-902 (Oct.,1982).

Early Tunable DBR Work

Pioneering Active-Passive interfaces

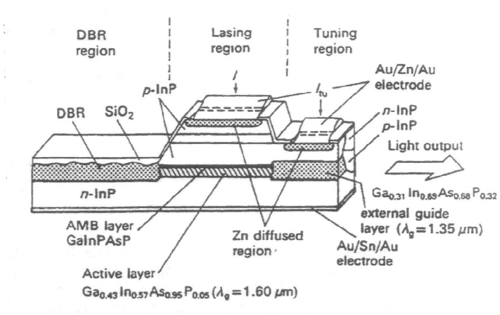

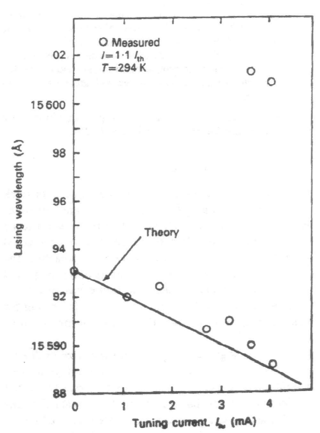

Tohmori, Suematsu, Tushima, and Arai, TIT, 1983

No-Regrowth Groove Etch: RIE/HCl/Q-etch/HCl

Bell Labs

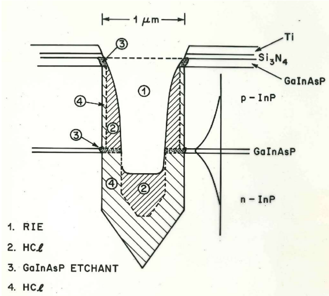

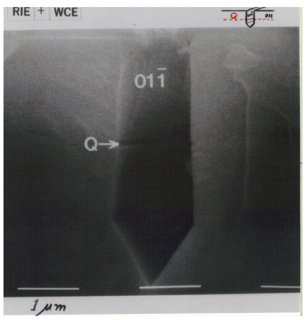

Threshold current density versus reciprocal cavity length (1/*l*) for cleaved and etched facet broad-area lasers.

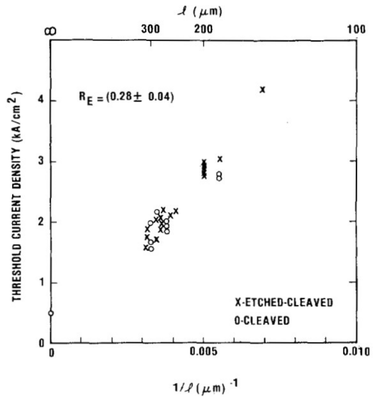

→ Kaz also demonstrated integrated polymer waveguide external cavity.

L. A. Coldren, K. Furuya, B. I. Miller and J. A. Rentschler, "Etched mirror and groove-coupled laser devices for integrated optics," *J. Quantum Electron.* **QE-18** (10) 1679-1688, Oct., 1982

15

UCSB

1984—One Year After Bell System Breakup

16

1980s: MBE; more MBE; and founding of Materials Dept.

Early MBE/Kroemer

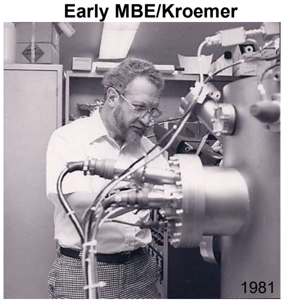

Physics/Electronics

Later MBE: 2 Gen-2s

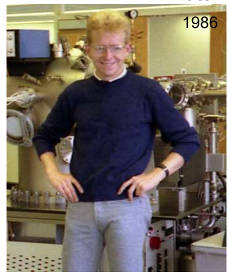

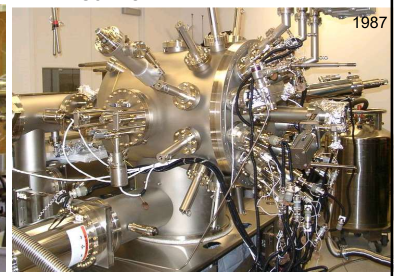

Electronic Materials Founders

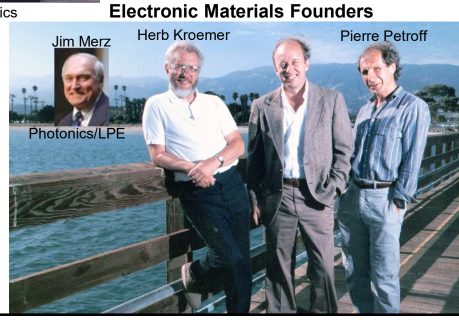

Materials Department (1986)

Slightly later ('87)

Art Gossard
Director of MBE Lab

John Bowers

Evelyn Hu later

17

Excellent MBE Enables Good Vertical-Cavity Modulators and Lasers

Reflection Modulator ('86-'91)

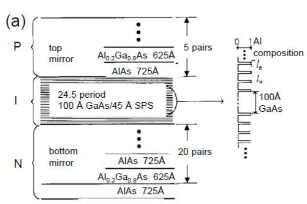

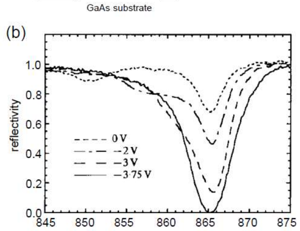

Asymmetric Resonant-cavities

K. K. Law, M. Whitehead, J. L. Merz, and L. A. Coldren, *Electron. Lett.* **27**, 1863 (1991).

VCSEL ('87→)

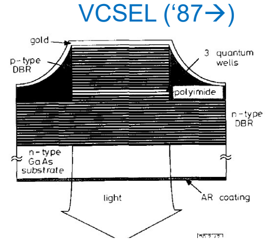

Gain limited to standing wave peaks (2X modal gain)

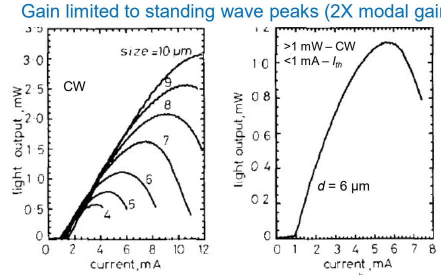

R. S. Geels & L. A. Coldren, *Electron. Letts*.,vol 27, no. 21, Oct., 1991

Recent Review: Larry A. Coldren, "Review of key vertical-cavity laser and modulator advances enabled by advanced MBE technology," JVST-A **39,** 010801 (2021); doi: 10.1116/6.0000574—tribute to Prof. A.C. Gossard.

18

UCSB

Tunable DBR Lasers (mid-late 1980's)

- One cavity: tune cavity modes and mode selection filter separately (or together)
- Coherent and WDM

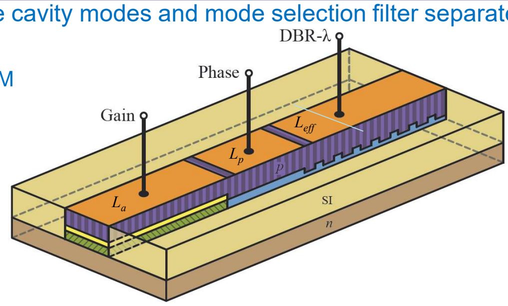

- The center wavelength of grating, λ_g, will tune in direct proportion to the index change Δn_{DBR}; however this will also tune the mode slightly as well, due to the penetration, L_{eff}.
- Tuning the Phase section electrode will tune only the mode location, λ_m, (tune together with DBR for wide continuous tuning: *JQE* **23** (6) 903, June, 1987)
- There also may be some slight active region index change (due to loss changes)

Limit on tuning range →
$$\frac{\Delta\lambda_g}{\lambda_g} = \frac{\Delta\bar{n}_{DBR}}{\bar{n}_{DBR}}. \approx 0.5\%$$
~ 7 nm @ 1.5 μm

$$\frac{\Delta\lambda_m}{\lambda_m} = \frac{\Delta\bar{n}_a L_a + \Delta\bar{n}_p L_p + \Delta\bar{n}_{DBR} L_{eff}}{\bar{n}_{ga} L_a + \bar{n}_{gp} L_p + \bar{n}_{gDBR} L_{eff}}.$$

UCSB

Multi-element Mirror 4-Section Tunable Laser

United States Patent [19] — Coldren

[11] Patent Number: 4,896,325

[45] Date of Patent: Jan. 23, 1990

[54] MULTI-SECTION TUNABLE LASER WITH DIFFERING MULTI-ELEMENT MIRRORS

[75] Inventor: Larry A. Coldren, Santa Barbara, Calif.

[73] Assignee: The Regents of the University of California, Berkeley, Calif.

[21] Appl. No.: 235,307

[22] Filed: Aug. 23, 1988

[51] Int. Cl.⁴ H01S 3/10

[52] U.S. Cl. 372/20; 372/99; 372/102; 372/38; 372/31; 372/29

[58] Field of Search 372/101, 20, 92, 99, 372/102, 29, 32, 38

[56] References Cited

U.S. PATENT DOCUMENTS

4,358,851 11/1982 Scifres et al. 372/6
4,504,950 3/1985 Au Yeung 373/101

OTHER PUBLICATIONS

Akiba et al.; "Self-Focusing Lens as Resonator enables 10 GHz Modulation"; Fiberoptic Technology Oct. 1981, p. 124.

Primary Examiner—Leon Scott, Jr.
Attorney, Agent, or Firm—Donald A. Streck

[57] ABSTRACT

An improvement for allowing selective tuning of the emitted beam over a broad bandwidth to a diode laser having an active section for creating a light beam by spontaneous emission over a bandwidth around some center frequency and for guiding and reflecting the light beam between a pair of mirrors bounding the active on respective ends thereof to create an emitted beam of laser light. The mirrors each have narrow, spaced reflective maxima with the spacing of the reflective maxima of respective ones of the mirrors being different whereby only one the reflective maxima of each of the mirrors can be in correspondence and thereby provide a low loss window at any time. The preferred mirrors each include a plurality of discontinuities to cause the narrow, spaced reflective maxima wherein the spacing of the discontinuities of one mirror is different from the spacing of the discontinuities of the other mirror so as to cause the wavelength spacing of the maxima to be different. Additionally, the preferred embodiment includes a vernier circuit operably connected to the mirrors for providing an electrical signal to the mirrors which will cause continuous tuning within a desired frequency band, an offset control circuit operably connected to the mirrors for providing a voltage signal to the mirrors which will shift the reflective maxima of the mirrors into alignment at a desired frequency mode, and a phase control circuit for adjusting the laser mode wavelength to be in correspondence with the low loss window.

27 Claims, 3 Drawing Sheets

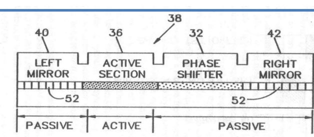

FIG. 5

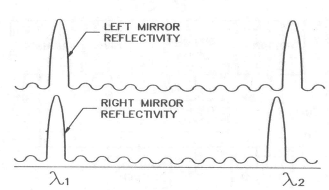

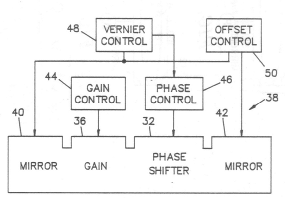

- **Vernier tuning of DBR mirror 'super modes'**
  (much wider spacing than cavity modes)

DESCRIPTION OF THE PREFERRED EMBODIMENT

The novel four section tunable laser of the present invention is shown in simplified form in FIG. 5 where it is generally indicated as 38. By combining discrete mode-jump tuning with continuous tuning, it will be seen that this design allows the relative tuning range to be extended by at least an order of magnitude larger than Δn/n. To achieve the objectives, two multi-element mirrors 40, 42 are employed, one at each end of the laser 38. The gain section 36 and phase shifter section 32 are as described above with respect to the three-section laser of FIG. 3, of which this is an improvement

UCSB — Sampled-Grating DBR Tunable Laser

- Initial results
- 3 sections—vernier tuning

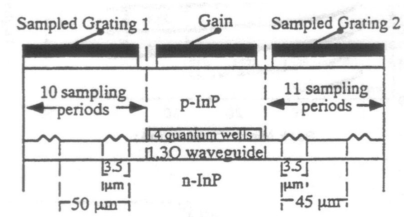

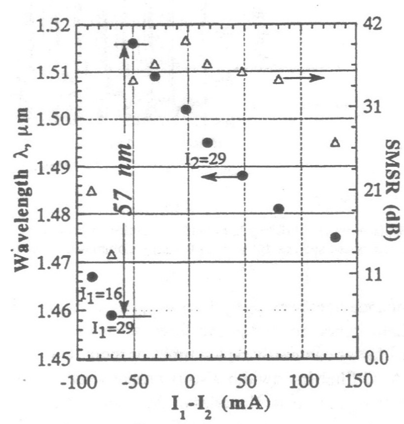

V. Jayaraman, A. Mathur, L.A. Coldren and P.D. Dapkus, ISLC 1992

21

UCSB — Super-structure Grating DBR laser

Distributed reflector and wavelength-tunable semiconductor laser

Tohmori, Yoshikuni, Ishii, Kano, Tamamura --filed 3/3/1993

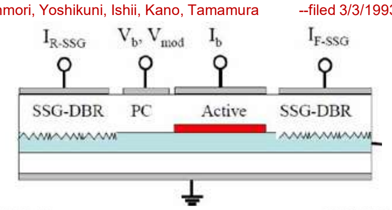

U.S. Patent June 28, 1994 Sheet 3 of 18 5,325,392

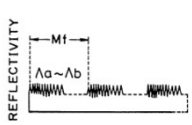

FIG.3A

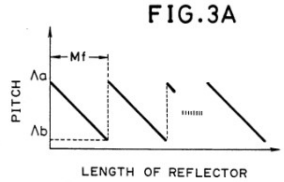

FIG.3B

NTT-NEL

IEEE JOURNAL OF QUANTUM ELECTRONICS, VOL. 32, NO. 3, MARCH 1996

Quasicontinuous Wavelength Tuning in Super-Structure-Grating (SSG) DBR Lasers

Hiroyuki Ishii, Hiromasa Tanobe, Fumiyoshi Kano, *Member, IEEE*, Yuichi Tohmori, *Member, IEEE*, Yasuhiro Kondo, *Member, IEEE*, and Yuzo Yoshikuni, *Member, IEEE*

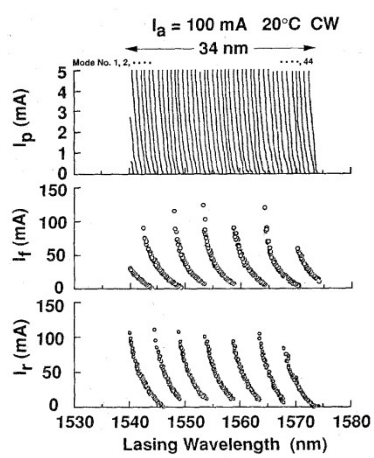

Fig. 12. Quasicontinuous wavelength tuning characteristics with three-tuning-current control.

22

SGDBR wide-tuning, high-power, high-reliability

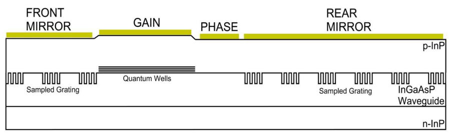

Agility Communications formed to Commercialize in 1998.

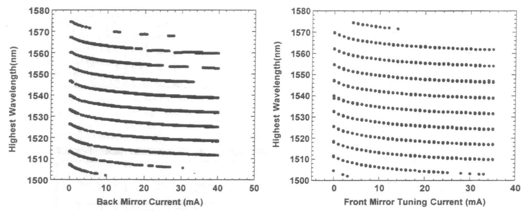

72 nm full wavelength coverage, Agility, 2001.

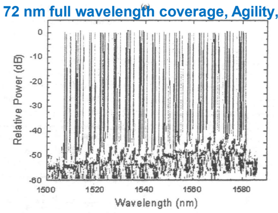

> 300 yr MTTF

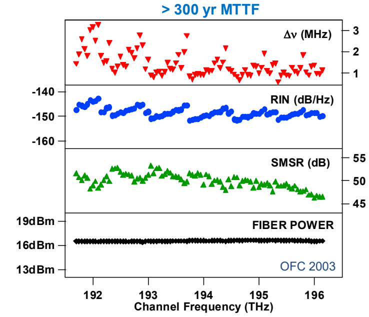

Sampled-Grating DBR: Monolithic and Integrable

SGDBR+X widely-tunable transmitter:
- Foundation of PIC work at UCSB

UCSB'90-- → Agility'99-'05 → JDSU'05→

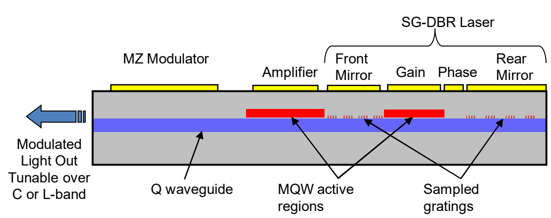

6 section InP chip

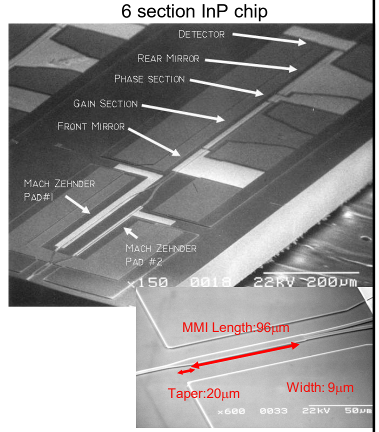

- Vernier tuning over 40+nm near 1550nm
- SOA external to cavity provides power control
- Highly reliable— < 10% of SGDBR is grating
- Integration technology for much more complex PICs*

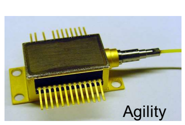

JDSU-ILMZ TOSA (~ 18mm)

~2008

J. S. Barton, et al, *ISLC*, TuB3, Garmish, (Sept, 2002)

PICs (2005-2013)

UCSB

Wavelength converters/switches

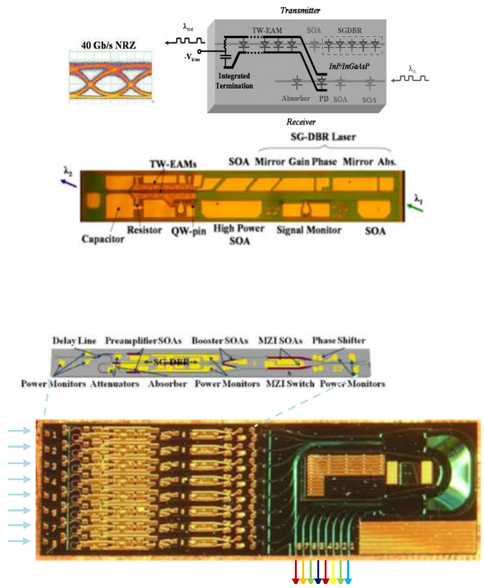

OPLL-Coherent RX & Beam Sweepers

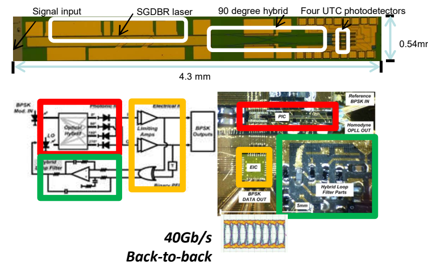

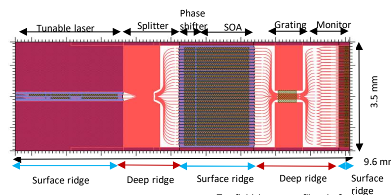

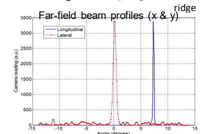

*For more information see: L. A. Coldren, et al, "A Review of Photonic Systems-on-Chip Enabled by Widely-Tunable Lasers," *IEEE J. Quantum Electron.*, **58**(4):1-1 August 2022; doi: 10.1109/JQE.2022.3168041

PICs (2015-2022)

UCSB

RF/fiber & trace gas detection

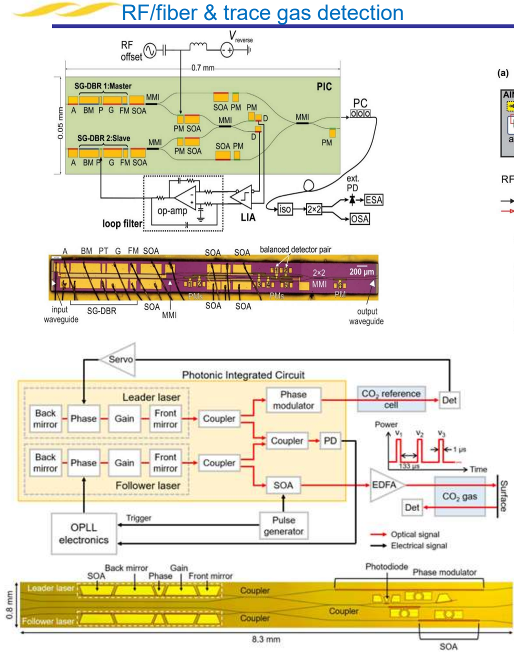

Rapid locking to narrowline microresonator

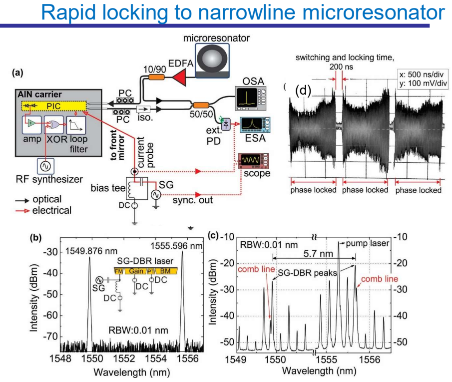

< 1 kHz linewidth

*For more information see: L. A. Coldren, P.A. Verrinder, J. Klamkin, "A Review of Photonic Systems-on-Chip Enabled by Widely-Tunable Lasers," *IEEE J. Quantum Electron.*, **58**(4):1-1 August 2022; doi: 10.1109/JQE.2022.3168041

Improved Dry etching & Flattened Ring Resonator Laser

- $Cl_2/H_2/Ar$ (9/18/2 sccm) ICP (Inductively-Coupled Plasma) etching at a chamber pressure of 1.5 mT.

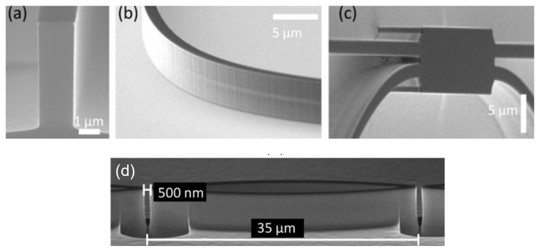

Scanning electron microscope (SEM) images of the etched waveguides showing: (a) 5 µm deep etch with vertical sidewalls, (b) waveguide bends with smooth sidewalls, (c) multimode interference (MMI) couplers, and (d) flattened ring-resonator laser with frustrated total-internal-reflection mirrors.

J.S. Parker, E.J. Norberg, Y.J. Hung, B. Kim, R.S. Guzzon, L.A. Coldren, "InP/InGaAsP Flattened Ring Lasers with Low-loss Etched Beam Splitters", *Photonics Technology Letters*, **23**, (9), pp. 573-575 (May 2011)

Micro-transfer Printing of III-V chips on Si-Photonics
(etched facets inherent)

Integration of III-V light sources on a silicon photonics circuit by transfer printing

Joan Juvert, Tommaso Cassese, Sarah Uvin, Andreas De Groote, Brad Snyder, Peter De Heyn, Peter Verheyen, António José Trindade, Christopher Bower, Marco Romagnoli, Günther Roelkens, and Dries Van Thourhout

2017 IEEE 14th International Conference on Group IV Photonics (GFP)
23-25 August 2017, Berlin, Germany

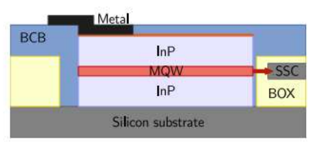

Fig. 1. Sketch of the integration approach. The III-V coupon is transfer printed directly in a trench in the buried oxide. No adhesive layer is used for the bonding. The output of the MQW device is directly coupled to a trident spot-size converter, SSC in the picture, in the photonic circuit. The whole structure is passivated with BCB after transfer printing.

- Many other recent publications on µTP. [These guys are not the originators.]
- Current DARPA—LUMOS program is based upon use of this approach

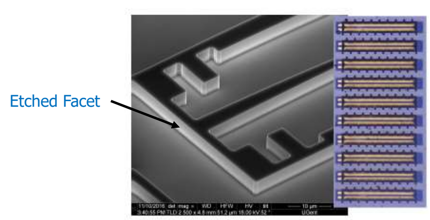

Fig. 2. SEM image of the front side of the main mesa. The trenches inside the mesa define the central waveguide. The notches in the trenches are used for pattern recognition during transfer printing. On the right, an optical image of an array of encapsulated coupons on their native III-V substrate is shown.

Summary
(for students?)

- Etched facets are needed for micro-transfer printing, and they now appear to function as well as cleaved facets.
- You never know where your current project will lead you, so best to be enthusiastic about it and learn what you can from it.
- The things that are different from the mainstream about your project may be the most important. Don't always follow the crowd.
- Unexpected results are not failed results, they provide learning opportunities. If your experiment gives the expected results, you may be happy, but you probably haven't learned anything new.

Backup

Narrow-linewidth Thermally-tuned SGDBR Laser

UCSB

- 70kHz linewidth and 50dB SMSR at +17dBm fiber power over 41nm range in C-band

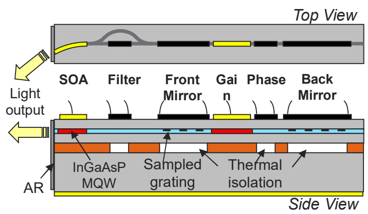

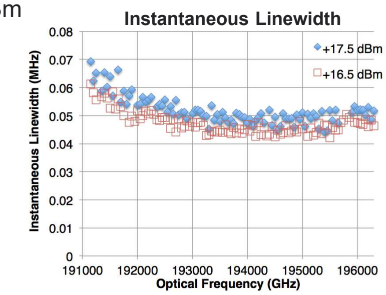

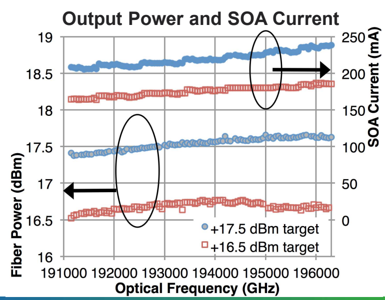

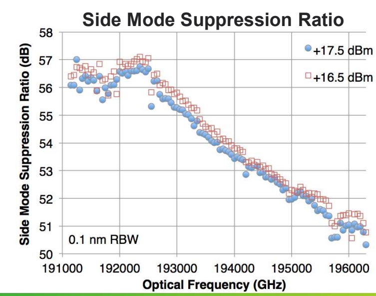

LUMENTUM

M.C. Larson et al., OFC 2015, M2D.1

31

Coupled-Cavity Etched-Groove Tunable Laser with Regrowth

Bell Labs

Monolithic two-section tunable laser

-- BH stripe lasers (CW)

-- BH regrowth simultaneously fills slots

-- Single HCl etch of only InP at mirrors

-- Planar etched facets and slots (all InP)

-- Single longitudinal mode

-- Tunable

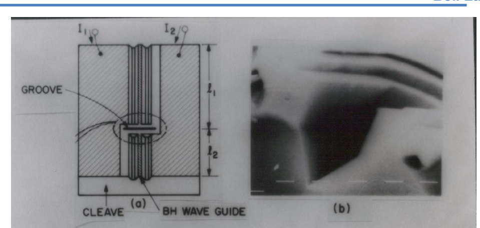

RIE etch, Q-etch, Regrow InP, HCl etch

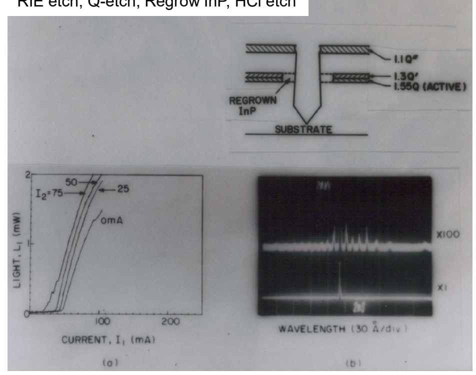

L. A. Coldren, T. L. Koch, T. J. Bridges, E. G. Burkhardt, B. I. Miller, and J. A. Rentschler, "Vapor-phase regrown monolithic two-section window lasers exhibiting DSM operation at 1.55 um," *ISLC*, Rio de Janeiro, Brazil, Sept., 1984

Widely Tunable 1030 nm Gallium Arsenide Sampled Grating Distributed Bragg Reflector Lasers and Photonic Integrated Circuits

Paul Verrinder[1], Lei Wang[1], Fengqiao Sang[1], Victoria Rosborough[1], Guangning Yang[2], Mark Stephen[2], Larry Coldren[1], Jonathan Klamkin[1]

[1]*Electrical and Computer Engineering Department, University of California, Santa Barbara, CA 93106 USA*

[2]*NASA Goddard Space Flight Center, Greenbelt, MD 20771 USA*

pverrinder@ucsb.edu

Abstract: A widely tunable 1030 nm gallium arsenide laser with an integrated semiconductor optical amplifier was demonstrated. Continuous tuning across 22.2 nm and up to 70 mW output power was achieved. © 2022 The Authors

1. Introduction

The ability to easily tune the output wavelength of a laser is important for a variety of applications ranging from fiber telecom systems to free space communications and Lidar [1, 2]. In wavelength division multiplexing (WDM) systems, for example, the role previously filled by multiple standalone distributed Bragg reflector (DBR) lasers or distributed feedback (DFB) lasers can be reduced to a single wavelength tunable laser. Lidar systems can take advantage of this wavelength agility to accomplish beam steering by combining a tunable laser with diffractive grating elements. The laser and photonic integrated circuit (PIC) platform presented here are realized on gallium arsenide (GaAs) and with a nominal target center wavelength of 1030 nm. The sampled grating distributed Bragg reflector (SGDBR) laser architecture enables wide tuning range. The 10xx nm wavelength regime is of interest for a variety of applications including airborne Lidar (the target application), industrial, and biomedical [3, 4]. PIC technology enables a significant reduction in overall system cost, size, weight, and power (CSWaP) compared to currently deployed architectures for 1030 nm Lidar [4-6]. This is critical for space and airborne applications. Tunable lasers near 970 nm have been demonstrated on GaAs [7], however, the majority of commercially available tunable lasers at 1030 nm are external cavity lasers rather than monolithically integrated devices. Similar to indium phosphide (InP) for 1550 nm applications [8], the GaAs platform utilized here and described in [9] possesses the ability to integrate active and passive elements such as lasers, semiconductor optical amplifiers (SOA), modulators, photodetectors, couplers, and optical filters. The SGDBR laser demonstrates 22.2 nm of continuous tuning and up to 70 mW output with an integrated SOA.

2. Device Design and Fabrication

Figure 1(a) shows a sideview schematic of a four section SGDBR laser, with gain, front and back mirrors, and phase sections. Optical gain for the laser is provided by the multi-quantum well (MQW) gain region, consisting of three 5 nm thick indium gallium arsenide ($In_xGa_{1-x}As$) quantum wells (QWs) with $x = 0.271$, surrounded by gallium arsenide phosphide ($Ga_{1-x}AsP_x$) barriers with $x = 0.1$, to provide strain compensation. The MQW layers are surrounded by GaAs waveguide layers, and aluminum gallium arsenide (AlGaAs) separate confinement heterostructures (SCH). Integration of the active QW regions with the passive mirror and phase sections is accomplished by selectively removing the QW layers in the passive sections and regrowing the upper cladding layers by metalorganic chemical vapor deposition (MOCVD) after etching gratings for the front and back mirrors. Gratings for the SGDBR mirrors are patterned on the GaAs waveguide layer using electron beam lithography (EBL), and designed with a pitch of 157 nm for a Bragg wavelength of 1032.8 nm. The gratings are etched to a depth of 35 nm using inductively coupled plasma (ICP) etching with chlorine (Cl_2) and nitrogen (N_2) gas. The front and back mirrors are designed with different reflectivity spectra to exploit the Vernier effect for wide tuning.

This fabrication process was used to fabricate multiple lasers on a single die as shown in Fig. 1(b). Some of the fabricated lasers are simple four-section SGDBRs and some incorporate an SOA at the output after the front mirror for increased optical power. These devices are shown in the top-view microscope images in Figs. 1(d) and 1(e), respectively. In this paper we demonstrate results from the two devices shown in Figs. 1(d-e); one without an SOA and one with SOA. In both cases the length of the gain section is 500 µm, and for the amplified device, the length of the SOA is 500 μm. After fabrication, individual lasers were cleaved out from the chip, anti-reflection (AR) coating was applied to the front and back facets, and the chip was mounted and wire bonded to a carrier as shown in Fig. 1(c).

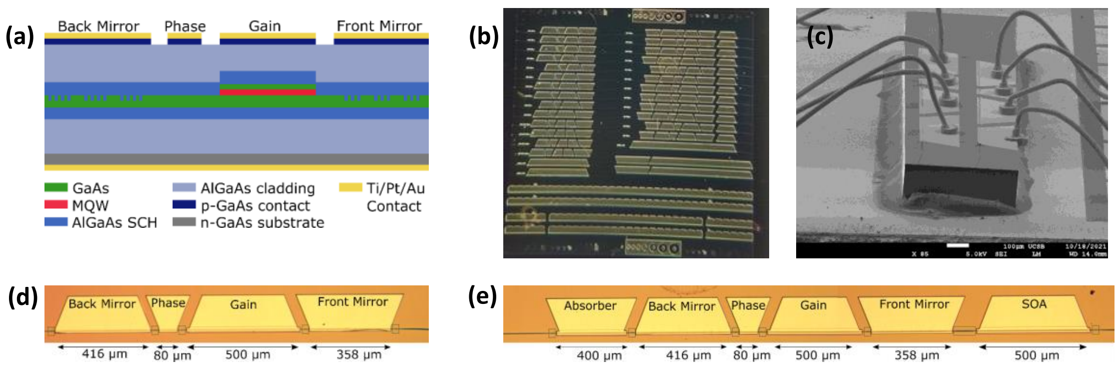

Fig. 1. (a) Side-view schematic of four section SGDBR laser, (b) plan-view microscope image of fabricated die, (c) SEM image of laser chip mounted and wirebonded to a carrier, (d) (e) top-view microscope image of fabricated laser without SOA, and with SOA, respectively.

3. Laser Performance and Characterization

Optical output power was measured by sweeping the current applied to the gain section of the laser and coupling the output to an integrating sphere. The continuous wave (CW) light-current (LI) characteristics are shown in Fig. 2(a) – the blue curve is for the laser without amplification, and the red curve represents the laser with an integrated SOA at the output biased at 100 mA. These devices can easily achieve 35 mW output power without amplification and greater than 70 mW with the SOA. Figure 2(b) shows SOA gain vs. total output power for 4 different current injection levels in the SOA, demonstrating over 25 dB of gain before saturation when the SOA is biased with 100 mA. The output from the laser was coupled to a lensed fiber and connected to an optical spectrum analyzer (OSA) to measure the output spectrum of the device. Figure 2(c) shows the free-running laser spectrum (i.e. current only applied to gain section, without mirror tuning) when the laser gain section is biased at 100 mA CW, demonstrating a peak wavelength of 1031.8 nm, and side-mode suppression ratio (SMSR) of 35 dB.

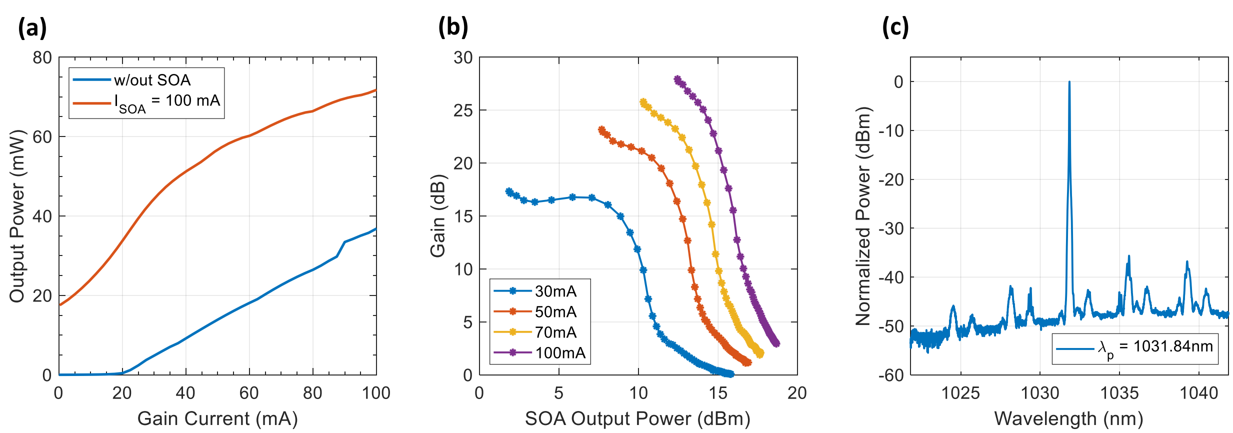

Fig. 2. (a) Optical power vs. current for laser without SOA (in blue) and laser with SOA (in red), (b) SOA gain vs. output power for varying SOA current levels, and (c) laser output spectrum without mirror tuning.

Tuning of the peak wavelength is accomplished by injecting current into the mirror and phase sections of the device. The injected current changes the index of refraction in that section, which shifts the peak of the reflectivity spectra and, therefore, the lasing wavelength. Tuning one mirror at a time will shift the output wavelength to the various available Vernier modes; this is shown in Fig. 3(a) where the spectra for 8 distinct Vernier modes are overlaid on a single plot to demonstrate a total tuning range of 22.2 nm (from 1026.1 nm to 1048.3 nm), with 30 dB SMSR at each

Vernier mode. Wavelengths between the peaks in Fig. 3(a) can be accessed by tuning both mirrors simultaneously, which shifts the peak continuously rather than hopping to adjacent Vernier modes. Figure 3(b) shows a contour plot for this laser, which was generated by tuning the front and back mirrors over every point from 0-150 mA to create a 150x150 grid of wavelength points as a function of mirror current. Figure 3(c) shows a contour plot of the SMSR associated with each point in Fig. 3(b). Tuning of the laser's phase section shifts the position of the cavity modes and, in conjunction with mirror tuning, can be used to avoid cavity mode hops as the laser is tuned from one Vernier mode to another. It should be noted that the SMSR contour plot in Fig. 3(c) was generated without any phase section tuning, and the very low SMSR data points in the plot are a result of mode hopping behavior. With fine tuning of the cavity modes, continuous mode-hop free tuning is possible with greater than 25 dB SMSR across the entire 22.2 nm range.

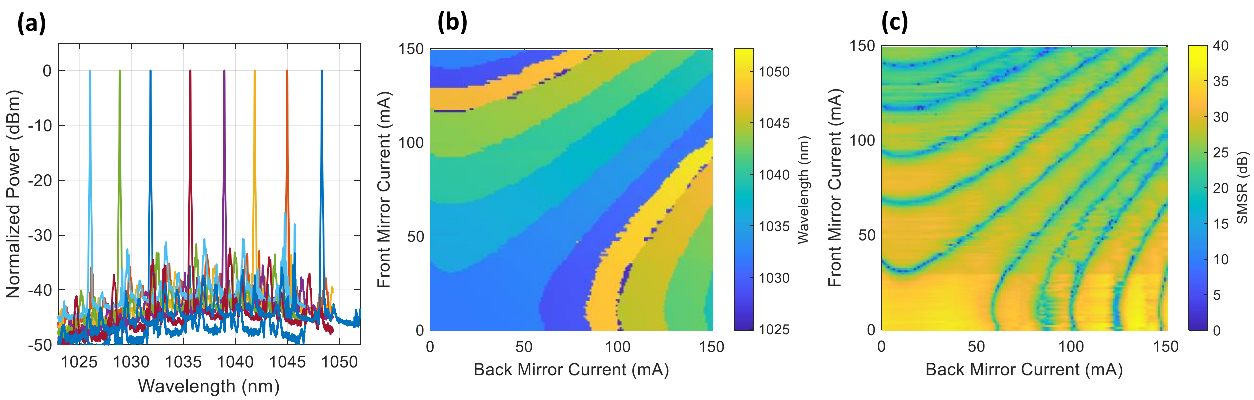

Fig. 3. (a) Overlaid lasing spectra showing Vernier mode positions. (b) Wavelength contour plot, and (c) SMSR contour plot

4. Conclusion

A widely tunable SGDBR laser on a GaAs PIC platform has been successfully demonstrated for operation near 1030 nm. The device demonstrates continuous, mode-hop free tuning across 22.2 nm with 30 dB SMSR, and greater than 70 mW of CW output power with amplification.

Acknowledgements

This work was supported by the NASA ESTO Advance Component Technology program. A portion of this work was carried out in the UCSB Nanofabrication Facility

References

[1] L. A. Coldren, G. A. Fish, Y. Akulova, J. S. Barton, L. Johansson, and C. W. Coldren, "Tunable Semiconductor Lasers: A Tutorial," *J. Light. Technol.*, vol. 22, no. 1, pp. 193–202, 2004, doi: 10.1109/JLT.2003.822207.
[2] B. J. Isaac, B. Song, S. Pinna, L. A. Coldren, and J. Klamkin, "Indium Phosphide Photonic Integrated Circuit Transceiver for FMCW LiDAR," *IEEE J. Sel. Top. Quantum Electron.*, vol. 25, no. 6, pp. 1–7, 2019, doi: 10.1109/JSTQE.2019.2911420.
[3] R. Kawakami *et al.*, "Visualizing hippocampal neurons with in vivo two-photon microscopy using a 1030 nm picosecond pulse laser," *Sci. Rep.*, vol. 3, pp. 1–7, 2013, doi: 10.1038/srep01014.
[4] A.W.Yu et al., "A 16-beam non-scanning swath mapping laser altimeter instrument" in Proc. SPIE LASE, San Francisco, CA, USA, 2013
[5] M. A. Krainak *et al.*, "Laser transceivers for future NASA missions," in Proc. SPIE Defense, Security, and Sensing, Baltimore, MD, USA, 2012
[6] A. W. Yu *et al.*, "Orbiting and in-situ lidars for earth and planetary applications," *IEEE J. Sel. Top. Appl. Earth Obs. Remote Sens.*, vol. 14, pp. 8999–9011, 2021, doi: 10.1109/JSTARS.2021.3103929.
[7] M. Tawfieq, H. Wenzel, P. Della Casa, O. Brox, A. Ginolas, P. Ressel, D. Feise, A. Knigge, M. Weyers, B. Sumpf, and G. Tränkle, "High-power sampled-grating-based master oscillator power amplifier system with 23.5 nm wavelength tuning around 970 nm," *Appl. Opt.,* vol. 57, no. 29, pp. 8680-8685, 2018
[8] H. Zhao *et al.*, "Indium Phosphide Photonic Integrated Circuits for Free Space Optical Links," *IEEE J. Sel. Top. Quantum Electron.*, vol. 24, no. 6, pp. 1–6, 2018, doi: 10.1109/JSTQE.2018.2866677.
[9] P. Verrinder *et al.*, "Gallium Arsenide Photonic Integrated Circuit Platform for Tunable Laser Applications," *IEEE J. Sel. Top. Quantum Electron.*, vol. 28, no. 1, 2022, doi: 10.1109/JSTQE.2021.3086074.